Adsorbate Induced Partial Passivation of Gas-Surface Interactions

Bart Berenbak

Promotiecommissie

promotoren:	prof.dr. Steven Stolte
	prof.dr. Aart W. Kleyn
overige leden:	prof.dr. Wim van der Zande
	dr. Geert-Jan Kroes
	prof.dr. Ben Nieuwenhuys
	dr. Maurice Jansen

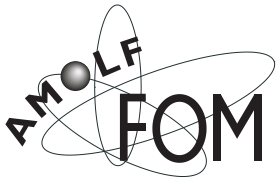

Omslag: Illya Cerjak

The work described in this thesis is part of the research programme of the *Stichting Scheikundig Onderzoek Nederland* SON (Dutch Foundation for Chemical Research) and was made possible by financial support from the *Nederlandse Organisatie voor Wetenschappelijk Onderzoek* NWO (Dutch Organization for Scientific Reasearch).

VRIJE UNIVERSITEIT

Adsorbate Induced Partial Passivation of Gas-Surface Interactions

ACADEMISCH PROEFSCHRIFT

ter verkrijging van de graad van doctor aan
de Vrije Universiteit te Amsterdam,
op gezag van de rector magnificus
prof.dr. T. Sminia,
in het openbaar te verdedigen
ten overstaan van de promotiecommissie
van de faculteit der exacte wetenschappen/scheikunde
op dinsdag 27 juni 2000 om 15.45 uur
in het hoofdgebouw van de universiteit,
De Boelelaan 1105

door

Bart Berenbak

geboren te Breukelen

promotoren: prof.dr. S. Stolte
prof.dr. A.W. Kleyn

This thesis is based on the following papers:

Chapter 2 B. Berenbak, D.A. Butler, B. Riedmüller, D.C. Papageorgopoulos, S. Stolte and A.W. Kleyn, *Sticking probability measurements in a reactive system*, Surface Science. 414 (1998), 271.

Chapter 3 B. Berenbak, S. Zboray, B. Riedmüller, D.C. Papageorgopoulos, D.A. Butler, S. Stolte and A.W. Kleyn, *Ar on Ru(0001), comparison to the washboard model and trajectory calculations*, in preparation.

Chapter 4 D.C. Papageorgopoulos, B. Berenbak, M. Verwoest, B. Riedmüller, S. Stolte and A.W. Kleyn, *A molecular beam study of the scattering and chemisorption dynamics of N_2 on Ru(0001)*, Chem. Phys. Lett., 305 (1999), 401

Chapter 5 B. Berenbak, B. Riedmüller, D.A. Butler, C.T. Rettner, D.J. Auerbach, S. Stolte and A.W. Kleyn, *Molecular beam study on interaction dynamics in a reactive system: NO on bare Ru(0001)*, Phys. Chem. Chem. Phys., 2 (2000) 919.

Chapter 6 D.A. Butler, B. Berenbak, S. Stolte and A.W. Kleyn, *Elastic Scattering in a Reactive Environment: NO on Ru(0001)-(1×1)H*, Phys. Rev. Lett., 78 (1997) 4653-4556.

Chapter 7 B. Berenbak, B. Riedmüller, C.T. Rettner, D.J. Auerbach, S. Stolte and A.W. Kleyn, *Rotational Excitation of NO on Ru(0001)-(1×1)H*, in preparation.

Chapter 8 B. Berenbak, S. Zboray, B. Riedmüller, D.C. Papageorgopoulos, S. Stolte and A.W. Kleyn, *Steric asymmetry in NO scattering from Ru(0001)-(1×1)H*, in preparation.

Contents

1 Introduction **1**
- 1.1 Catalysis: a historic overview . . . 1
- 1.2 Basics of catalysis . . . 2
- 1.3 This thesis . . . 4
- 1.4 Crash course on surface science terminology . . . 8

2 Sticking probability measurement in a reactive system **11**
- 2.1 Introduction . . . 12
- 2.2 Experimental . . . 13
  - 2.2.1 Sticking probability measurement . . . 13
- 2.3 Application to the NO/Ru(0001) system . . . 19
- 2.4 Conclusion . . . 21

3 Ar/Ru(0001) experiments compared to Washboard model and trajectory simulations **23**
- 3.1 Introduction . . . 24
- 3.2 Scattering experiments . . . 25
  - 3.2.1 Experimental setup . . . 25
  - 3.2.2 Angular distributions . . . 26
  - 3.2.3 Time of flight distributions . . . 27
- 3.3 Comparison to the Washboard model . . . 29
- 3.4 Classical trajectory calculations . . . 31
  - 3.4.1 Computational . . . 31
  - 3.4.2 Simulation results . . . 33
- 3.5 Discussion . . . 33
- 3.6 Conclusions . . . 36

4 A molecular beam study of the scattering and chemisorption dynamics of N_2 on Ru(0001) **37**
- 4.1 Introduction . . . 38
- 4.2 Experimental . . . 38

4.3 Results and discussion 39
4.4 Conclusions 45

5 Molecular beam study on interaction dynamics in a reactive system: NO on bare Ru(0001) 47
5.1 Introduction 48
5.2 Experimental 48
5.3 Results and discussion 50
5.3.1 Thermal energy helium atom scattering 51
5.3.2 Initial sticking probability 53
5.3.3 Angular and energy distributions 55
5.4 Summary 56

6 Elastic scattering in a reactive environment: NO on Ru(0001)-(1×1)H 59
6.1 Introduction 60
6.2 Experimental 60
6.3 Results 60
6.4 Conclusions 66

7 Rotational Excitation of NO on Ru(0001)-(1×1)H 67
7.1 Introduction 68
7.2 Experimental 69
7.3 Results and Discussion 71
7.3.1 Possible double rainbow 75
7.4 Conclusions 75

8 Steric asymmetry of NO scattering on Ru(0001)-(1×1)H 77
8.1 Introduction 78
8.2 Experimental 79
8.3 Results and discussion 79
8.4 Conclusions 82

9 Orientation dependent sticking of NO on Al(111) 83
9.1 Introduction 84
9.2 Experimental 85
9.3 Results and discussion 88
9.4 Preliminary conclusions 90

10 Summary 101

11 Samenvatting 105

Nawoord 111

Chapter 1

Introduction

Typically the first sentence of a thesis on gas-surface interactions contains a general remark emphasizing the importance of gas-surface interactions in the world around us. This should then be supported by recognizable examples from every day life: the oxidation of iron to iron-oxide, also known as rust, or the 3-way catalyst, mandatory in each modern car exhaust.

This is a typical surface science thesis. The the research presented is of highly specialized fundamental nature. Not directly aimed at solving applied technical problems, our studies contribute to the basic framework of surface chemistry. In this introduction I will try to picture various aspects of both applied and fundamental surface science, providing a context for this work. Alongside I will introduce some of the surface science *slang* which hopefully makes chapters 2-9 of the thesis more accessible to readers from outside the community.

1.1 Catalysis: a historic overview

With limited knowledge, catalysis was already used in 1746 to produce sulphuric acid. Nitrous vapours were used as catalyst. Later the reaction rates were boosted by constructing the walls of the reaction chamber from lead. In the nineteenth century scientist like Davy, Faraday and Berzelius instigated the development towards modern surface science by attempts to mathematically model catalyst behaviour. In the late 1940's Eugene Houdry developed a catalytic converter to reduce the output of hazardous exhaust gases from internal combustion engines. Quite advanced for that time, the platinum catalyst was on a monolith to allow large gas flows.

As already becomes clear, most dramatic breakthroughs were not initiated by fundamental interests. In the early twentieth century ammonia (NH_3) synthesis was developed by Haber and Bosch in order to produce artificial fertilizer out of nitrogen (N_2) and hydrogen (H_2) gas. During the first world war more ammonia was need for

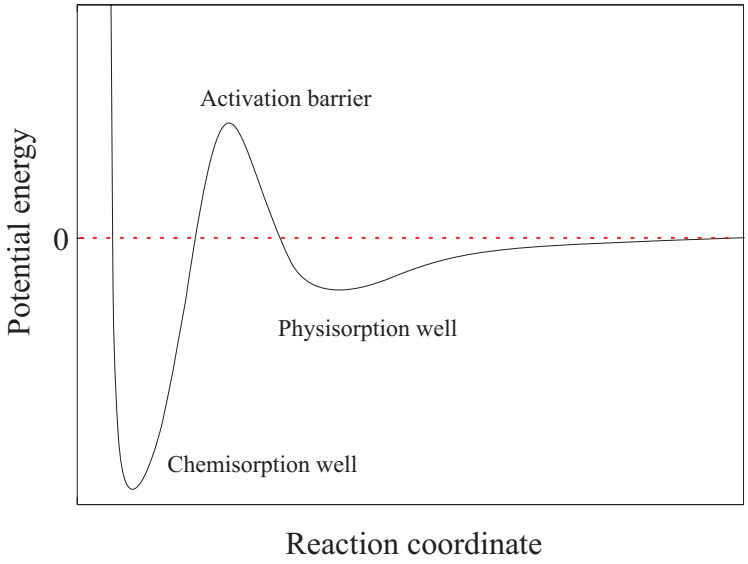

Figure 1.1: *A simple one dimensional example of possible energy levels in a chemical reaction. An activation barrier separates the shallow physisorption well from the deeper chemisorption.*

the manufacturing of explosives. Iron was know to promote the breaking of the N_2-bond, but still 4000 variations to the iron based samples were tested for their chemical activity. Probably world war II would have lasted shorter if German scientists would not have managed to produce liquid fuels out of coal with the Fisher-Tropsch process, thus compensating for the absence of crude oil resources.

1.2 Basics of catalysis

Typically an energetically favorable chemical reaction is limited or hindered by an *activation barrier*. Fig. 1.1 shows a schematic energy diagram of such a system. Energy has to be supplied to the reaction candidates to overcome the chemical barrier. This extra energy can be brought in the system several ways. Simply increasing the incidence energy of the gaseous reactants or increasing the (surface) temperature works in most cases. This kind of activation is also referred to as *shake and bake*.

A different approach to boost reaction rates is to lower the activation barrier by smart application of an active *catalyst*, a substrate which participates in the reaction without being 'consumed'. Amazingly simple as this might sound, there are some fundamental limitations to the behaviour of catalysts. As first formulated by Ostwald, catalysts do not influence the thermodynamic equilibrium of reactants and products

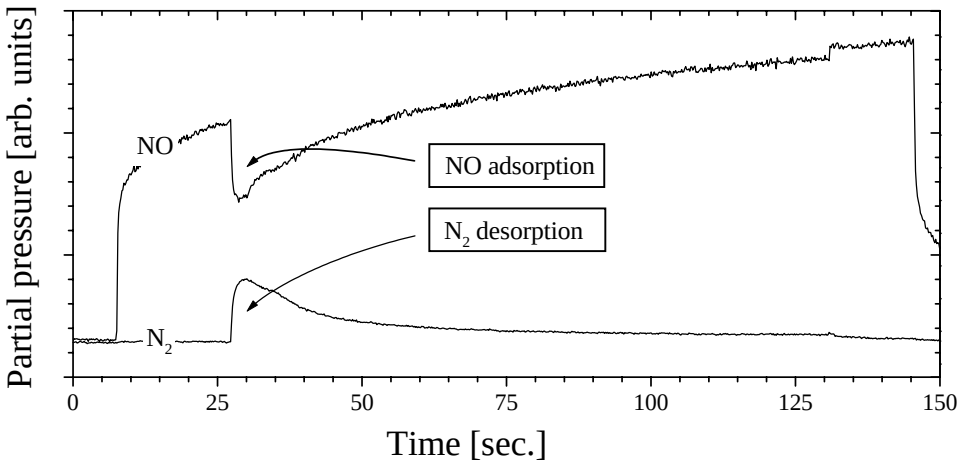

Figure 1.2: *Nitric oxide gas conversion into nitrogen gas, catalyzed by the 900 K (627^o C) Ru(0001) crystal surface. The partial pressure increases when the NO gas beam enters the chamber (t = 7.5 s). Upon retraction of an inert flag (t = 27 s), the Ru surface is exposed to the beam. Subsequent adsorption of NO molecules reduces the NO partial pressure, immediately followed by an increase in the N_2 signal due to desorption of N_2 molecules which have been formed on the surface ($2NO_g \rightarrow N_{2,g} + O_{2,g}$). Because the surface temperature is too low for O-atoms to recombine and desorb, the NO_g adsorption rate goes down as O_{ads} coverage builds up. Gas phase oxygen molecules can be formed at surface temperatures exceeding 1600 K ($\leq$ 1300^o C) .*

but only affects the rate of chemical reaction [70]. The increase in reaction rates can be many orders of magnitude. In most applications however, a pure end product is wanted instead of a mixture of chemicals, making *selectivity* between different reaction paths often far more important than the rate. A good example is the production of drugs and other so-called 'fine' chemicals, where mono-chirality is forced by legislation; only the active component of a stereo symmetric chemical is allowed in order to eliminate unwanted side effects. In situations like these, the demands on the catalyst are so severe that expensive bio-catalysis yields the best results, employing immobilized enzymes to perform complicated manipulations.

In our case this substrate is a (single crystalline metallic) surface, but in homogeneous catalysis a metal (ion) complex in the liquid phase operates as the active catalyst. The ruthenium surface is capable of converting toxic NO molecules to harmless N_2 and O_2 molecules; a reaction that does not occur spontaneously in the gas phase. First the NO molecules adsorb on the surface ($NO_g \rightarrow NO_{ads}$). Subsequent dissociation leaves adsorbed nitrogen and oxygen atoms on the surface ($NO_{ads} \rightarrow N_{ads}$+$O_{ads}$). The N-atoms are mobile at surface temperatures above 520 K

and can recombine to form adsorbed nitrogen molecules ($N_{ads} + N_{ads} \rightarrow N_{2,ads}$). Finally desorption brings the nitrogen molecules in the gas phase ($N_{2,ads} \rightarrow N_{2,g}$). In Fig. 1.2 this conversion appears as a decrease in the NO partial pressure concomitant with an increase in the N_2 signal, as soon as the NO beam is exposed to the hot Ru surface (at t = 27 s). Oxygen molecules can be formed in the same manner but demand surface temperatures exceeding 1600 K (1300^o C) in order to overcome the much higher binding energy of the O-atoms to the surface.

A nice illustration of the parallel existence of different reaction channels, complicating surface chemistry, is the inability of gold to be oxidized even though this is energetically attractive. Molecular oxygen will stick to the gold surface provided the temperature is low enough. Oxidation however requires the molecules to break up to give adsorbed oxygen atoms. The increase in surface temperature needed leads to desorption of the molecule long before it can dissociate. The shiny gold surface is 'saved' by the molecular precursor to sticking; phase space wins.

Control over competing reacting channels is one of the driving forces behind applied surface chemistry. Molecular beam methods have proven to be a very powerful tool for the study of elementary reaction steps, for they allow control over the incidence angle and energy of the molecules impinging on the sample of interest. Information, for instance, about the height and shape of an activation barrier can be obtained by studying the reaction rate as a function of incidence energy. Through *micro-reversibility* such information can be analyzed to yield information about the desorption rates of species.

Though many insights have been obtained, and computers have been effectively applied to quantitatively predict reactions, a remarkable resemblance between applied catalysis now and in 1746 is the 'trial and error' method often used. Fundamental research, like the work presented in this thesis, contributes to the very basic knowledge behind each step in a catalytic cycle.

1.3 This thesis

The title of this thesis, *Adsorbate Induced Partial Passivation of Gas-Surface Interactions*, is covered in eight chapters, mostly about nitric oxide (NO). This gaseous molecule has a bad reputation in our society. It is know for it's poisonous character to living creatures and the negative contributions to the ozone layer and acid rain. Inhalation of this gas is not recommended for it attacks the nervous system. In surface chemistry, however, the use of NO is widespread. Besides the many interesting reactive properties for most metallic surfaces, its electronical structure exhibits a lone pair $^2\Pi$-electron, which makes laser spectroscopy extremely fertile and allows state selection (orientation) by a hexapole electrostatic lens.

Each chapter focuses on different aspects of the collision process of gas particles on metallic crystal surfaces. Using molecular beams, insights can be obtained in the *dynamics* of the interaction. Does the dissociation of NO molecule on the Ru(0001)

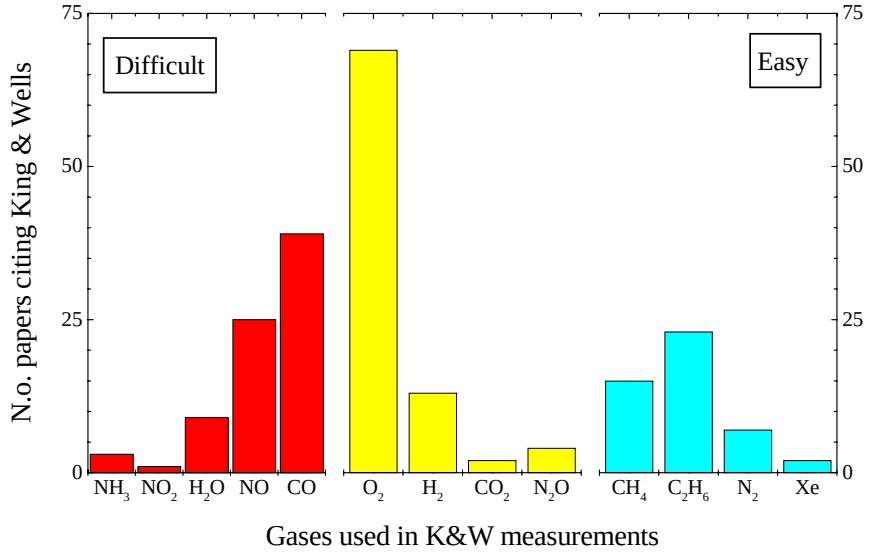

Figure 1.3: *Number of papers citing the original publications by King and Wells [31, 32] (first published in 1972) as a function of the gas used. The gases are roughly ordered to the degree of difficulty encountered due to interactions with the stainless steel walls of most vacuum systems.*

surface for instance, occur after first adsorbing as a molecule, or is the dissociation prompt? This information in reaction mechanisms forms the main difference with microscopic and spectroscopic techniques, exposing *steady states* at surfaces.

Besides this Chapter 1 (the introduction), different aspects will be handled in the following way:

Chapter 2 will present an important extension to the analysis of the *adsorption-reflection* technique, developed by King and Wells to measure the initial sticking coefficients of gases on surfaces [31, 32]. Since this technique is based on changes in the partial pressure in the vacuum chamber, some sort of modification is needed for those gases that interact with the (usually stainless steel) walls. This very common problem was already addressed by King & Wells in their original papers. Very few publications however contain any information about the analysis procedure invoked to circumvent these problems caused by interactions with the chamber walls. Fig. 1.3 shows a histogram of the amount of publications with the term 'sticking coefficient' in the title, grouped per gas, roughly ordered to the amount of difficulties likely to be encountered when used in King & Wells sticking measurements. Application of our simple and elegant analysis procedure could probably have resulted in more reliable absolute initial

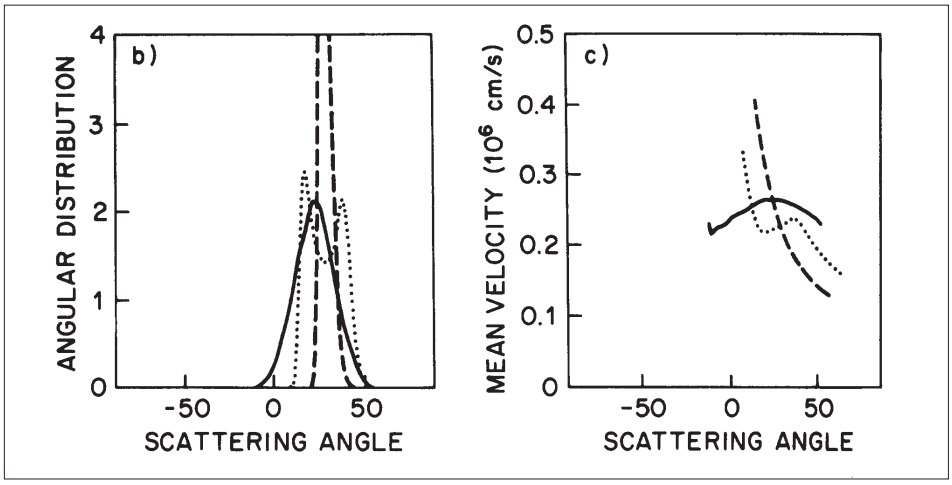

Figure 1.4: *From Tully* et al. *[85]. The washboard model applied to the Ar argon scattering of various faces of the platinum. The dashed curve in the right panel, 'explained' by Tully as a failure of the washboard model, shows exactly those features we observe for our Ar/Ru(0001) system.*

sticking coefficients for most of these ≈1500 articles.

Chapter 3 reports about the unexpectedly complicated scattering of argon from the clean Ru(0001) surface; one of the most simple gas-surface systems thinkable. If surface science could ever be simple, the straightforward scattering of a noble gas (argon) from a very high quality, well ordered single crystal like ruthenium should be it. Initiated to provide a clearly understandable reference in anticipation of the complicated N_2/Ru scattering described in Chapter 4, the results turned out quite surprising. Needles to say that being fooled by apparent simplicity, its surprising data provides an excellent opportunity to gain much insight in the basics of surface scattering. Especially when the energy distributions reveal features similar to those observed by John Tully when testing his newly developed *washboard* model; the simplest extension to the well know *hard cube* model (see Fig. 1.4) [85]. Fascinatingly our results on Ru(0001) very much resemble the results Tully obtained for the Pt(111) surface and interpreted as unphysical.

Chapter 4 was instigated by theoretical predictions from Nørskov *et al.*, presented at the *Gordon Research Conference on Dynamics at Surfaces* in 1997. This inspired us to apply perhaps the only technique capable of direct observation of a short lived metastable molecular state on the surface. Such a state was calculated for N_2 on clean Ru(0001) and was thought to cause a measurable

residence time of particles on the surface. In this case a delay in the Time Of Flight (TOF) should be observed. Direct evidence of this metastable state has not been observed, but the sharp increase in the width of the angular distribution with increasing particle energy clearly indicate a change in corrugation of the Potential Energy Surface (PES); fully consistent with a very shallow metastable state.

Chapter 5 is about the interaction of nitric oxide with the clean Ruthenium surface. The special characteristic of this combination is the possibility for molecules to dissociate spontaneously leaving nitrogen and oxygen atoms on the surface. The sticking on this surface is so effective that almost no molecules manage to scatter of the surface. The higher detection efficiency of the setup used at IBM in San Jose (U.S.A.) made it possible to measure the energy of the scattered fraction. While the angular spread of scattered NO molecules is large, as to be expected for *reactive* scattering, the energy transfer in the collisions is surprisingly small.

Chapter 6 contains a fascinating data set that we were lucky to encounter quite early in the project. Now, a few years later, the main features are still puzzling. After accidentally covering the surface with the hydrogen, present in the molecular beam as seeding gas, the specularly scattered amount of NO molecules shot up and the particles seemed to exhibit extremely small translational energy losses in the collision event. Well controlled experiments with pre-dosed hydrogen layers at the liquid nitrogen cooled surface (T_s= 140 K = -133^o C) revealed an unprecedented narrow angular spread of the scattered flux with close to elastic scattering; like a *molecular mirror* the molecules bounce specularly of the flat surface (incidence angle = outgoing angle) while maintaining most their initial velocity.

Surprising as this apparent absence of surface corrugation seems, the story got an extra special turn when the sticking probability for NO molecules turned out to be quit high: ∼50%. This *reactive* sticking seems intuitively in conflict with the *inert* scattering for it usually is encountered in combination of broad angular distributions. This observation of *elastic scattering in a reactive environment* was good for a publication in Physical Review Letters [10], a highly appreciated magazine. The additional techniques employed to unravel this mystery will be described in Chapters 7 and 8.

Chapter 7 is the result of measurements performed at the *Almaden Research laboratory* of IBM in San Jose (USA). This joint study program became financially possible with the help of the *Dr. J.E. van Dierendonck Stipendium*. During this 10 weeks visit Charlie Rettner, Dan Auerbach and I managed to determine the rotational state distribution of NO scattered from the hydrogen covered Ru(0001) surface. Little rotational excitation was expected since this system had already revealed surprising little energy loss in the gas-surface collision

(Chapter 6). The rotational temperature however turns out to be 'cool' but not extremely 'cold'; the molecule apparently maintains the conventional *egg*-shape.

Chapter 8 contains a very simple and elegant piece of surface chemistry research. Though the experimental details are quit demanding, the basics is simple: the ability of a hexapole beam source to orient NO molecules before impinging on the sample surface, allows a direct study of the difference in interaction for the two ends of the molecule. Clearer than ever before it is shown that the *inert* O-side of the molecule scatters in a relatively sharp angular distribution with high intensity in the specular direction, while the *reactive* N-side result in a wider angular spread with a relatively high intensity in the wings of the distribution. The width of the distribution can be used as a measure of reactivity of the interaction.

Chapter 9 presents the preliminary results of a collaborative study with Andrew Komrowski and Andrew Kummel (UCSD, USA) into the interaction of NO with (111) face of aluminum. The recent interest in this system has been instigated by controversy around the closely related O_2/Al(111) system. When NO molecules break up on the surface, N-atoms seem to be 'missing'; most probably ejected into the vacuum. Our experimental setup enables orientation of the NO molecules prior to the collisions. With this hexapole beam source we determined molecules with the N-end preferentially directed towards the surface to yield the highest sticking probability.

Chapter 10 [1] is a summary of the work presented. Especially Chapters 5 - 8, are closely linked by the mysterious scattering of NO molecules from the hydrogen covered ruthenium surface which we investigated with various experimental techniques. The aim of this chapter is to summarize and combine the results of the different studies so that a consistent picture of the interaction potential can be constructed.

1.4 Crash course on surface science terminology

English is of course the scientific language. Much of the language used amongst surface scientist however is supplemented by typical expressions, which allows better communication. For those readers who are not familiar with the surface science slang, this section contains an introduction to some of the essential terminology.

Direct elastic scattering occurs when the gas particle has a single collision with the surface, without transferring any energy to the surface.

Direct inelastic scattering stands for collisions in which the gas particle transfers energy to the surface in the collision event.

[1] Go straight to this chapter if you've already lost it here

Rotational excitation is an energy transfer process in (gas-surface) collisions in which energy is converted in rotational energy.

Chemisorption stands for bonding of a particle to the surface by sharing electronic orbitals with the electronic states of the surface.

Physisorption means bonding of a particle to the surface by so-called *van der Waals* forces; a polar bond is induced without sharing electrons. This bond is much weaker than chemisorption.

Sticking and trapping are more loosely defined terms indicating particles that loose all translational energy in the collision and make a bond with the surface. In this thesis *sticking* stands for chemisorption while *trapping* is used for physisorption.

Corrugation is the ripple in the surface as experienced by an impinging gas particle. Depending on the nature of the interaction, the impinging gas particle experiences a certain smoothness or roughness. The washboard model is a way to study the influence of this corrugation on direct inelastic scattering.

A unit cell is the smallest building block of a (single) crystal that still contains the all information about the spatial geometry of the crystal.

Steric asymmetry denotes the difference in the interaction of two ends of an hetronuclear molecule; in our case the two sides of the NO-molecule.

Thermal energy particles are produced with molecular beams. In contrast to the enormously energetic beams generated by nuclear physics related particle accelerators, the energies used in surface chemistry are generally in the order of electron Volts (eV). Velocities related to these thermal energies are similar to those of air particles surrounding us; about $\frac{3}{2}kT \cong 300$ meters per second at room temperature.

Normal or parallel momentum indicate the components of the total momentum (is mass $\times$ velocity) directed normal or parallel to the surface. One often speaks of normal energy while strictly spoken this is not allowed while energy is a not vector but a scalar (a quantity without direction).

The (0001) face of crystalline ruthenium has the hexagonal close packed (HCP) structure; the indices indicate to which crystal face the sample is polished.

Sub-, super- and specular scattering are terms to denote the different angular regimes. We speak of *specular* scattering when the outgoing angle is the same as the incoming angle as holds for a mirror. *Super-* and *sub specular* denote outgoing angles more parallel and perpendicular to the surface respectively.

Chapter 2

Sticking probability measurement in a reactive system

The sticking probability of reactive molecules on surfaces is usually measured using the well established beam reflectivity technique of King and Wells [31, 32]. The fundamental problem of this technique results from the interaction of the gas with the walls of the chamber. For the majority of gases used in King and Wells sticking probability measurements, the exposure of the chamber walls to the gas causes changes in the effective pumping speed of the vacuum chamber. A simple model is presented which shows the influence of the residence time of particles on the walls, on the effective pumping speed of the system. In combination with test data, this model reveals a very symmetric response to changes in the beam flux. This insight is used to develop a straightforward method for the determination of the initial sticking coefficient S_0, which allows for changes in pumping speeds. In applying the technique to the adsorption of NO on Ru(0001) the initial sticking coefficient is observed to be very high ($S_0 \geq 0.9$) and almost constant for incident energies between $0.3 < E_i < 2.5$ eV, suggesting more than one dissociation pathway. For the Ru(0001)-(1×1)H surface S_0 increases from 0.2 to 0.6 in the same energy range, indicating a partially activated process.

2.1 Introduction

One of the fundamental parameters describing the interaction of gases with surfaces is the sticking coefficient, defined as the ratio of adsorbing to impinging particles. Initial sticking coefficients between 0.01 and 1 are usually measured by the adsorption-reflection technique of King and Wells (K&W), in a molecular beam setup [31, 32]. In this method, the partial pressure due to molecules reflected from a reactive surface (the non-sticking component) is compared with that due to reflection from an inert surface. To use the chamber pressure as a direct measure of the number of reflected molecules in this way, requires the pumping speed of the chamber to be constant. In this ideal case the response of the chamber to changes in gas load is programmed by the vacuum time constant (~ 0.4 sec). Most gases of interest however, do stick to the stainless steel walls of the vacuum chamber. Depending on the residence time of the adsorbed particles the response of the system can be dramatically affected. Only in the two extreme cases of zero or infinite residence time the response is not affected; the chamber walls will either stay clean, or will turn inert after a dose sufficient to completely passivate the entire chamber. For gasses like NO, CO, O_2, NH_3, etc. the residence time will be in the order of seconds to minutes, seriously complicating the analysis of the K&W measurement. Although the technique of K&W is widely used, with the original papers [31, 32] being cited more than 500 times since 1981, little is mentioned about the evaluation of the data. For example, Luntz et al [45] neglected the change in pumping speed of the chamber walls in evaluating their O_2/Pt(111) measurements. The influence of the rather large vacuum time constant ($\sim$0.6 sec) was handled by simply averaging the partial pressure over several seconds. Especially for reactive systems with sticking probabilities close to unity, the sample surface can be substantially covered in this period. To overcome this problem attenuated beams have been used. Rettner *et al.* tackled this problem rigorously for the sticking of O_2 on tungsten by adapting the measurement procedure [64]. Their procedure consisted of two consecutive measurements, comparing the partial pressure rise upon hitting the clean or the fully saturated sample surface. Variations in pumping speed are accounted for by comparing the pressure in one trace at time t with the pressure at time t' from the other, with times t and t' being the times at which the chamber walls have been exposed to the same dose of gas. This procedure would be correct for an infinite residence time, but not for a limited (real) residence time, since the desorption of particles is not treated. A similar procedure is apparently developed by Hopkinson *et al.* [28, 27], where the change in pumping speed of the system due to adsorption/desorption from the chamber walls is treated by a series of exponential relaxation terms determined from a separate blank experiment. In this paper a simple adsorption/desorption model is developed which leads to an alternative, more accurate and far simpler approach which provides an extension to the procedure of King and Wells to more demanding systems. The new analysis procedure is tested for the highly reactive interaction of NO molecules with the Ru(0001) surface.

2.2 Experimental

The experiments were carried out in a surface scattering machine described in detail elsewhere [58, 56]. It consists of a scattering chamber, to which a three-stage supersonic molecular beam source is attached. The volume of the chamber is ∼120 l, and it is pumped by a 520 ls^{-1} turbo-molecular pump (TMP), mounted such that the effective pumping speed is ∼300 ls^{-1}, resulting in an overall base pressure of approximately $1{\cdot}10^{-10}$ mbar. The translational energy (E_i) of the incoming molecules, as measured by their time of flight, was varied between 0.07 and 2.7 eV by changing the seeding ratio of NO in either H_2 or He, and heating the nozzle. Due to effective pumping, no pressure rise can be detected in the last stage of the source. This ensures a negligible effusive beam contribution in the main chamber.

The beam flags required for the sticking probability measurement were positioned in the second stage of the beam source and in the scattering chamber, and were constructed of stainless steel and quartz respectively. A quadrupole mass spectrometer (QMS, Balzers QMG-420), mounted on the wall of the scattering chamber provided the angle integrated measurement of the NO partial pressure. Chopped beams (2.5, 10 or 50% duty cycle) were used to reduce the total flux of NO incident on the surface, allowing the collection of a large number of data points at low surface coverages.

The Ru sample was aligned and polished to within 0.1^o of the (0001) crystal face. It could be heated by electron bombardment (600 V, 80 mA) at up to 25 Ks^{-1}, regulated by a programmable controller (Eurotherm 900 EPC) and cooled to ∼100 K with liquid nitrogen. The sample temperature was measured with a type C thermocouple. This was calibrated against a type K thermocouple for temperatures below 273 K. Cleaning was performed in situ by repeated cycles of flashing in a background pressure of oxygen ($2 \cdot 10^{-8}$ mbar) to 1500 K. An oxygen free surface could be obtained by a single flash to 1600 K in UHV [10]. Helium thermal energy atom scattering (TEAS) was found to be an extremely sensitive probe of the surface cleanliness and order. This proved to be particularly useful because the main contaminant (C) is difficult to detect in small concentrations by Auger electron spectroscopy (AES) due to overlap with the Ruthenium peaks [20, 61]. Low energy electron diffraction is available for calibration of the azimuthal orientation of the crystal surface.

2.2.1 Sticking probability measurement

The technique of King&Wells is performed by sequentially retracting two beam flags. Opening the first flag, positioned in the second stage of the beam source, allows the beam to hit the second flag, positioned inside the main chamber. For an inert beam flag and a totally passivated chamber the beam flux will cause a pressure rise from P_{Bg} to $P_f (= P_{BG} + P_{rise})$, according to the relation

$$P_{rise} = \frac{Q_{beam}}{S_{TMP}} \tag{2.1}$$

where Q_{beam} is the gas flow volume of the molecular beam, and S_{TMP} the pumping speed of the TMP. Opening the second flag allows the beam to hit the sample surface. This will cause a pressure drop ($P_{drop} = P_f - P_s$) if the surface adsorbs part of the beam flux. Given a constant pumping speed S_{TMP}, the initial sticking coefficient simply follows as

$$S_0 = \frac{P_{drop}}{P_{rise}}. \tag{2.2}$$

However, for gases that interact strongly with the stainless steel chamber walls, the transitions to equilibrium pressures, upon opening the beam flags, take longer than predicted by the vacuum time constant of the chamber (in our case $\tau_{vac} \cong 0.4$s). This increase in response time of the system is due to molecules going through a sequence of adsorption and 'delayed' desorption on their way to the pump. The combination of the vacuum time constant τ ($= S_{TMP}/V$), the sticking coefficient s_w and residence time τ of particles on the chamber walls now program the pumping characteristics. The problem of determining P_{rise} and P_{drop} is shown in the typical data set of Fig. 2.1 which shows the course of the partial NO-pressure in the main chamber upon opening and subsequently closing the first beam flag. Closing the first beam flag is equivalent to the situation of retracting the second flag in combination with full adsorption of the beam on the sample surface ($S = 1$), since in both cases no particles from the beam can contribute to the partial pressure. The characteristics of pressure rise and drop are studied using a model, which explicitly compares the temporal dependence of the number of particles in the gas phase (N_g) and the number of particles adsorbed on the chamber walls (N_w).

$$\frac{dN_g}{dt} = n_d - n_s + F_{tot} - JN_g \tag{2.3}$$

$$\frac{dN_w}{dt} = -n_d + n_s \tag{2.4}$$

Here n_d is the number of desorbing particles per unit of time, n_s the number of adsorbed particles, F_{tot} the total particle flux entering the chamber and $J = S_{TMP}/V$ the number of particles being pumped, all per unit of time, and V the chamber volume. The number of particles that hit the chamber walls per unit of time equals $n_h = \frac{\bar{c}A}{4V}N_g$, with $\bar{c} = \sqrt{\frac{8kT}{\pi m}}$ the average velocity of the particles and A the surface area of all the material used in the main chamber. We assume the coverage of the chamber walls to remain small ($\Theta \ll 1$), which allows the use of a constant sticking coefficient for particles at the chamber walls s_w. The number of adsorbing particles per unit of time (n_s) becomes:

$$n_s = s_w n_h = s_w \frac{\bar{c}A}{4V}N_g \tag{2.5}$$

The particles have a limited residence time (τ) on the walls. Assuming first order desorption, the number of desorbing particles, per unit of time, is:

$$n_d = \frac{N_w}{\tau} \tag{2.6}$$

Substituting Eqns. 2.3 and 2.4 into 2.1 and 2.2 gives:

$$\frac{dN_g}{dt} = \frac{N_w}{\tau} - \left[\frac{s_w \bar{c} A}{4V} + \frac{S_{TMP}}{V}\right] N_g + F_{tot} \tag{2.7}$$

$$\frac{dN_w}{dt} = -\frac{N_w}{\tau} + \frac{s_w \bar{c} A}{4V} N_g \tag{2.8}$$

We separate the flux (F_{tot}) into two contributions, the pulsed beam flux (F_{MB}) and a continuous background contribution (F_{Bg}). The latter is required to mimic the resident gas pressure in the scattering chamber when $F_{MB} = 0$. We can now construct the two necessary boundary conditions $N_g = F_{Bg}/J$ and $N_{w(0)} = F_{Bg} s_w \bar{c} A \tau / 4VJ$, and solve the two coupled first order differential equations:

$$N_g(t) = \frac{F_{Bg}}{J} + \frac{F_{MB}}{2J}\left[2 - (1-X)\cdot e^{-\frac{1}{2}(\lambda_1+\lambda_2)t} - (1-X)\cdot e^{-\frac{1}{2}(\lambda_1-\lambda_2)t}\right] \tag{2.9}$$

with

$$X = \frac{\frac{S_{TMP}}{V} - \frac{1}{\tau} - \frac{s\bar{c}A}{4V}}{\sqrt{-4\frac{S_{TMP}}{\tau V} + \left(\frac{1}{\tau} + \frac{s\bar{c}A}{4V} + \frac{S_{TMP}}{V}\right)^2}} \tag{2.10}$$

and

$$N_w(t) = \frac{F_{Bg}}{J}\frac{\tau s_w \bar{c} A}{4V} + \frac{F_{MB}}{2J}\frac{\tau s_w \bar{c} A}{4V}\left[2 - (1-Y)\cdot e^{-\frac{1}{2}(\lambda_1+\lambda_2)t} - (1-Y)\cdot e^{-\frac{1}{2}(\lambda_1-\lambda_2)t}\right] \tag{2.11}$$

with

$$Y = \frac{\frac{S_{TMP}}{V} - \frac{1}{\tau} - \frac{s\bar{c}A}{4V}}{\sqrt{\left(\frac{1}{\tau}\right)^2 + \frac{2}{\tau}\left(\frac{s\bar{c}A}{4V} - \frac{S_{TMP}}{V}\right) + \left(\frac{s\bar{c}A}{4V} + \frac{S_{TMP}}{V}\right)^2}} \tag{2.12}$$

With $\lambda_1 = \frac{1}{\tau} + \frac{s\bar{c}A}{4V} + \frac{S_{TMP}}{V}$ and $\lambda_2 = \sqrt{-4\frac{S_{TMP}}{\tau V} + \left(\frac{1}{\tau} + \frac{s\bar{c}A}{4V} + \frac{S_{TMP}}{V}\right)^2}$. From Eqn. 2.10, it can be seen that the two pre-exponentials are mainly determined by s_w, whereas the time scale of the slow exponential ($\tau_{slow} = 1/(\lambda_1 - \lambda_2)$) is dominated by $1/\tau$. This is illustrated in Fig. 2.1(c) and (d) where N_g and N_w are shown for three combinations of $1/\tau$ and $\frac{s\bar{c}A}{4V}$. Note the absolute scale of Fig. 2.1(c) and (d), which correspond to an arbitrary beam flux of 5 s^{-1}.

Reasonable values for residence time and the sticking coefficients are difficult to predict, since the walls of the actual vacuum chamber are not constructed from just stainless steel. Furthermore, not all the stainless steel components have the same history. This will lead to deviations, from the double-exponential solution of Eqn. 2.9,

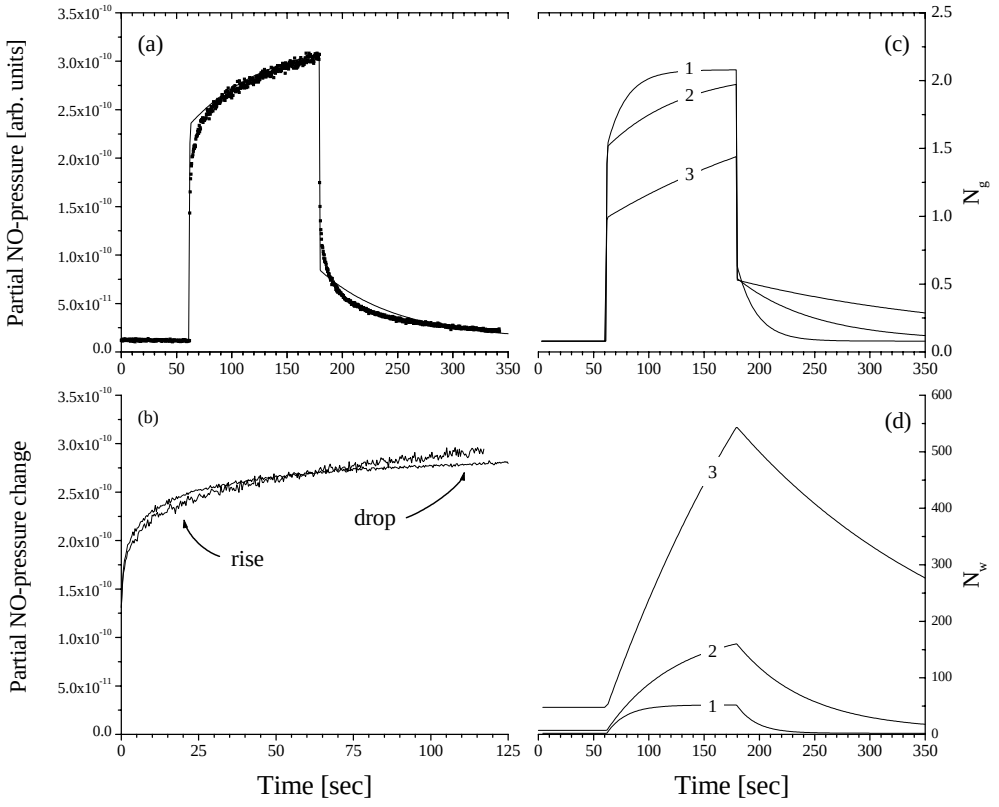

Figure 2.1: *(a) The measured response of the partial NO-pressure upon opening and closing the first beam flag, with a fit to expression 2.9 ($1/\tau$ = 0.01587 ~ (63 s)$^{-1}$, $\frac{s\bar{c}A}{4V}$ = 1.0597 s^{-1}, and S_{TMP}/V = 2.5 s^{-1} fixed). (b) Comparison of the magnitude of the pressure rise, $P(t_{rise} + t_i) - P_{Bg}$, and drop, $P(t_{drop}) - P(t_{drop} + t_i)$ for the data of panel (a) of this figure. (c) The simulated response of the number of gaseous particles (N_g) in the chamber upon opening and closing the first beam flag for three different combinations of ($1/\tau$, $\frac{s\bar{c}A}{4V}$): 1. is (0.06, 2), 2. is (0.02, 2) and 3. is (0.02, 6). (d) The corresponding number of particles adsorbed on the chamber walls (N_w).*

especially on a short time scale. On a longer time scale the material with the largest residence time will dominate the pressure change. If we extend our model such that the chamber walls are treated as consisting of two different materials, by a third differential equation to the set, a very good resemblance to the data can be obtained. Additional simplification are the assumption of first order desorption, the neglect of diffusion in pores and cracks, the non uniform behavior in the effective pumping speed and coverage of the walls. For simplicity we choose to use a τ and s_w that is averaged over all the different materials used inside the UHV chamber. Fixing the know value for S_{TMP}/V ($= 300$ ls$^{-1}/120$l $= 2.5$ s^{-1}), fitting the data of Fig. 2.1(a) to Eqn. 2.9 gives us $1/\tau = 0.01587 \sim(63\text{ s})^{-1}$, and $\frac{s\bar{c}A}{4V} = 1.0597$ s^{-1}. Ignoring the deviations in the first few seconds of pressure change, the fit appears realistic, despite the simplifications (see Fig. 2.1(a)).

Although we don't have an accurate number for the surface area of the chamber, the obtained value for $\frac{s\bar{c}A}{4V}$ allows us to estimate the order of the sticking coefficient for NO on the stainless steel to be <1%. The time constants in the two exponentials of Eqn. 2.9 now become $\tau_{fast} = 1/(\lambda_1 + \lambda_2) \cong 0.28$ s and $\tau_{slow} = 1/(\lambda_1 - \lambda_2) \cong 89.85$ s. Note that τ_{fast} is faster than the vacuum time constant as expected from the increased effective pumping speed, by the sticking of particles on the chamber walls. The slow one is slower than the residence time of the molecules on the walls, as to be expected from the multiple adsorption-desorption events likely to occur before particles are pumped by the TMP.

Comparing the magnitude of the pressure drop and rise change, upon opening or closing the beam flag, shows comparable responses for times in the order of the vacuum time constant, while for larger times the curves start to deviate substantially. The origin of this asymmetry results from the absence of equilibrium when switching the beam off. When allowing equilibrium to be reached before switching the beam off, complete overlap of the simulated curves can be observed. Crucial is the observation that the amplitude of the fast pressure change does not depend on the presence of an equilibrium. This result allows us to extrapolate back to $t = 0$ in order to obtain the initial sticking coefficient. That the instantaneous pressure change does not depend on the time the beam has been switched on has been verified both experimentally and by the model. It shows that taking the instantaneous pressure change ratio, the actual coverage of the walls is irrelevant, thus giving the initial sticking coefficient directly. The coverage of the walls does not change on the time scale of the fast change, and can be ignored. It cannot be ignored when comparing data at some time t' to some earlier time t. In this case the change in wall coverage and pumping speed had to be taken into account explicitly, such as done by Rettner *et al.* [64]. Due to the limited residence time, this wall coverage strongly depends on the entire pressure history of the experiment.

The equivalent form of the ratio of the magnitude of the pressure change in discreet

steps, like the experimental data, is:

$$S(t_i) = \frac{P(t_{drop}) - P(t_{drop} + t_i)}{P(t_{rise} + t_i) - P_{Bg}}, \qquad t_i = i \cdot \delta t \tag{2.13}$$

with $P(t_{drop})$ the pressure just before allowing the beam on the surface, i = 0, 1, 2, 3, ... and δt is the measurement time per data point. The changing sticking coefficient of the sample with increasing coverage causes an increasing error as time proceeds. In practice the determination of the initial sticking coefficient this is no problem because $S(t_i)$ shows a linear change over the first few seconds, allowing easy extrapolation to t=0:

$$S_0 = \lim_{i \to 0} S(t_i) \tag{2.14}$$

The result of Eqns. 2.13 and 2.14 are illustrated in Fig. 2.2(a) and (b), for the test data of Fig. 2.1(b). Upon removing the beam from the chamber a 'sticking probability' of 1 should be observed. In fact a value of 1.035 is measured, suggesting an error of less than 4% for the technique, small compared to the error incurred by assuming a constant pumping speed (C $\cong$ 40%).

An automated version of the analysis is developed which needs only t_{rise} and t_{drop} as input. The background pressure (P_{Bg}) is determined by a linear fit through the data prior to t_{rise}, and the pressure just before the second switching point, $P(t_{drop})$, is determined from a fit to $P(t) = P_{rise}\left[1 - C \cdot (1 - e^{-(t - t_{rise})/\tau})\right]$.

An adsorption-desorption model is presented explaining variations in the effective pumping speed of the UHV chamber in terms of sticking probability and residence time of particles on the chamber walls. The surprising conclusion to the most fundamental problem in analyzing K&W data is that no corrections are needed, to obtain the initial sticking probability, due to canceling of the deviations. The resulting analysis procedure, described above, gives slightly overestimated (4%) but very reproducible initial sticking coefficients. The analysis of sticking probability measurements for NO on Ru(0001) has been performed by a computerized version of this procedure. The method allows the reproduction of S_0 with a spread of less than 4%.

In an earlier paper we reported values for S_0 for NO on Ru(0001), without the benefit of this analysis procedure [10]. The previous analysis procedure consisted of exponentials being fitted, attempting to correct the data. The values for S_0 obtained with the procedure described above, which will be presented in the next section, are 20 to 30% higher, compared to the previously reported sticking coefficients. We believe that the energy dependence in the deviation on particle energy is an artifact of the previously used method, and that the values reported here are more accurate. The discrepancies emphasize the need for careful analysis in such reactive systems.

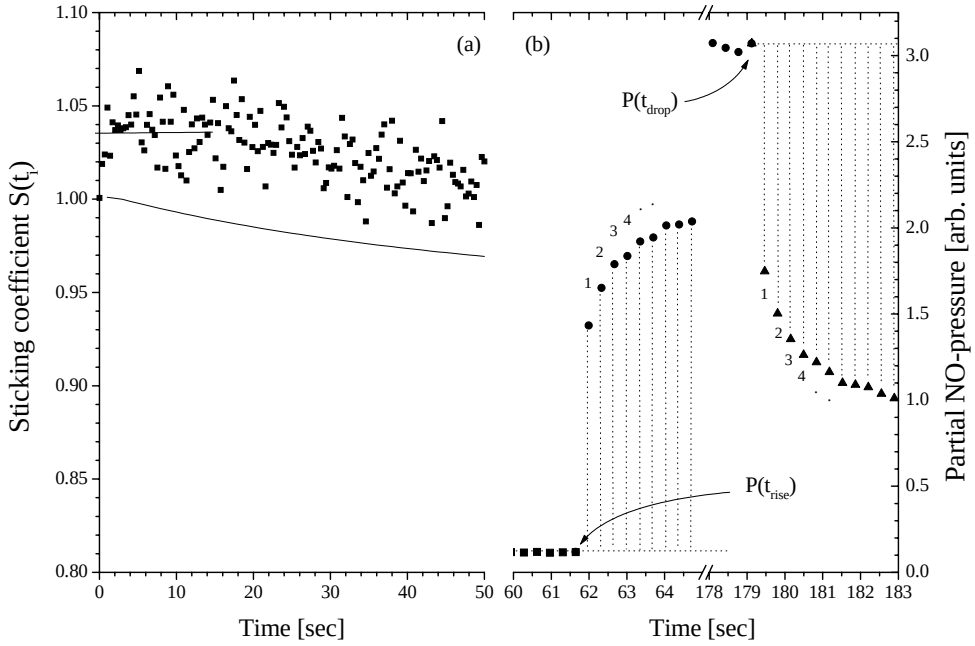

Figure 2.2: *Graphical representation of expressions 2.13 and 2.14: (b) an array of sticking coefficients is constructed by taking the ratio of pressure drop to rise on equal time intervals after t_{rise} and t_{drop}, (a) the ratio of the pressure change is plotted for the test data and the simulated test data. A linear fit through the data is used to obtain the initial sticking coefficient. For the test data the initial sticking coefficient has an error of only 3.5%.*

2.3 Application to the NO/Ru(0001) system

The above described analysis procedure for the beam reflectivity method of King and Wells is applied to the NO/Ru(0001) and NO/Ru(0001)-(1×1)H systems. NO adsorbs on Ru(0001) in a number of different states, depending on the surface temperature (T_s). Below 200 K a strongly bound chemisorbed molecular state is formed [86, 16]. Above 200 K, NO can dissociate into N_{ads} and O_{ads} ad-atoms, given the availability of free sites. Above 450 K, any remaining molecular NO_{ads} desorbs from the surface. The results presented below, in combination with scattering data, will be further elaborated in a forthcoming article [4]. Fig. 2.3 shows the dependence of S_0 on the translational energy (E_i) of NO molecules incident on the Ru(0001) surface. Within the accuracy of our experimental setup, S_0 did not depend on incoming angle (θ_i), or surface temperature (T_s). The absence of any change in S_0 at surface temperatures above and below the molecular desorption temperature is consistent with the same

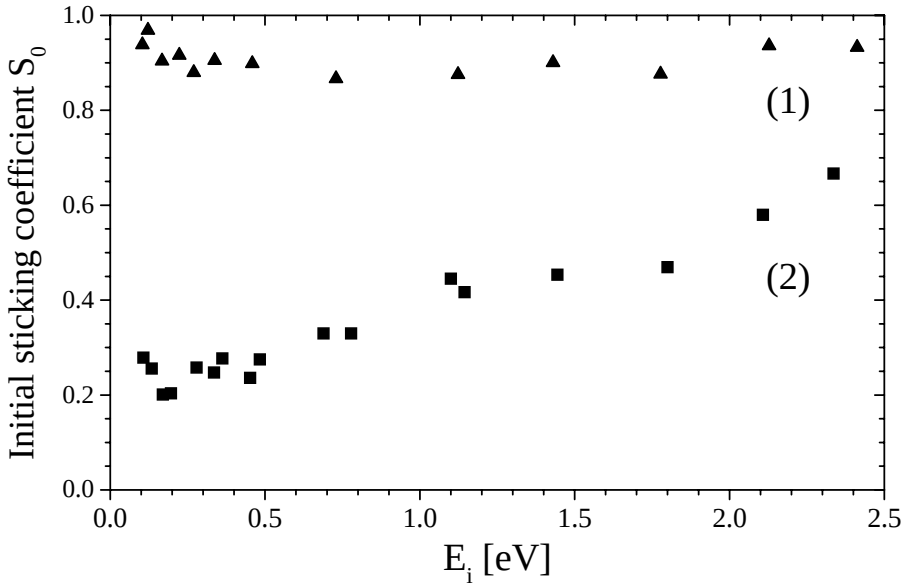

Figure 2.3: *The initial sticking probability for NO molecules on the clean (1) and H-covered Ru(0001) (2). The high and almost constant S_0 on the clean surface can be explained through (at least) two adsorption mechanisms, a non-activated precursor mediated and an activated one, combining to maintain a high sticking probability. The (1×1)H overlayer partially passivates the surface showing the characteristics of an activated channel.*

dynamic processes limiting both molecular and dissociative adsorption. Apparently, dissociative adsorption is mediated through the molecular state, which dissociates efficiently at surface temperatures above 200 K, in agreement with previous studies [86, 16].

S_0 Falls from $\sim$ 100% (E_i= 0.07 eV) to 90% at E_i= 0.3 eV and then remains constant for energies up to E_i= 2.3 eV. This is remarkable, since the probability of trapping into a non-activated chemisorbed state would drop rapidly for incidence energies exceeding the depth of the binding well [39], while the presence of an activation barrier would lead to a sticking probability which increased with energy. The binding energy of NO on Ru(0001) is known to be $\sim$1.5 eV [86, 16]. For a particle with a total energy of particle (translational energy plus 1.5 eV due to the attractive potential) to lose more than 2.3 eV in a binary collision, the effective mass of the surface atom should be unphysically low (<18amu). It does not seem possible that a simple trapping mechanism, involving non-attractive chemisorption alone could yield near unity sticking coefficients at incidence energies as high as 2.3 eV. An almost constant initial sticking probability over such a wide energy range can only be explained

through the simultaneous occurrence of (at least) two adsorption mechanisms, a non-activated precursor mediated and an activated one, combining to maintain a high sticking probability.

Fig. 2.3 also shows the sticking probability of NO on the hydrogen covered Ru(0001) surface. S_0 is greatly reduced [10] but increases with E_i, from 20% at to 60% at 2.3 eV, suggesting an activated process. If the molecular adsorption dynamics involve both a non-activated, trapping mediated channel, and an activated, direct adsorption channel, it is possible that the effect of the hydrogen atoms is to block the non-activated channel, reducing the sticking probability at low energies and revealing the activated nature of the channel at higher energies.

2.4 Conclusion

In conclusion, we have demonstrated that the method of King and Wells can yield reliable values for sticking coefficients of reactive molecules that also exhibit a clear residence time on the walls of the vacuum system. We have observed, that the sticking coefficient for NO on Ru(0001) is close to unity for a remarkable long interval of incidence energies. We attribute this to the presence of two channels for chemisorption. In the case of H-adsorption on the crystal, one of the channels is significantly modified.

Chapter 3

Ar/Ru(0001) experiments compared to Washboard model and trajectory simulations

The scattering of Ar atoms on a Ru(0001) surface has been studied by applying supersonic molecular beam techniques. Variation of the incidence energy (E_i) results in a rich variety of angular and energy distributions. At a low energy clear zero-order diffraction has been identified. Higher energies ($\geq$1 eV) result in unconventional energy distributions. Generally these distributions can be intuitively interpreted by combining binary collisions for sub-specular scattering with hard cube super-specular scattering. The ($\geq$1 eV) argon scattering of Ru(0001) however, seems to be dominated by a totally different mechanism, which are almost quantitatively reproduced by the washboard model, developed by Tully [85]. This is surprising since his comparison of the washboard model to a reference of classical trajectory calculations for the Ar/Pt(111) system showed essential deviations. Our attempt to reproduce the experimental Ar/Ru(0001) data by similar simulations were unsuccessful, most likely due to shortcomings in the description of the solid state.

3.1 Introduction

Scattering atoms from surfaces with the help of molecular beam techniques has been successfully applied to study the fundamentals of gas-surface interaction. Though a lot has been achieved over the last decades, still simple systems with noble gases scattering from crystalline metallic surfaces are non-trivial to analyze. (Semi-) Classical trajectory calculations have proven to yield substantial insight but are obviously limited due to simplifications of the (pair) potentials as well as the large number of surface atoms necessary to generate a realistic phonon bath [40, 91]. Even if the simulation reproduces the data set, full understanding of the essential mechanisms is not directly obtained. Furthermore the quantized phonon excitation can have big influences on the character of the interaction. The diffraction of for instance Argon on W(100)-2H, observed by Schweizer *et al.* [71, 72], has been found to occur without phonon excitation. A wide variety of scattering effects has been explained by them in terms of classical and quantum models. We report a similar zero order diffraction peak for the scattering of thermal argon from Ru(0001) surface.

Basic models are desirable to feed intuition on basic trends in gas-surface interaction. A combination of the simplest models, the *binary collision model* for sub-specular and *hard cube model* for super-specular deflection angles often suffices for qualitative analysis. The *washboard model*, the simplest corrugated extension to the flat hard cube model, developed by Tully [85], serves as a useful tool to elucidate trends the scattering from corrugated surfaces. As shown in Fig. 3.1, a ripple is introduced to allow off-normal momentum transfer to the surface. This simple addition permits (double) rainbow structures to emerge in the angular distributions. When applying the washboard model to argon scattering from various crystal faces of platinum, almost quantitative agreements with stochastic trajectory calculations were reported by Tully. Only the smooth (111) surface gave rise to some remarkable deviations in the velocity distribution. Tully attributed this malfunction to an overestimated corrugation parameter α_m.

In this paper we present angular and velocity distributions of Argon scattered from Ru(0001) for a range of beam energies, surface temperatures and incoming angles. Energy distributions determined for relatively high incidence energies ($\geq$2 eV) show exactly those washboard features that Tully found to be doubtful for the (111) face of platinum. Two solutions seem possible: either the Ru(0001) surface possess a larger surface corrugation than Pt(111), or Tully's trajectory calculations do not accurately represent the real system. The seconds option should be considered since our similar trajectory calculations on the Ar/Ru(0001) system failed to reproduce the experimental data. Especially the competition between energy transfer to the surface through (binary) collisions and energy uptake from the warm surface from phonons seems subtle.

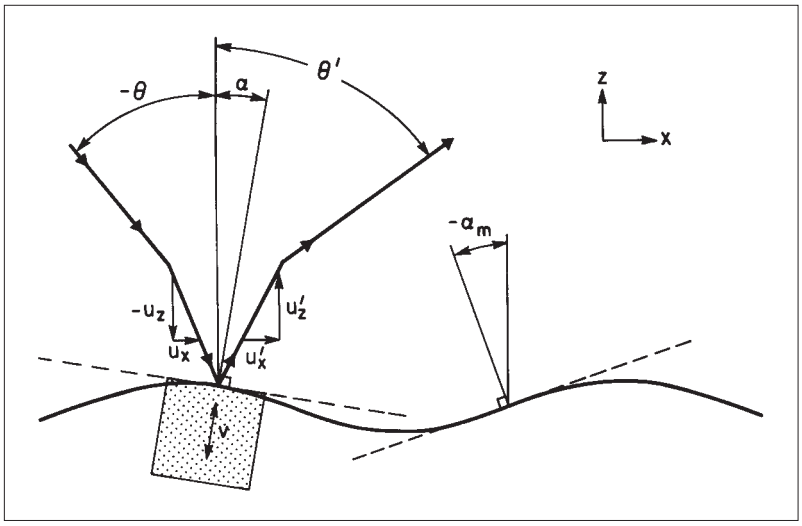

Figure 3.1: *From Tully* et al. *[85]. A ripple with maximum angle α_m is introduced as a modification to the hard cube model, allowing of-normal momentum transfer to the surface.*

3.2 Scattering experiments

3.2.1 Experimental setup

The experiments were carried out in a UHV scattering chamber described in detail in a number of earlier studies [58]. It consists of a main chamber with a base pressure of $1 \cdot 10^{-10}$ mbar, which contains the sample, mounted on a 3-axis goniometer [59] enabling the study of azimuthal dependencies. To this chamber is attached a three stage supersonic molecular beam source with an 80 mm alumina (Al_2O_3) nozzle. A rotating disk chopper, positioned in the second stage, provides pulses of 0.5 to 50% duty cycle duration at up to 500 Hz. The translational energy of the NO was varied between 0.1 and 2.5 eV by changing the seeding ratio of NO in either H_2 or He and heating the nozzle. This was done by electron bombardment (500 V) of a tungsten tube around the nozzle. For the H_2-seeded beam the nozzle temperature is restricted to ∼1300 K, since higher temperature will allow the H_2 to reduce the Al_2O_3 nozzle.

Beam energies were determined by measuring the time-of-flight (TOF) of a short pulse (10 ms) of gas from the chopper to a differentially pumped rotatable quadrupole mass spectrometer (QMS) in the scattering chamber. The final energy of scattered molecules was obtained by deconvolution of their TOF signals with the direct beam profiles as described elsewhere [55]. Angular resolved scattered beam intensities were measured using a 50:50 modulated beam and fitting the output of the multi channel

scaler (MCS) with a modified square wave function in order to directly obtain the background corrected signal (S_{ignl}): $MCS_i = B_{ackgr} + (S_{ignl} - B_{ackgr})/(e^{[(\Delta - i)/\tau]} \cdot e^{-[(\Delta + T_{open} - i)/\tau]})$, with T_{open} the open time of the chopper. The quadrupole mass spectrometer used for these measurements (Extranuclear Labs.) is mounted on a doubly differentially pumped rotatable cover in order to provide angular resolution.

The Ru sample was aligned and polished to within 0.1^o of the (0001) crystal face. It could be heated by electron bombardment (600 V, 80 mA) at up to 25 Ks^{-1}, regulated by a programmable controller (Eurotherm 900 EPC) and cooled to ~100 K with liquid nitrogen. The sample temperature was measured with a type C thermocouple. This was calibrated against a type K thermocouple for temperatures below 273 K. Cleaning was performed in situ by repeated cycles of flashing in a background pressure of oxygen ($2 \cdot 10^{-8}$ mbar) to 1500 K. An oxygen free surface could be obtained by a single flash to 1600 K in UHV. Helium thermal energy atom scattering (TEAS) was found to be an extremely sensitive probe of the surface cleanliness and order. This proved to be particularly useful because the main contaminant (C) is difficult to detect in small concentrations by Auger electron spectroscopy (AES) due to overlap with the Ruthenium peaks [20, 61]. Low energy electron diffraction is available for calibration of the azimuthal orientation of the crystal surface.

3.2.2 Angular distributions

Depending on incidence energy and surface temperature the angular distributions of argon scattered from the (0001)-face of ruthenium show scattering phenomena qualitatively similar to those observed for the Ar/W(100)-2H system by Schweizer *et al.* [72]. For the 140 K Ru surface, scattering the lowest energy beam (80 meV) revealed a diffraction peak positioned on top of a broad background of collision events in which phonons are excited (see Fig. 3.2 and also Fig. 6.4). For this energy, the higher order diffraction peaks are expected at $\theta_{spec} \pm n \cdot 1.6^o$ (n = 1, 2, 3, ...). This separation is smaller than the experimental resolution of $\simeq 2^o$ but might explain the repeatedly observed shoulders around the zero-order diffraction peak (inset of Fig. 6.4). A liquid nitrogen cooled nozzle, as used by Schweizer *et al.* [72] will produce a slower Ar beam with a sharper velocity distribution which will result in more pronounced diffraction peaks with larger angular separation. Upon increasing the beam energy the diffraction peak disappears. The broad background sharpens from a FWHM of about 22^o at 0.08 eV to 15^o at E_i= 0.56 eV. At this energy the experienced surface corrugation at this surface temperature causes a double rainbow structure to develop which is absent for the comparable T_s= 550 K data of Fig. 3.3. of which the origin will become clear in section 3.3. At even higher energies, 1.40 eV, a single peak with a FWHM of 8.5^o is formed. Note the super specular shift of the distributions with for harder collisions, indicative of an increasing amount of normal momentum being transferred to the surface.

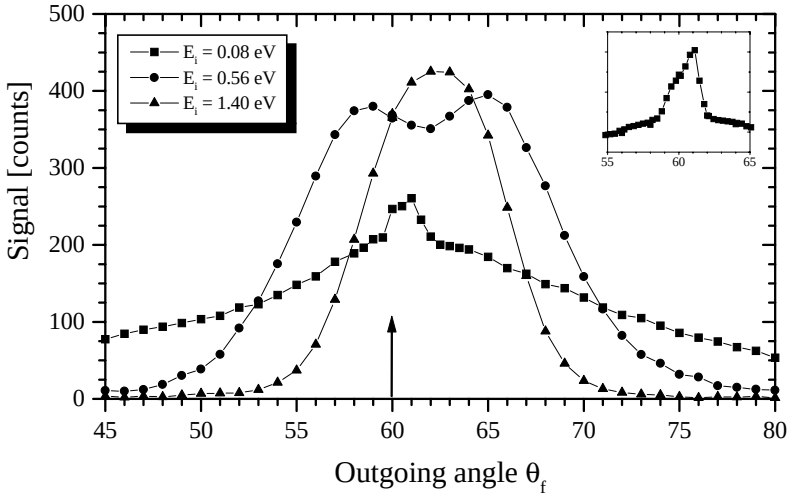

Figure 3.2: *Argon reflectivity of the 140 K Ru(0001) surface at $\theta_i = 60^o$: $E_i = 0.08$ eV (squares) shows a zero-order diffraction peak, $E_i = 0.56$ eV (bullets) shows a rainbow like double structure and $E_i = 1.40$ eV (up triangles) shows a single peak. The vertical arrow indicates the specular scattering direction ($\theta_f = \theta_i$). The inset shows a zoom in on the specular diffraction region.*

3.2.3 Time of flight distributions

The most surprising part of the data set consists of the final energy distributions obtained by Time Of Flight (TOF) measurements of argon scattered from the Ru(0001) surface. The energy distribution (Fig. 3.3) shows a peculiar pattern for the highest incoming energy of 1.56 eV. A remarkable transition in scattering mechanisms is clearly observed for energies in the range $0.44 \leq E_i \leq 1.56$ eV. The lower incidence energy results in an energy distribution which can qualitatively be understood by combining the binary collision model for the sub-specular ($\theta_f < \theta_i$) scattering and the parallel momentum conservation for super-specular scattering ($\theta_f > \theta_i$). Upon increasing the beam energy this simple trend no longer holds and other mechanisms seem to dominate energy transfer and uptake.

Sub-specularly ($\theta_f = 35^o$), nearly elastic collisions are observed for both the lowest and the highest energy, while the intermediate shows substantial energy loss. The broadness of thermal Ar TOF spectra caused severe problems with the analysis for low energies, and only spectra for $E_i \geq 0.2$ eV could be deconvoluted. The raw TOF data presented in Fig. 3.4 however clearly illustrates momentum gain of the Ar atoms from *hot* surface phonons. The bending down for the sub-specular scattering for the intermediate energy ($E_i = 1.05$ eV) is probably due to relatively hard collisions with a turning point closer to the surface. This allows more momentum transfer

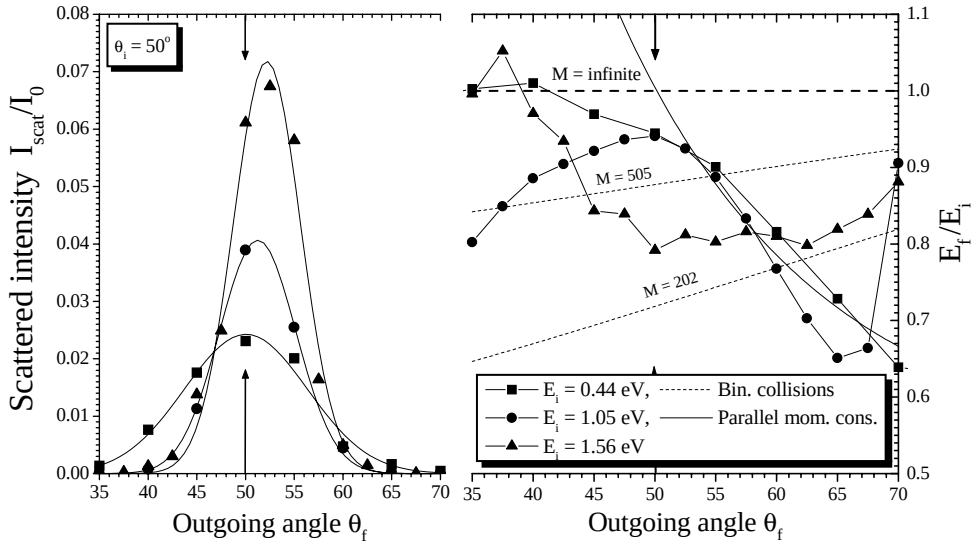

Figure 3.3: *Argon scattering form the T_s= 550 K Ru(0001) surface, θ_i= 50°, for three different incident energies E_i= 0.44, 1.05 and 1.56 eV. The solid lines (left panel) are drawn to guide the eye only. Dashed lines in the right panel represent the energy losses for binary collisions of Ar (m = 40 amu) from various masses (M = 202, 505 and infinite). The solid line holds for parallel momentum conservation. While the angular distributions narrow and shift super specular with increasing E_i, the energy distributions develop features which no longer resemble the binary collision or hard cube model.*

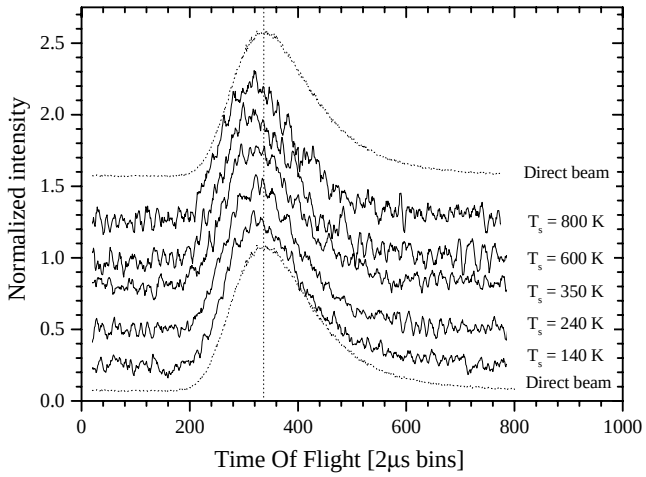

Figure 3.4: *Raw TOF data showing the shorter flight time for low energy (≈0.08 eV) Argon scattered of Ru(0001) surface (θ_i= 40°, θ_f= 20°) at different temperatures (T_s).*

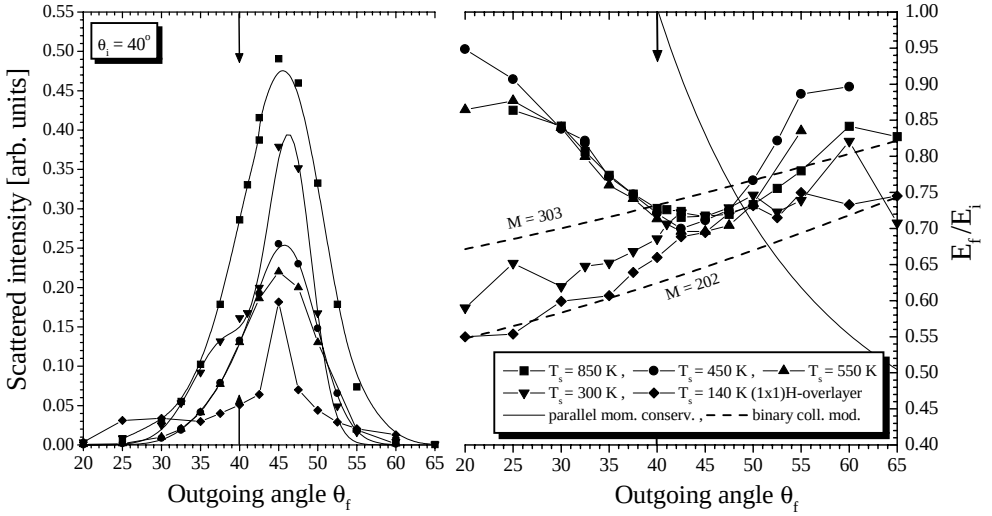

Figure 3.5: *Argon reflectivity of the Ru(0001) surface, θ_i= 40°, E_i= 2.2 eV for different surface temperatures (T_s). Vertical arrows indicate the specular scattering direction ($\theta_i = \theta_f$).*

to individual atoms instead of a heavier surface cluster, as is the case for softer super-specular scattering where generally the momentum transfer only takes place in the direction normal to the surface while leaving the parallel component conserved. These are common trends, but apparently do not hold for the higher energy particles of the 1.56 eV curve, where effective energy uptake from surface phonons seems to compensate for the expected momentum transfer. The super specular scattering again shows remarkable deviations, while the low and intermediate energy curves follow the parallel momentum conservation curve nicely.

When considering the coupling to phonons, the interaction time could be the crucial parameter. The influence of surface temperature at high energies is shown in Fig. 3.5. Surprisingly the lowest temperature curves T_s= 140 K (H-covered surface) and 300 K follow the binary collision trend fairly well over the entire angular region. The resemblance of these two curves might be due to partial hydrogen coverage at T_s= 300 K from the H_2/Ar mixed beam. Above the hydrogen desorption temperature, the T_s= 450, 550 and 850 K curves appear within the expected error bars.

3.3 Comparison to the Washboard model

As mentioned in the introduction the washboard model is a simple extension of the hard cube model which allows off-normal momentum transfer. Diffraction will not

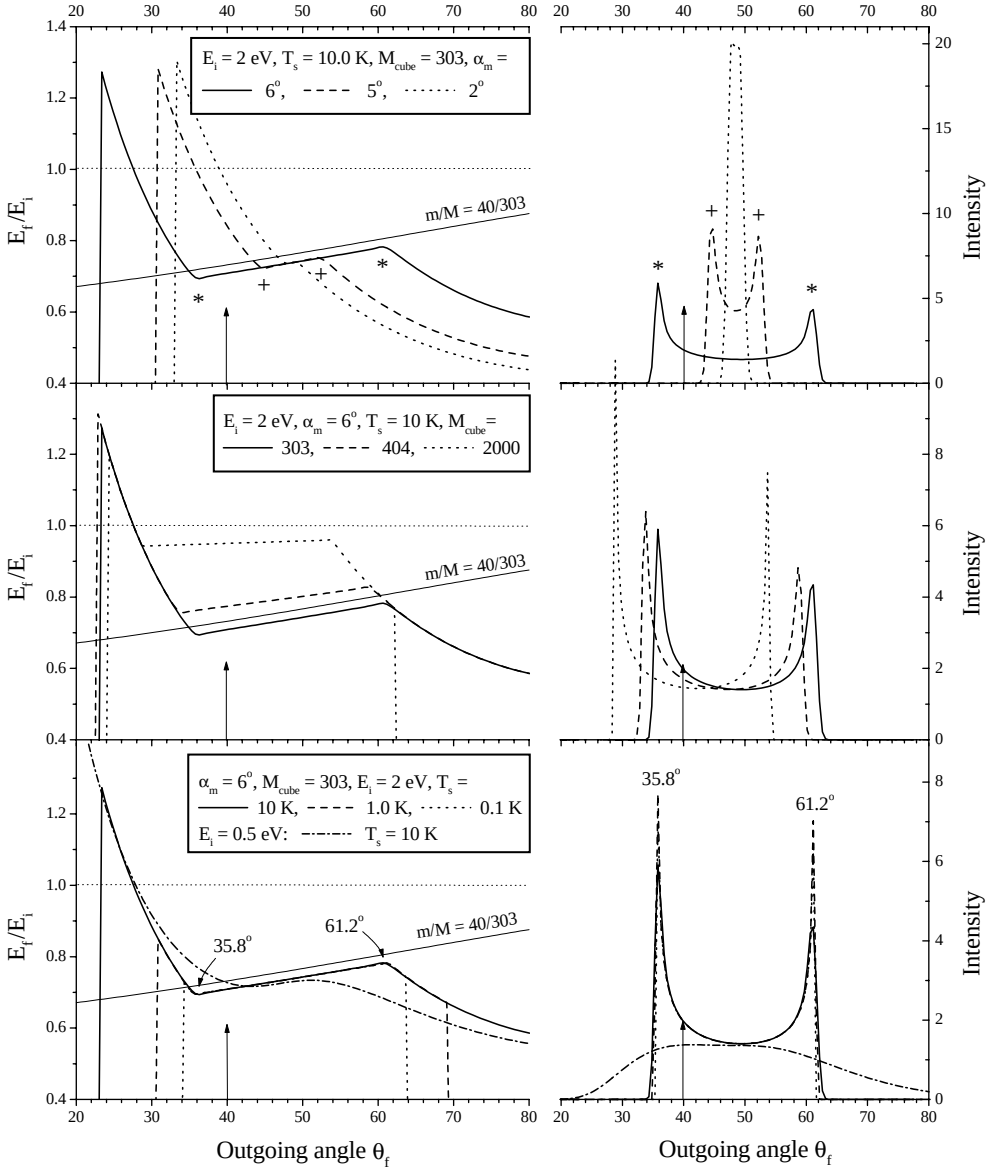

Figure 3.6: *Variation of three input parameters of the washboard model, developed by Tully [85]: the maximum angle in the washboard ripple α_m (top panel), the cube mass M_{cube} (middle panel) and the surface temperature T_s (bottom panel). The increased effect of surface temperature on lower energy scattering is also shown in this panel (E_i= 0.5 eV, T_s= 10 K). Fixed parameters are the well depth (W = 0.1 eV) and the incoming angle (θ_i= 40°).*

be observed since quantized energy transfer to surface phonons is not included. The appearance of the double peak structure in the 0.56 eV curve of Fig. 3.2 however can clearly be understood by the introduction of a surface corrugation, as can be observed in the top-right panel of Fig. 3.6. When focusing on the energy distribution measured for the highest beam energy (2.32 eV) presented in Fig. 3.7, quite surprising, almost quantitative correspondence of the washboard model to the experimental data is achieved, with very reasonable input parameters ($\alpha_m = 6^o$ and $m_{Ar}/M_{cube} = 40/303$). This agreement does however not accompanied by optimum correspondence in the angular distribution. We choose however to focus on the qualitative analysis of the unconventional energy distribution.

Fig. 3.6 shows the response of the output of the washboard model upon variation of the essential input parameters. In the specular region E_f/E_i follows the binary collision curve. Scattering to outgoing angles beyond the sub- and super specular rainbow maxima ($\theta_{f,sub} = 35.8^o$ and $\theta_{f,sup} = 61.2^o$) is prohibited for the 0 K surface. Only specific *thermal* fluctuations of the washboard can result in these scattering angles (bottom row Fig. 3.6). Outgoing angles of $\theta_f < \theta_{f,sub}$ can be achieved by scattering of a maximum backwards tilted rising cube. Similarly $\theta_f > \theta_{f,sup}$ is possible when scattering of a maximum forward tilted dropping cube. The subsequent energy gain or loss with respect to the binary collision result is clearly reflected in the left column of Fig. 3.6. For sub-specular angles the final energy is determined by competing mechanisms. The balance between energy uptake from the surface phonons vs. the transfer of momentum to the surface due to binary collisions is largely determined by the velocity and mass of the surface cube. Furthermore, larger deflection angles, i.e. harder collisions, are generally concomitant with turning points of the trajectories closer to the surface, leading to interaction with less surface atoms simultaneously and thus relatively light cube masses. A dependence of the cube mass on the deflection angle is not invoked in the cube model which therefore overemphasizes influence of the surface vibrations. Moreover, it must be noted that the temperature invoked in the washboard model makes the entire ripple vibrate as a whole. In reality the coupling between the surface atoms will allow thermal vibrations causing the shape of the unit cell to be distorted. Also difference in the Debye temperatures are not included.

3.4 Classical trajectory calculations

3.4.1 Computational

The computational code used to simulate the Ar/Ru(0001) system has been described in great detail elsewhere [40]. In short the classical trajectory calculations consist of solving the classical molecular dynamics by integrating the Newtonian mechanical equations using the Verlet algorithm. The pair potential describing the forces between

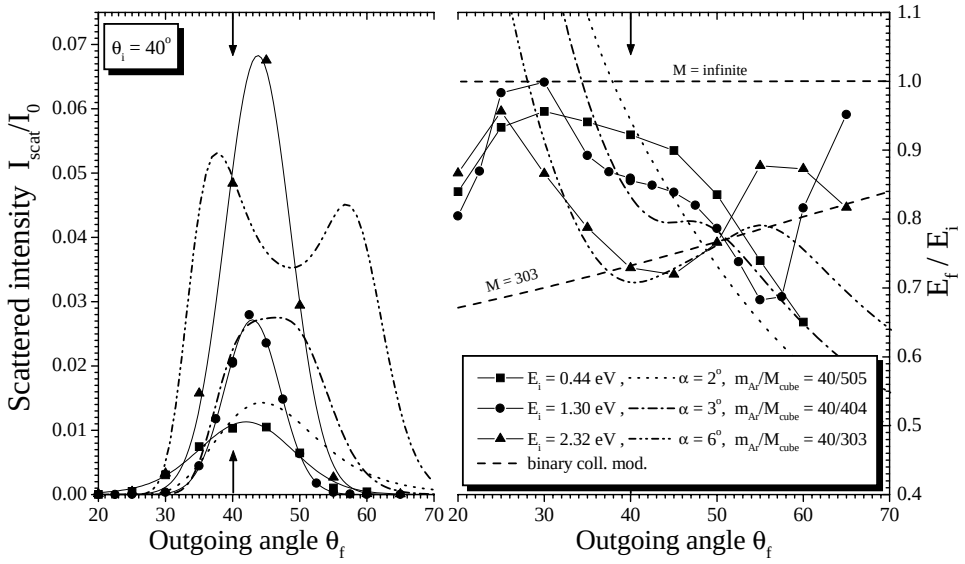

Figure 3.7: *Comparison of the the washboard model to the actual data for three beam energies (at θ_i= 40°, T_s= 550 K). Dashed lines in the right panel represent the energy losses for binary collisions of Ar (m = 40 amu) from various masses (M = 303 and infinite). Vertical arrows indicate the specular scattering direction ($\theta_i = \theta_f$). Optimum agreement is achieved for the highest beam energy of 2.32 eV. Lower incidence energies result in large deviations in the specular region of the angular distributions.*

the nearest neighbors in the solid is of the following form:

$$V(r) = \frac{1}{2}k_1(r-d)^2 + \frac{1}{3}k_2(r-d)^3 + \frac{1}{4}k_3(r-d)^4 \tag{3.1}$$

$$k_1 = \frac{3}{8}M(k_B\Theta/\hbar)^2, \quad k_2 = \frac{21}{2d}k_1, \quad k_3 = \frac{371}{6d^2}k_1 \tag{3.2}$$

With the anharmonic force constants k_2 and k_3 determined from a Tailor expansion of a Lennard-Jones potential. The surface Debye temperature is accounted for by an additional set of force constants for all atoms connected to a surface atom according to the same equations 3.1 and 3.2. A finite surface temperature is introduced by initially imposing a Maxwell-Boltzmann velocity distribution on the crystal atoms in their equilibrium position. With evolving time half of the kinetic energy is transferred to potential energy. The potential of the gas-solid interaction is a combined repulsive Born-Mayer pair potential and an attractive van der Waals like z-dependent

interaction:

$$V_{tot}(\mathbf{R}) = \sum_{i\epsilon\{C\}} Ae^{-\alpha(|\mathbf{R}|)} - \sum_{i\epsilon\{S\}} B(Z_i - z_0)e^{-\gamma|Z_i|^4} \cdot \frac{e^{-\sigma(X_i^2+Y_i^2)}}{\sum_{k\epsilon\{S\}} e^{-\sigma(X_k^2+Y_k^2)}} \quad (3.3)$$

$$\mathbf{R_i} = (X_i, Y_i, Z_i) = \mathbf{R} - r_i \quad (3.4)$$

With $\mathbf{R}$, the position of the Ar atom and r_i the position of each i-th crystal atom, $\{C\}$ and $\{S\}$ denote the ensemble of crystal and surface atoms, respectively.

In fitting the potential energy data, as calculated by standard LDA-techniques, to the from of Eq. 3.3, emphasis has been put on the agreement for the a-top position. The resulting parameters are: $A = 120664$ eV, $\alpha = 5.8063$ Å^{-1}, $B = 2.520$ eVÅ^{-1}, $z_0 = 2.514$ Å and $\gamma = 0.0304$ Å^{-4}. The range of the attractive potential set to be about 10 surface atoms ($\sigma = 0.149$ Å^{-2}).

3.4.2 Simulation results

Running classical trajectory calculations for the best known set of input parameters (see Table 3.1) did not result in quantitative correspondence with the experimental data. As can be seen in (the up-triangle curve of) Fig. 3.8, even qualitative washboard like similarities are mostly absent. In order to gain insight in the mechanisms responsible for the malfunctioning of the simulation code, various input parameters have been tested. A more accurately calculated pair potential of the Ar/Ru pair potential seemed to have minor influence on the results. The increase of the bulk and surface Debye temperatures of ruthenium (415 K and 216 K respectively) turned out more effective. As shown in Fig. 3.8, a trend similar to the washboard model develops when increasing both the Debye temperatures of the crystal with a factors of 1.5 - 2.0. The increased lattice *stiffness* invoked by the stronger links between the crystal atoms increases the effective surface mass, explaining the reduced average energy transfer in the collisions. Furthermore, double rainbow structures appear in the angular distributions due to the lesser thermal disordering of the crystal. This trend can also be observed when comparing of the scattering data on the T_s= 140 K and 550 K surfaces shown in Figs. 3.2 and 3.3.

A significantly better correspondence to the data is obtained when limiting the impact parameters to a string over the atop sites, as shown in Fig. 3.9. In this way the scattering is mostly in plane, excluding *chattering* between rows of surface atoms. This especially affects the behaviour in the specular region. The overlapping curves in the wings indicate the extremer sub- and super-specular angular regions to be hardly reached by particles with impact parameters lying outside the atop string.

3.5 Discussion

Highest incoming energies yield the most surprising result: the washboard model reproduces the peculiar experimentally obtained energy distributions, while both Tully's

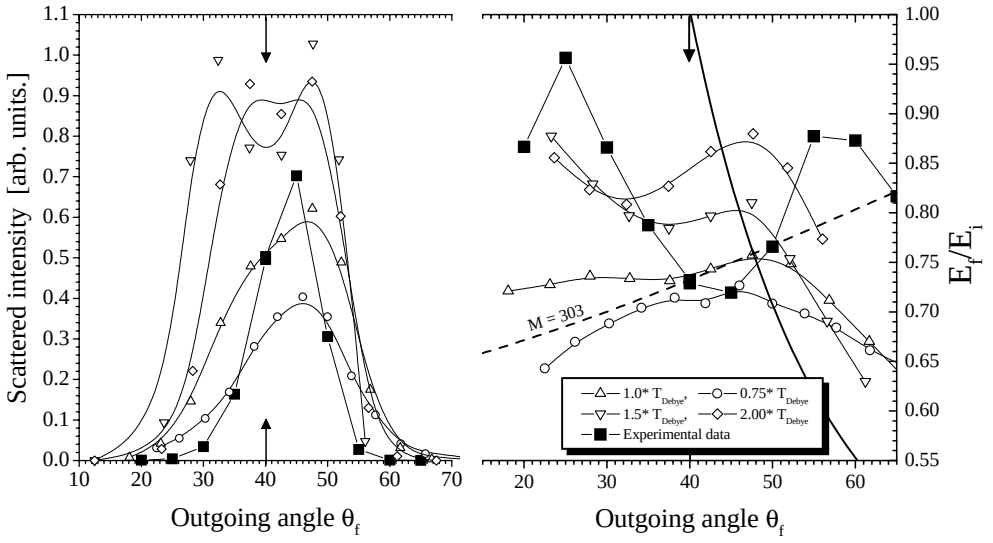

Figure 3.8: *The output of the classical trajectory calculations using the TACO-code for four different sets of bulk and surface Debye temperatures (0.75, 1.0, 1.5 and 2.0 times the default Debye temperatures* Θ_{bulk}*= 415 K and* Θ_{surf}*= 216 K), for a fixed surface temperature of* T_s*= 550 K, compared to the experimental data (*θ_i*= 40° and* E_i*= 2.32 eV).*

trajectory calculations for the Ar/Pt(111) as well as ours for the Ar/Ru(0001) system failed to do so. Comparison of the experimental data, washboard model and classical trajectory calculations raises several questions. Could the washboard model, despite the simplicity, contain all the essential physics on energy transfer processes, or is the agreement more a coincidence? Though Tully showed the washboard model to work surprisingly well (almost quantitatively) for various corrugated faces of platinum, the model is meant to elucidate simple trends in gas-surface scattering only. When comparing the washboard model to the calculations for relatively smooth Pt(111) system, Tully observed effects in the energy distribution that did not seem to have any physical meaning [85] (similar to Fig. 3.7). Much to our surprise, the Ar/Ru(0001) measurements show exactly those unexpected *washboard* features that seemed erroneous for the Ar/Pt(111) system.

Direct comparison of the trajectory calculations to the washboard is facilitated by limiting the impact parameters to the a-top string; thus performing pseudo 2-dimensional calculations. A sinusoidal approximation of the washboard ripple seems valid in this situation. The results, depicted in Fig. 3.9, clearly show different trends in the specular region for the 2 and 3-dimensional simulations, probably caused by a substantial amount of multiple collisions and scattering from the heavy hollow

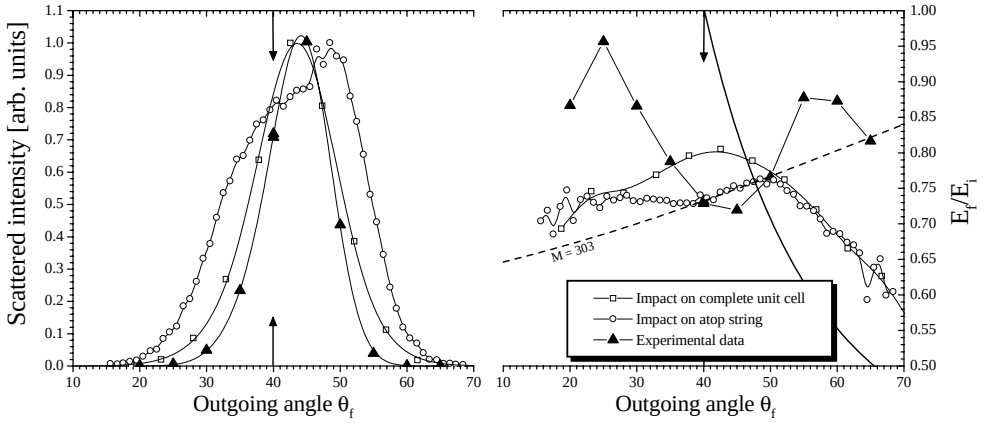

Figure 3.9: *The effect of limiting the impact to the atop string vs. the entire unit cell for E_i= 2.32 eV scattering at θ_i= 40° and T_s = 550 K. Clearly the string impacts resemble the washboard results in the specular region (see Fig. 3.6 and 3.7), contrary to scattering from the whole unit cell.*

sites. Surface phonons are treated fundamentally different by the Washboard model and TACO. The washboard oscillates as a whole maintaining the sinusoidal shape, whereas the more realistic trajectory calculations include thermal distortion of the lattice. Furthermore, the Debye temperature is not accounted for in the washboard model; a conventional Maxwellian distribution of vibration frequencies and amplitudes is assumed. Other possible sources of discrepancies are the *hard* collisions and the constant cube mass for all scattering angles (Section 3.3). Especially for the larger scattering angles (sub-specular scattering) the closer approach of the surface causes the argon atom to interact with less surface atoms simultaneously, i.e. a lower cube mass. Note that extending the washboard model for such details could improve quantitative agreement with experiments but at the expense of the accessibility for intuition. Deducing the crucial problem in the simulation method could lead us to the difference between the Ar/Ru(0001) and Ar/Pt(111) systems. The observed effective *tuning* of the Debye temperature suggests the main reason of our trajectory simulations failing to reproduce the experiment lies in the implementation of the interactions in the solid state. The oscillation amplitude and frequency of (real) surface atoms is likely to result in a interaction time dependent coupling to the surface phonons. In this way changes in the incidence energy will affect the balance between energy loss or uptake.

This opens the question why Ru(0001) scatters argon in a qualitatively different way than Pt(111), behaving so much like a washboard. In order to facilitate comparison, the most important parameters describing the two crystals are presented in Table 3.1. Both the atomic masses and the Debye temperature's differ a factor of

Parameter	Ru(0001)	Ref.	Pt(111)	Ref.
Mass [amu]	101		195	
Lattice structure	HCP		FCC	
Nearest neighbor distance [Å]	2.669	[25]	2.77	[40]
Bulk Debye temperature [K]	415	[25]	230	[40]
Surface Debye temperature [K]	216	[25]	110	[40]
Argon physisorption well [meV]	62	[25]	78	[24]

Table 3.1: *Comparison of the main parameters describing the interaction between argon and the Ru(0001) and Pt(111) crystal faces.*

two. Our trajectory calculations showed the effect of the Debye temperatures on the energy distributions (Fig. 3.8) which could account for the difference in the observed sub-specular energy distributions.

3.6 Conclusions

As simple as scattering of a noble gas atom from a single crystalline surface might seem, we observe multiple competing scattering mechanisms for Ar/Ru(0001). Zero-order diffraction at the lowest incidence energy, rainbow scattering at intermediate and washboard like energy transfers for the highest reachable energy. Especially these peculiar energy distributions, qualitatively different from Ar/Pt(111)-system, are nicely reproduced by the washboard model. While not too much significance should be attached to quantitative aspect of the output, this simple model does prove to be a powerful tool in the straightforward analysis of the competing mechanisms behind energy exchange of gases and surfaces.

Comparison of pseudo 2-dimensional and full 3-d classical trajectory simulations show the 1-d washboard ripple to be clearly insufficient to describe the Ru(0001) surface corrugation. Satisfactory correspondence to the experimentally determined energy distributions was however not obtained, most likely due to shortcomings in the representation of the phonon bath in our simulation code (TACO).

Chapter 4

A molecular beam study of the scattering and chemisorption dynamics of N_2 on Ru(0001)

The chemisorption of N_2 on Ru0001 has been studied with supersonic molecular beams in the translational energy regime from 0.1 to 1.8 eV. No sticking with a probability of more than 10^{-4} has been observed. Angular flux distributions and variations in the kinetic energy of the scattered molecules provide evidence for the existence of different scattering regimes. The scattering behavior is explained in terms of scattering from a dual repulsive wall, which is attributed to the existence of a metastable molecular precursor state to nitrogen dissociation, thus providing indirect proof for recent theoretical predictions for this system.

4.1 Introduction

The dissociative chemisorption of nitrogen has been well established as the rate limiting step of ammonia synthesis over iron based catalysts [15]. While promoted iron is still the current catalyst of choice, ruthenium has received considerable attention in the past years, as probably the only alternative to replace it [83]. Alkali promoted Ru catalysts were reported to exhibit enhanced activities at elevated temperatures and pressures [83, 52]. The exact mechanism for N_2 dissociation on Ru is still unknown and it should have similarities and differences with that of the reaction on the iron surface, which would determine its efficiency as an ammonia synthesis catalyst. A clear understanding of the interaction of nitrogen with Ru may lead to an improvement of these catalysts.

In a theoretical study Nørskov and coworkers have performed a series of density functional calculations of the minimum energy reaction path for dissociation of N_2 on the Ru(0001) surface [49, 48]. The calculations presented, showed that dissociation is highly activated, the minimum barrier being 1.36 eV. They predicted the existence of a new metastable molecular precursor state to dissociation, where the molecule is rotated from its stable molecularly chemisorbed state, with the N_2 bond oriented perpendicular to the surface, to a down lying position, which eventually leads to dissociation into two adjacent hollow sites of the hexagonal closed packed (hcp) surface. A barrier of 0.5 eV was calculated for rotating the molecule into this state. In a more recent density functional calculation, with the N_2 molecule oriented parallel to the surface, Murphy *et al.* suggested the presence of a metastable molecular state with an energy of $\sim$0.5 eV above that of the free N_2 [50]. A sizable activation barrier to dissociation is in agreement with the small sticking coefficients observed for this system [50, 47, 77, 11, 69, 13].

Angle and energy resolved measurements of the directly scattered molecules provide an important informative probe of the gas surface interaction dynamics, especially for a system like the one currently studied where the error in the evaluation of the sticking probabilities for dissociation is large due to its small value. In the present study scattering experiments were carried out to probe the repulsive part in the nitrogen-ruthenium interaction potential. Evidence is provided for the existence of two different scattering regimes, with the results being explained in terms of a dual repulsive wall present in the interaction potential.

4.2 Experimental

The experiments were carried out in a molecular beam apparatus described elsewhere [79]. It consists of a three stage differentially pumped molecular beam line connected to an ultra high vacuum (UHV) chamber equipped with low energy electron diffraction (LEED), ion sputter gun and a residual gas analyzer for monitoring the background gas. A differentially pumped quadrupole mass spectrometer (QMS), which can be ro-

tated in a horizontal plane around the sample, is used to detect the particles scattered from the surface.

The sample is mounted on a three-axis goniometer [59]. It allows for incidence parameters, such as the angle of incidence with respect to the surface normal and the azimuthal angle, with respect to a high symmetry direction on the surface to be set under computer control. In conjunction with the rotatable QMS, particles leaving the surface in and out of plane can be measured. The Ru sample used was aligned and polished to within 0.1^o of the (0001) crystal face and cleaned by repeated flashing to a surface temperature of 1500 K in $2{\cdot}10^{-8}$ mbar of oxygen. The remaining oxygen was removed by flashing to 1600 K. The surface quality was found to be excellent as checked by LEED and by the Debye-Waller analysis of the thermal helium reflectivity which extrapolated to $I/I_0 = 1.0$ at 0 K, where I_0 is the incident He beam intensity.

The molecular beam is generated by supersonic expansion of a N_2 (5.0 purity) gas, seeded in either He (4.6 purity) or H_2 (5.0 purity) from an 80 μm alumina nozzle. The energies of the beams were varied from thermal to about 1.8 eV by changing the seeding ratios and/or by heating the nozzle in the 300 - 1100 K temperature range. The translational energies of the beams were derived from the TOF distributions. The spectra were corrected for a trigger time delay and the ion flight time through the QMS and fitted to shifted Maxwell-Boltzmann distributions convoluted over the finite chopper opening time yielding the mean energy per particle in the beam. The TOF experiments were performed with a 0.5% duty cycle chopped beam while, in order to get more flux, 50% duty cycle chopped beams were used for measuring the angular intensity distributions.

4.3 Results and discussion

To get a better insight into the dynamics of the nitrogen surface interaction, flux and energy distributions of the inelastically scattered particles were measured. The measurements were performed in the plane through the incident beam and the surface normal. They were carried out at a surface temperature of 550 K, in order to avoid CO and hydrogen residual gas adsorption. The beam energies ranged from 0.09 to 1.86 eV. There was no nitrogen signal in the Thermal Desorption Spectra after measurements at normal incident energies less than the maximum beam energy used, 1.09 eV. From the exposure time and the sensitivity of the setup an upper limit for the dissociative chemisorption probability of 10^{-4} is estimated. The distributions were perfectly reproducible.

Fig. 4.1 shows angular flux distributions for various incident beam energies displayed for an incident angle of 40^o. The distributions are normalized to the incident beam flux. The lines through the data points act as a guide to the eye. A broad distribution, centered on the specular is observed for a 0.09 eV beam. A steady increase in the maximum of the scattered flux distributions and a decrease in width of the scattered particles are observed with increasing E_i. Above 0.81 eV a broadening

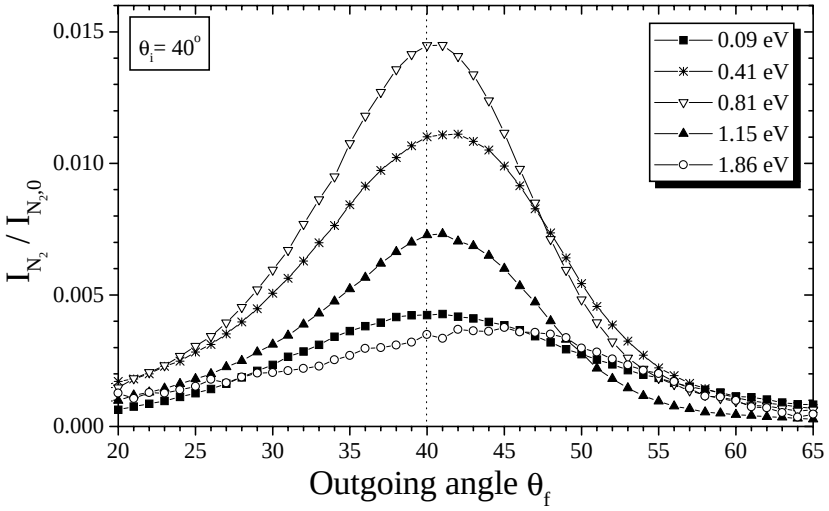

Figure 4.1: *Angular resolved flux distributions of N_2 molecules scattered from Ru(0001) for θ_i= 40^o at T_s= 550 K. The distributions are normalized to incident flux. Lines through the data points are to guide the eye only.*

is observed, with a broad asymmetrical distribution for the highest energy (1.86 eV). The widths of the distributions (FWHM) are displayed in Fig. 4.2 for three different incident angles. A decrease in FWHM with increasing energy is observed which can be rationalized by a decrease of the influence of the velocities of the surface atoms due to the higher incidence velocities of the impinging molecules; a decrease of thermal broadening with increasing E_i [63]. This is corroborated by the sensitivity of the width on surface temperature, with the width increasing from 11.2^o at 130 K to 15.6^o at 550 K for E_i= 0.36 eV.

An abrupt increase in width is observed at 1.1 eV, as seen in Fig. 4.2a, for θ_i= 40^o. There is an increase for θ_i= 50^o, with the onset being at higher E_i, while it is not observed for θ_i= 60^o. This increase in width with increasing E_i is due to an increase in the surface corrugation being probed (structure scattering). The effect is pronounced for θ_i= 40^o since the velocity component normal to the surface is higher, for the same translational energy, than for the other two incident angles. Higher normal energies guarantee more corrugation, due to higher penetration to the underlying structure of the atomic cores. This is seen in Fig. 4.2b where the widths of the distributions are plotted against normal energy. The onset for structure scattering is at ∼0.65 eV. The FWHM values do not saturate at the highest energies indicating that a maximum in the corrugation, as observed by the incident molecules, is not reached.

The existence of two scattering regimes is evident from the results, with thermal scattering dominating at low incident energies and structure scattering at higher

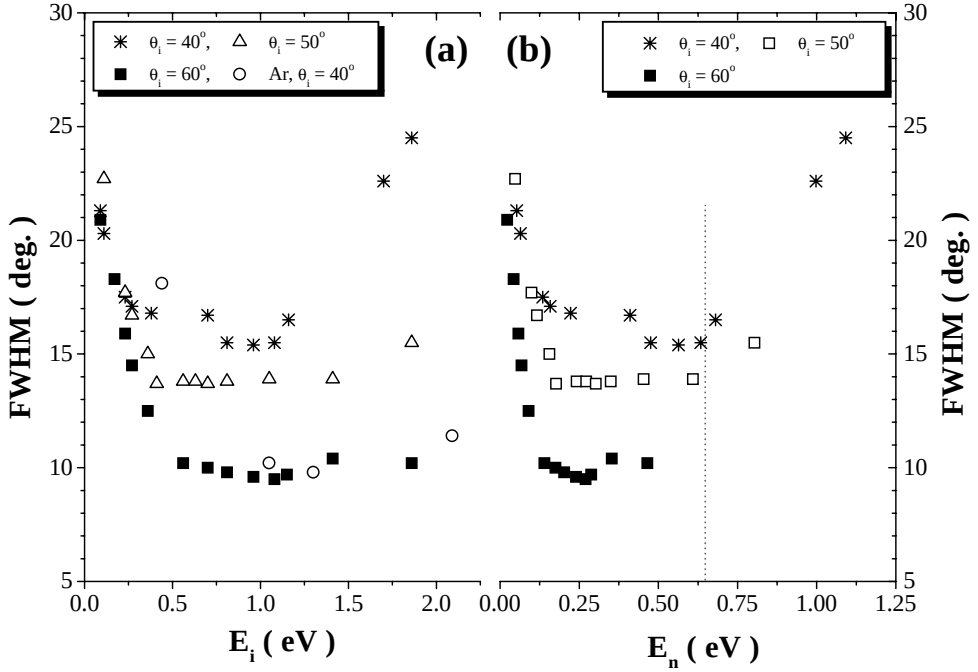

Figure 4.2: *The full widths at half-maxima (FWHM) of the angular flux distributions of N_2 and Ar scattered from Ru(0001) as a function of (a) incident energy E_i for three different incident angles and (b) incident normal energy E_n ($= E_i \cdot \cos^2\theta$, T_s= 550 K).*

energies. The widths of the flux distributions of Ar as a function of E_i are also plotted for comparison in Fig. 4.2a, for $\theta_i = 40^o$. It is obvious that the scattering dynamics are different. Similar to nitrogen, a decrease of thermal broadening with increasing E_i is observed for Ar, but the distribution broadens only slightly at 2.09 eV, indicating a smaller degree of corrugation being probed. Argon exhibits the dynamics of a physisorption system with a rather shallow well and a repulsive wall relatively far out of the surface [6] (Chapter 3).

A better understanding of the nitrogen ruthenium interaction is given by examining the energy transfer mechanism of the inelastically scattered molecules. The angular resolved ratios of the mean final translational energy of the scattered particles, as derived from the TOF distributions, over the mean incidence energy, denoted as E_f/E_i, are plotted in Fig.s 4.3a and 4.3b for $\theta_i = 50^o$ and 40^o. The lines connecting the data points act as a guide to the eye only. The solid lines (marked $p_{//}$ cons.) hold for a situation, in which the parallel momentum of the scattered molecules is conserved, while the dashed lines hold for binary collisions of hard spheres

with different masses as indicated in the graph. Both of these models express limiting cases for gas surface scattering. Looking at the results for 50^o incidence angle, one can see that for E_i= 0.38 eV, the velocity distributions essentially follow parallel momentum conservation for super-specular angles (closer to the surface than specular). In this model the momentum parallel to the surface is conserved with deviations from specular scattering resulting from transfer of momentum normal to the surface, with the molecule essentially seeing a flat surface. The distribution deviates from this model for sub-specular angles (closer to the surface normal), since in reality, a small lateral corrugation always persists even for the high incidence angles, as seen in molecular dynamics simulations of Ar scattering from Ag(111) [41]. As E_i increases, energy transfer becomes more efficient and larger deviations are observed with the data for the highest energy (1.92 eV) converging towards the binary collision model, reminiscent of scattering from a highly corrugated surface. In this case the E_f/E_i ratio is derived from energy and momentum conservation for a two-body collision, assuming that no energy goes into the internal degrees of freedom (rotation and/or vibration). For 40^o there is an obvious change from one regime to the other. At energies higher than 0.81 eV, the impinging molecules transfer a larger amount of energy, with the distributions closely following hard sphere scattering, but lying above the line describing a two body collision between a nitrogen molecule and a ruthenium atom.

It is not apparent whether the molecule transfers its energy to the surface or whether internal degrees of freedom, such as rotation, are excited in the process. Although N_2 is a weakly aspherical molecule, for which a small degree of rotational excitation is expected, a translational to rotational energy transfer has been measured for scattering from W(110) and Pt(111) with an efficiency of 0.09 and 0.06 respectively [23]. For O_2 scattering from Ag(111) the energy ratios converged to a line below the hard sphere scattering line for a two-body collision between an oxygen molecule and a single silver atom suggesting that internal degrees of freedom were excited [58].

The trend in the energy ratio distributions is in total agreement with the flux distributions presented earlier. There are two scattering regimes evident from the results, with a dramatic changeover in the process for molecules with normal energies above $\sim$0.65 eV. There is an abrupt change in scattering from a relatively smooth surface, with the turning point fairly far out, to scattering from a corrugated surface, with the molecules being repelled close enough to feel the underlying structure. This behavior cannot be described by a simple interaction potential, since in that case, the scattering would resemble that of Ar, as it does for N_2/Ag(111) [58]. The results for Ru(0001) show a pronounced transition to a much larger degree of corrugation. The behavior can be explained by invoking scattering from a dual repulsive wall, a simple one-dimensional picture of which is drawn in Fig. 4.4, for two different molecular orientations. In the case of N_2 on Ru(0001) the dashed curve corresponds to the interaction potential seen by the molecule oriented perpendicular to the surface and the solid line to the potential corresponding to the molecule coming in with its axis

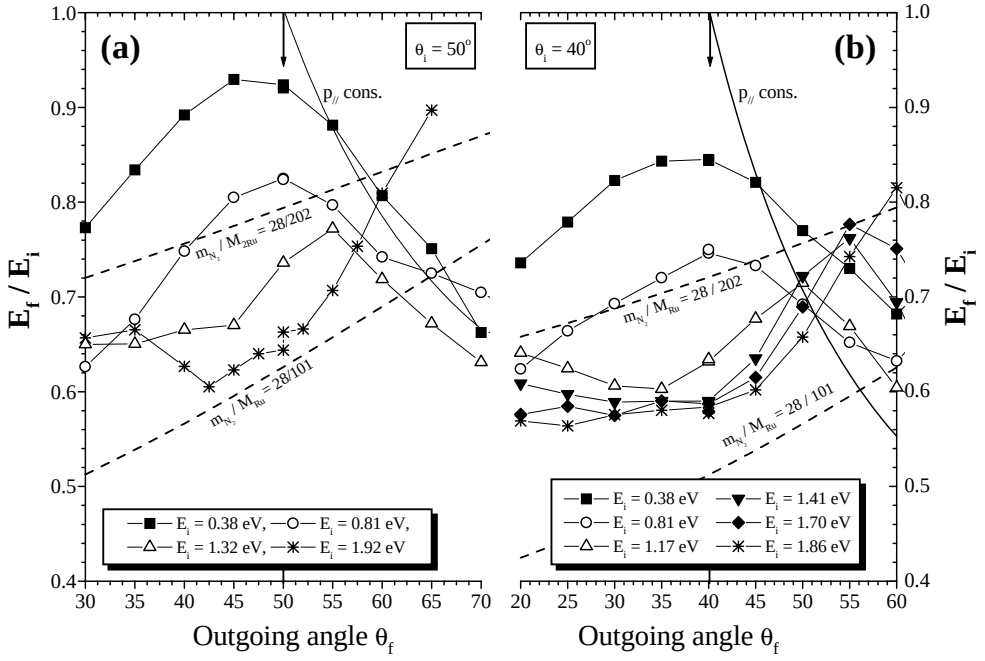

Figure 4.3: *Angular resolved energy distributions of N_2 molecules scattered from Ru(0001) for different incident energies, at a surface temperature of 550 K, for (a) θ_i = 50° and (b) θ_i = 40°. Lines through the data points are to guide the eye only. The thick lines hold for parallel momentum conservation and the dashed lines for hard sphere scattering of a nitrogen molecule from one (mass ratio m_{N_2}/M_{Ru} = 28/101) and two ruthenium atoms (m_{N_2}/M_{Ru} = 28/202).*

parallel to the crystal plane, as will be explained later. In the concept of a dual repulsive wall (solid curve), molecules with low incident energy are scattered from the repulsive wall positioned furthest from the surface. At higher energies the majority of the incoming molecules have sufficient energy to overcome the barrier and scatter from the repulsive part of the second wall which is situated closer to the surface. In the case of O_2 on Ag(111) [58], where the concept of a dual repulsive wall was used to account for the scattering behavior, molecules can scatter from the repulsive parts of either the physisorption or the chemisorption part of the interaction potential.

While a physisorption state has been identified for N_2 on Ru(0001) at 40 K by HREELS [75], N_2 can exist in a weakly chemisorbed molecular state between 70 and 120 K [17, 1]. Using Redhead's approximation and a typical pre-exponential of 10^{13} Hz these temperatures correspond to well depths of ∼10 and ∼30 meV, for the physical and chemisorption respectively. Mullins and co-workers have conducted a

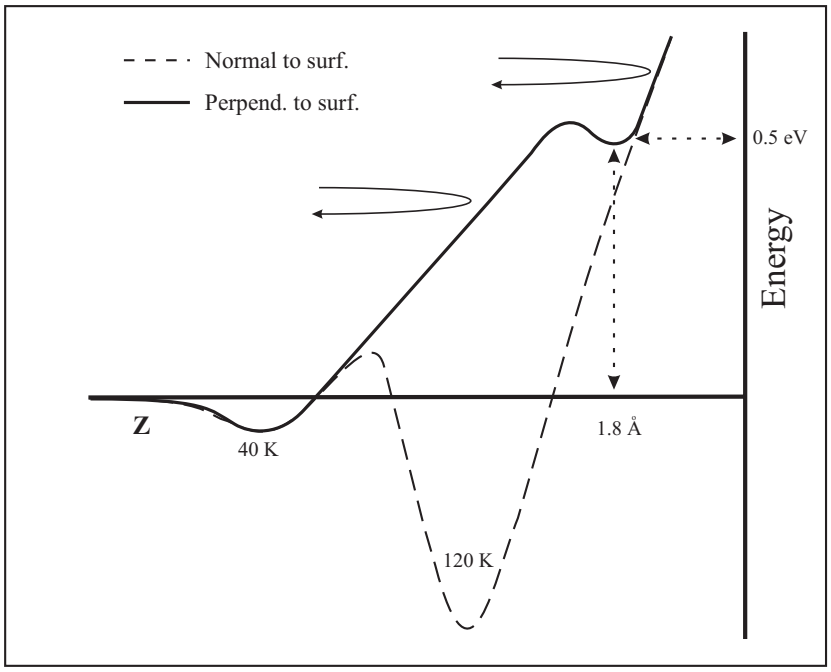

Figure 4.4: *Simplified potential energy diagram of the N_2-Ru interaction for the vertical standing (dashed line) and the flat lying (solid line) molecule along the molecule surface distance. See also [50]. The repulsive walls of the potentials have been arbitrarily drawn to merge at higher energies.*

beam study of the molecular chemisorption of N_2 on Ru(0001) [73, 74], suggesting that low energy nitrogen enters a physically adsorbed state on the surface prior to molecular chemisorption, with a direct mechanism dominating at higher energies. They proposed that the final state of molecular chemisorption is the same vertical standing state for both energy regimes. In contrast to Fe(111) [66] where high kinetic energies increases the population of the side-bound molecular chemisorbed nitrogen state, no evidence was detected for the population of a second state in their study. A hard cube model was used to fit their data and to predict the change in the physisorption trapping probability with energy. There was no trapping observed for normal energies of ~0.15 eV and higher, with all molecules having sufficient energy to overcome the barrier to chemisorption. This energy could represent the barrier the molecules need to surmount in order to reorient perpendicular to the surface into the molecular chemisorption state. The dashed line in Fig. 4.4 depicts this regime. This state was not populated in our experiment since the surface temperature was kept at 550 K, far above the desorption temperature of molecular nitrogen on this surface.

The presence of a metastable molecular precursor state has been theoretically predicted [49, 48, 50], with a barrier of ∼0.5 eV [49, 48]. Murphy *et al.* [50] have calculated this state near Z = 1.8 Å, where Z is the molecular center of mass distance. The presence of this state reduces the repulsion between N_2 and the surface, allowing the molecule to approach close in, parallel to the surface, without a large cost in energy. The molecule is able to approach in a favorable geometry for sticking, with a potential produced with a large curvature of the reaction path, which favors vibrational excitation.

Direct experimental evidence for the existence of a metastable molecular chemisorption state has been observed for O_2 on Ag(111) [60, 57], where transient trapping desorption was observed in the time-of-flight data. The transient trapping probability showed a sharp increase above a threshold and a subsequent decrease with increasing incidence energy. It was accompanied by a strong broadening in the angular direct-inelastically scattered flux distribution. In the present study, no evidence was seen in the time of flight for transient trapping desorption. The fact that trapping into a thermalized precursor state has not been observed is consistent with the unstable nature and the shallow well predicted by the theoretical calculations.

While no evidence for an abrupt change in adsorption/desorption behavior around the energy of the metastable state has been seen [50] the existence of the well should effect the scattering behavior. The notion of a dual repulsive wall in the potential is attributed to the presence of the metastable state, as seen in the simplified potential energy diagram of Fig. 4.4. By looking at the figure, one would also expect a change in scattering behavior as the molecule overcomes the barrier to molecular chemisorption. This effect is not experimentally observed, since thermal broadening dominates at the relatively low energies at which it would occur. The change in scattering behavior is at a threshold energy $E_n = E_i \cos^2 \theta_f > 0.65$ eV reasonably close to predictions and the magnitude of the corrugation probed is readily explained by the density functional theory calculations. It should be kept in mind that the favorable orientation of the majority of incoming molecules has its axis oriented parallel to the surface. As the molecule approaches the surface it crosses the small barrier to molecular chemisorption and is attracted by this potential which has the tendency to align the molecular axis along the surface normal. At low energies the molecules are scattered by the repulsive wall of this potential. At higher energies N_2 has sufficient energy to overcome the barrier to the precursor state and orient its axis parallel to the surface (solid line, Fig. 4.4). This allows the molecules oriented parallel to the surface to approach very close to the surface, as predicted, which results in the high degree of surface corrugation probed.

4.4 Conclusions

It has been shown that scattering experiments are able to probe the repulsive part in the particle-surface interaction potential. Two scattering regimes are evident which

can be explained by invoking the notion of a dual repulsive wall in the potential. This is due to the existence of a flat lying metastable molecular precursor state, with a repulsive wall close to the surface, which is consistent with recent theoretical predictions.

Chapter 5

Molecular beam study on interaction dynamics in a reactive system: NO on bare Ru(0001)

The interaction dynamics of NO with the reactive Ru(0001) surface has been investigated with the use of supersonic molecular beam techniques. Helium scattering, King & Wells sticking measurements and Time Of Flight (TOF) experiments are performed. The initial sticking coefficient is remarkably high with incident energy, varying from unity at thermal energies to ∼90% for 0.25 eV ≤ E_i ≤ 2.4 eV and does not seem to depend on surface temperature for 400 ≤ T_s ≤ 850 K. Counter intuitively, the non-sticking ∼10% of the incident flux has only about 12% translational energy transfer in the specular scattering direction. Molecular sticking is observed at low surface temperatures for above thermal incident energies, up to at least 0.45 eV. An attempt is made to distinguish between molecular precursor mediated pathways and direct dissociation. In order to account for the surprisingly constant initial sticking coefficients, the opening of a direct dissociative channel is proposed for beam energies exceeding the depth of the molecular chemisorption well. Several open problems are identified.

5.1 Introduction

Molecular beam scattering techniques have shown to be a powerful tool to study the dynamic processes at the gas-surface interface. The possibility to perform both oriented and state resolved scattering experiments using NO molecules enabled detailed studies on the energy transfer processes that occur during the collision with the Ag(111) and Pt(111) surfaces [33, 62]. In turn, this has allowed potential energy surfaces to be constructed and classical trajectory calculations tested against the experimental data [42, 8].

Though highly informative, both the Ag(111) and Pt(111) surfaces are inert towards NO reaction, since the thermodynamic barrier to dissociation of the molecule is above energies accessible with standard molecular beam techniques. Clearly it would be very interesting to extend the scope of the previous studies to a reactive (dissociative) system. This paper reports about the interaction dynamics of NO with the highly reactive Ru(0001) surface. This system is an ideal candidate for study since the adsorption of thermal NO on Ru(0001) has already been well characterized using a variety of structural techniques [86, 16] and offers a range of surface temperature and coverage regimes in which to work and where different processes may be probed.

At low surface temperatures (<200 K) adsorption of thermal NO is exclusively into molecular states chemisorbed at bridged and on-top sites [86]. Above 200 K the thermodynamic barrier to dissociation can be overcome and up to 450 K both dissociative and molecular chemisorption occur. According to Zambelli *et al.* dissociation occur efficiently at the atomic step edges, on the 300 K surface [93]. The amount of dissociation depends on the number of free sites available. Above 450 K, molecular NO desorbs from the surface and only the dissociative chemisorption products, N_{ads} and O_{ads}, are stable until they desorb associatively as N_2 and O_2 at ∼500 and ∼1500 K respectively.

In this paper we report the results of various experimental techniques, applied to discriminate between the different adsorption pathways. The high cross-section of helium diffracted from surface adsorbates gives sensitivity for surface order-disorder and overlayer structures can be probed by analyzing the interference patterns. The technique of 'King & Wells' gives the initial sticking probability as the fraction of molecules removed from the beam upon exposure to the clean surface. Furthermore, the angular and translational energy distributions of scattered NO molecules, determined by Time Of Flight (TOF) experiments, contain information on surface corrugation and energy transfer efficiencies.

5.2 Experimental

The experiments, except the TOF-measurements on the clean Ru surface, were carried out in a UHV scattering chamber, at the FOM-Institute, described in detail in a number of earlier studies [58]. It consists of a main chamber with a base pressure of $1 \cdot$

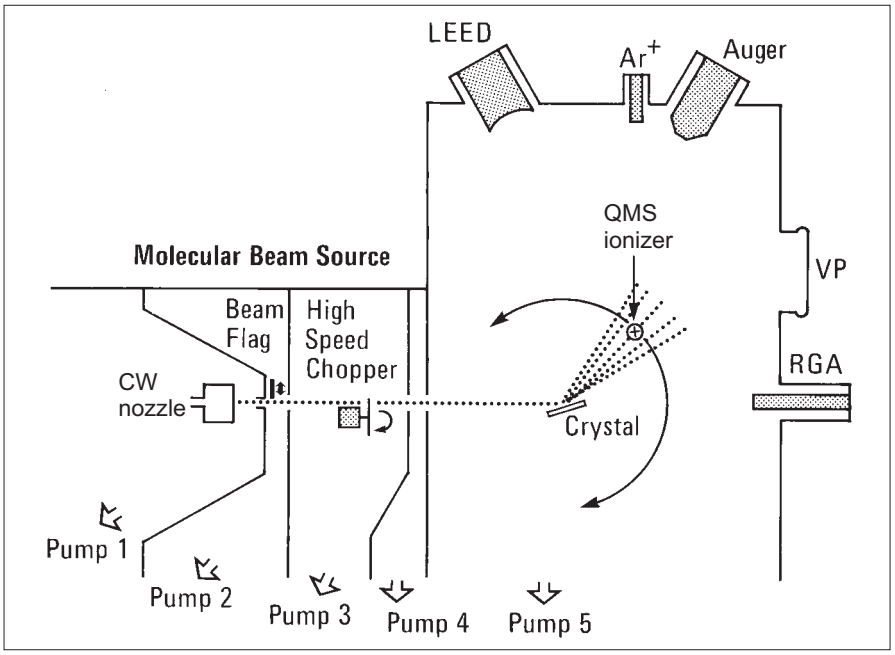

Figure 5.1: *The IBM molecular beam machine used to measure the time of flight distributions of NO scattered from the Ru(0001) surface. It consists of a 4 stage differentially pumped beam source, a two axis goniometer as sample mount and a doubly differentially pumped QMS.*

10^{-10} mbar, which contains the sample, mounted on a 3-axis goniometer [59]. To this chamber is attached a three stage supersonic molecular beam source with an 80 μm alumina (Al_2O_3) nozzle. A rotating disk chopper, positioned in the second stage, provides pulses of 0.5 to 50% duty cycle duration at up to 500 Hz. The translational energy of the NO molecules was varied between 0.1 and 2.5 eV by changing the seeding ratio of NO in either H_2 or He and heating the nozzle. This was done by electron bombardment (500 V) of a tungsten tube around the nozzle. For the H_2-seeded the nozzle temperature is restricted to ~1300 K, since higher temperature will allow the H_2 to reduce the Al_2O_3 nozzle.

Beam energies were determined by measuring the time-of-flight (TOF) of a short pulse (10 μs) of gas from the chopper to a differentially pumped rotatable quadrupole mass spectrometer (QMS) in the scattering chamber. The average final energy of scattered molecules was obtained by deconvolution of their TOF signals with the direct beam profiles. The quadrupole mass spectrometer used for these measurements is mounted on a rotatable covering flange in order to provide angular resolution. A second QMS, provides overall integrated partial pressures of gases in the chamber.

Angular resolved scattered beam intensities were measured using a 50:50 chopper, to modulate the beam, and fitting the detected signal with a modified square wave function to subtract the background from the signal.

The TOF-measurement on the clean surface were performed on a very similar setup at the IBM Almaden Research Centre [64]. Due to higher ionisation efficiencies, better ion optics and double differential pumping of the QMS probe, one to two orders of magnitude better signal to noise ratios could be obtained.

The Ru sample used at the FOM-Institute was aligned and polished to within 0.1^o of the (0001) crystal face. It could be heated by electron bombardment (600 V, 80 mA) giving rates up to 25 Ks^{-1}, controlled by a programmable regulator (Eurotherm 900 EPC) and cooled to $\sim$90 K with liquid nitrogen. The sample temperature was measured with a type C thermocouple. This was calibrated against a type K thermocouple for temperatures below 273 K. Cleaning was performed in situ by repeated cycles of flashing in a background pressure of oxygen ($2 \cdot 10^{-8}$ mbar) to 1500 K. An oxygen free surface could be obtained by a single flash to 1600 K in UHV. Helium Thermal Energy Atom Scattering (He-TEAS) was found to be an extremely sensitive probe of the surface cleanliness and order, as will be shown in section 5.3.1. This proved to be particularly useful because the main contaminant (C) is difficult to detect in small concentrations by Auger Electron Spectroscopy (AES) due to overlap with the ruthenium peaks [20, 61]. The sample used at IBM was determined to have a miss-cut of $\simeq 0.5^o$. Bulk cleaning by argon sputtering in combination with the oxygen treatment described above resulted in AES-spectra indistinguishable from the reference data. The surface quality was further checked for possible carbon contamination by the reproducibility of Temperature Programmed Desorption (TPD) spectra and TOF's of NO from the Ru(0001)-(1×1)H surface.

Sticking probability measurements were carried out using the adsorption-reflection technique of King & Wells [31], with beam flags positioned in the second stage of the beam source and in the main chamber. A correction was made for the change in effective pumping speed due to adsorption-desorption of molecules from the chamber walls. The correction is based on the observation (experiment and simulation) that the deviations from the ideal response upon pressure changes, resulting from the limited residence time of particles on the chamber walls, are a very similar for both pressure rise and drop [3].

5.3 Results and discussion

As mentioned in the introduction, the sticking of NO on clean ruthenium with a surface temperature higher than 200 K is dissociative. Depending on incident kinetic energy the dissociation can be mediated by physisorption/chemisorption precursor states or can occur along a direct pathway. A way to distinguish between a mediated or direct channel is to study the composition of the overlayer upon dosage with various energies at low surface temperatures. A direct pathway will give N_{ads}+O_{ads} below

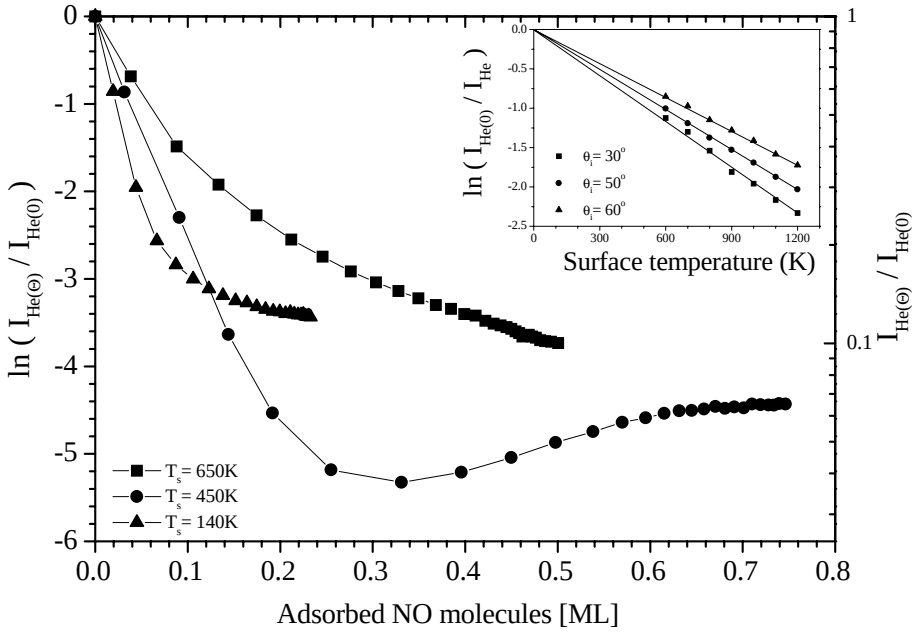

Figure 5.2: *The inset shows the specular thermal (65 meV) helium reflectivity of the bare Ru(0001) surface, normalized to the direct beam intensity, as a function of the surface temperature for incidence angles* $\theta_i = 30^o$, 50^o *and* 60^o *along the close packed* $< 11\bar{2}0 >$ *azimuth. The main body contains the normalized specular helium reflectivity, as a function of the amount of NO molecules adsorbed at* T_s= *140, 450 and 650 K,* E_i= *0.065 eV,* $\theta_i = \theta_f = 60^o$, *along the* $< 11\bar{2}0 >$ *azimuth.*

T_s= 200 K, while a (chemisorption) mediated pathway will only give NO_{ads}.

5.3.1 Thermal energy helium atom scattering

The inset of Fig. 5.2 shows the natural logarithm of the intensity helium scattered along the close packed $< 11\bar{2}0 >$ azimuth and specular scattering conditions ($\theta_f = \theta_i$) as a function of the surface temperature. At all incidence angles investigated the specular intensity decays exponentially with increasing surface temperature. It is also found that the relative scattered intensity I/I_0 extrapolates to 1.0 at T_s= 0 K consistent with a perfectly ordered, smooth surface, with no scattered intensity in the diffraction peaks.

A model for the decay in the specular scattered intensity with surface temperature, based on a Debye-Waller factor, has been developed by Beeby *et al.* [2]. Using this formalism it is possible to make an estimate of the Debye temperature ($T_{D,S} \cong$

842 K) and of the well depth for helium ($D_{He} \cong 76$ meV) on Ru(0001) surface. Both of the obtained values are much larger than can be reasonably expected. However, the inadequacy of this model to account for collisions which experience the long range attractive potential of several surface atoms has been pointed out by [14] and we will restrict our interpretation of helium scattering simply to that of a sensitive probe of the local surface order.

Application of the technique to elucidate the precursor mediated vs. direct channel is shown in Fig. 5.2. The dependency of the normalized helium specular scattered intensity as a function of the NO surface coverage is shown in three adsorption regimes. The molecules were dosed at $\theta_i = 60^o$ with a helium seeded NO beam ($E_i = 0.45$ eV) allowing simultaneous dosage and data acquisition, also referred to as MB-TEAS [78]. From the saturation coverage we determine that the adsorption is entirely into the molecular chemisorption state, at a surface temperature of 140 K. At 450 K the NO molecules dissociate to form a mixed N_{ads} + O_{ads} overlayer, and at 650 K the N_{ads} atoms associatively desorb, leaving an O_{ads} overlayer on the surface.

While the helium reflectivity is decreased efficiently by all the surface adsorbates, it is clear that the reflectivity from the molecular overlayer (T_s = 140 K) follows a significantly different form from that of the atomic overlayers. At $\Theta_{NO} \cong 0.3$ML, close to half the saturation coverage, the reflectivity reaches a minimum value of 0.005 before recovering to 0.012 of the initial reflectivity. This minimum can be explained by the existence of a strongly disordered ad-layer as slow molecular diffusion prohibits ordering of the partly covered (non-saturated) layer. The higher surface temperatures allow continuous restructuring and possibly island formation resulting in a monotomous decrease in the specular reflectivity. The asymptotic value of I/I_0 appears to be very similar for all three surface temperatures. This may be coincidental because the scattering cross sections for the adsorbates will be different as well as the Debye Waller factors.

From the initial decrease of reflectivity the helium scattering cross section for NO molecules ($\Sigma_{He,NO}$) can be determined to be 94 ± 10% Å^2. For both the mixed N_{ads} + O_{ads} and the O_{ads} overlayers the reflectivity falls smoothly with increasing surface coverage to values of 0.016 and 0.013 respectively. The initial decay on the 450 K surface appears to be far more rapid than at 650 K. This is because at 450 K two adsorbate atoms (N_{ads} + O_{ads}) are formed from every adsorbed NO molecule, while at 650 K only one adsorbate atom is left on the surface (O_{ads}), giving $\Sigma_{He,N+O} = 154$ ± 10% Å^2 and $\Sigma_{He,O} = 66$ ± 10% Å^2 respectively. The cross section for $\Sigma_{He,N}$ can be calculated if we assume the initial distance between the O_{ads} and N_{ads} to be large. In this case, subtraction of the value of $\Sigma_{He,O}$ from this N+O combined cross section to obtain $\Sigma_{He,N}$ is allowed and determined to be 88 ± 15% Å^2.

The molecular sticking observed at low surface temperatures is consistent with the thermal NO adsorption studies [86, 16] and apparently also holds for above thermal incident energies, up to at least 0.45 eV. This is supported by the earlier reports from us on He-diffraction patterns of the (2×2)NO overlayer, also produced with 0.45 eV

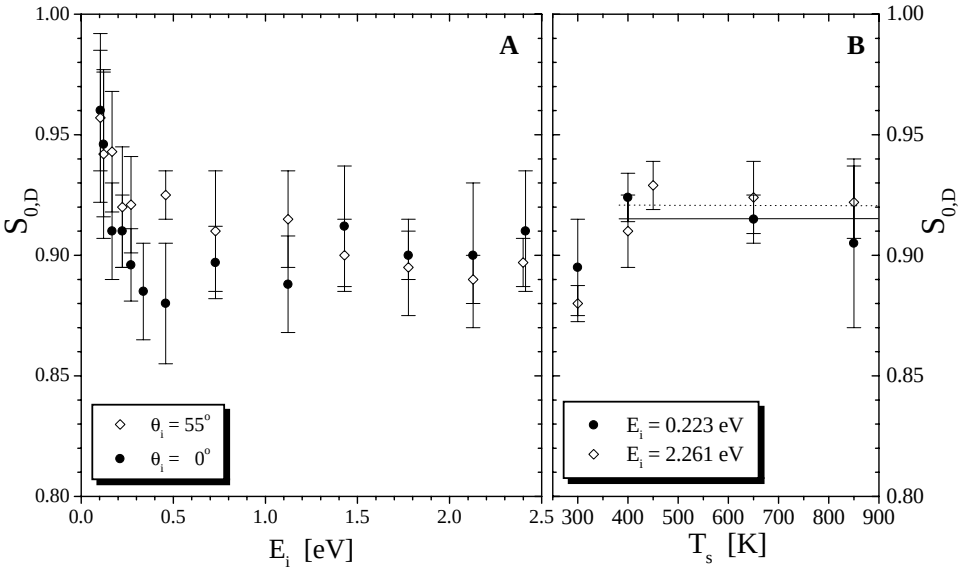

Figure 5.3: *Panel* **A***: Initial sticking probability of NO on Ru(0001) as a function of the incidence beam energy for incidence angles of θ_i= 0° and 55° along the $<11\bar{2}0>$ azimuth, at T_s= 650 K. Panel* **B***: Initial sticking probability of NO on Ru(0001) as a function of the surface temperature for incidence energies of E_i= 0.22 eV and E_i= 2.26 eV. θ_i= 0°. The solid and dashed lines are linear fits to the 0.22 and 2.26 eV data respectively.*

molecules [10]. Note that we can not perform these experiments for much higher energy beams (∼2 eV) for the inevitable heating of the nozzle would first decrease the He-scattering cross-sections and ultimately H_2 seeding be needed, excluding MB-TEAS.

5.3.2 Initial sticking probability

In Fig. 5.3.A the initial sticking probability $S_{0,D}$, determined using the technique of King & Wells (see Chapter 2), for NO/Ru (T_s= 650 K) is shown as a function of the incidence energy of the molecules for the incoming angles θ_i= 0° and 55°. At this surface temperature, the dissociation of NO and subsequent recombination of N_2 as reported in literature and observed in our He-scattering experiments (Section 5.3.1), can nicely be confirmed by the observation of a partial pressure rise proportional to the decrease in partial NO pressure upon exposure of the surface to the NO beam.

Values of the initial dissociative sticking coefficient ($S_{0,D}$) have previously been reported for θ_i= 60° [10] but have since been improved using a newly developed

analysis procedure [3]. At $\theta_i = 0^o$, a smooth decrease in the sticking probability from 1.0 to 0.9 occurs as the incidence energy is increased to 0.25 eV. $S_{0,D}$ then remains constant up to the maximum energy available in our experiment (~2.5 eV). At $\theta_i = 55^o$ the initial decrease of $S_{0,D}$ appears to be extended to slightly higher incidence energies, indicating a possible normal energy scaling.

In Fig. 5.3.B the initial NO sticking probability is shown as a function of the surface temperature for two incidece beam energies (E_i= 0.22 eV and 2.26 eV). Within the experimental uncertainty no dependence of $S_{0,D}$ on surface temperature could be found. The slightly lower values of $S_{0,D}$ observed at the 300 K surface, could well be connected to the fact that T_s= 300 K is below the desorption temperature of hydrogen, which allows a build up of contamination from the ambient gas over the couple of minutes it takes to cool down. As shown previously [10] the adsorption of hydrogen effectively reduces the sticking coefficient for NO molecules on the Ru(0001) surface.

While the fall off in $S_{0,D}$ over the range 0 - 0.25 eV, shown in Fig. 5.3.A is consistent with a physisorption mediated precursor, the striking feature of Fig. 5.3 is the insensitivity of $S_{0,D}$ to a wide range of both beam energies and surface temperatures: $0.3 \leq E_i \leq 2.4$ eV and $400 \leq T_s \leq 850$ K. When comparing to the NO/Pt(111) system, which has a similar deep molecular chemisorption well (1.0 eV), the probability for molecular chemisorption is expected to drop considerably for incoming molecules with energies exceeding the well depth [88, 8]. We can use the cube model, on the other hand, to make a simple estimate of the critical escape energy:

$$E^{cr}_{i,norm} = \frac{4\mu}{(1-\mu)^2} \cdot \epsilon \tag{5.1}$$

While this results in $E^{cr}_{i,norm}$= 0.86 eV for the NO/Pt system ($\mu = 30/195$, $\epsilon = 1.0$ eV), this value is 3.6 eV for the Ru surface ($\mu = 30/101$, $\epsilon = 1.49$ eV). Though one might wonder if 101 amu is a realistic cube mass for Ru, the difference suggests a much slower decrease of the initial sticking coefficient.

A direct dissociation probability, is expected to increase with E_i [62, 8]. In combination with the molecular precursor mediated dissociation pathway, this could nicely account for the nearly constant sticking coefficient. In all cases the trapping mechanisms would need efficient transfer of translational energy to the lattice to account for 90% sticking at high incident energies. Rotational excitation has proved to be an effective energy loss process for the NO/Pt(111) system.

The absence of a surface temperature dependence in $S_{0,D}$ can intuitively be understood considering the dynamics/kinetics. As pointed out in the introduction it only takes 200 K thermal energy to dissociate the molecule, where T_s= 475 K is the molecular desorption temperature. Combined with the energetic gain, due to the high binding energies of both the N and O atoms on the Ru(0001), a molecule trapped in the molecular chemisorption precursor at T_s= 650 K, will clearly favor dissociation over desorption, making a surface temperature dependence in $S_{0,D}$ unlikely.

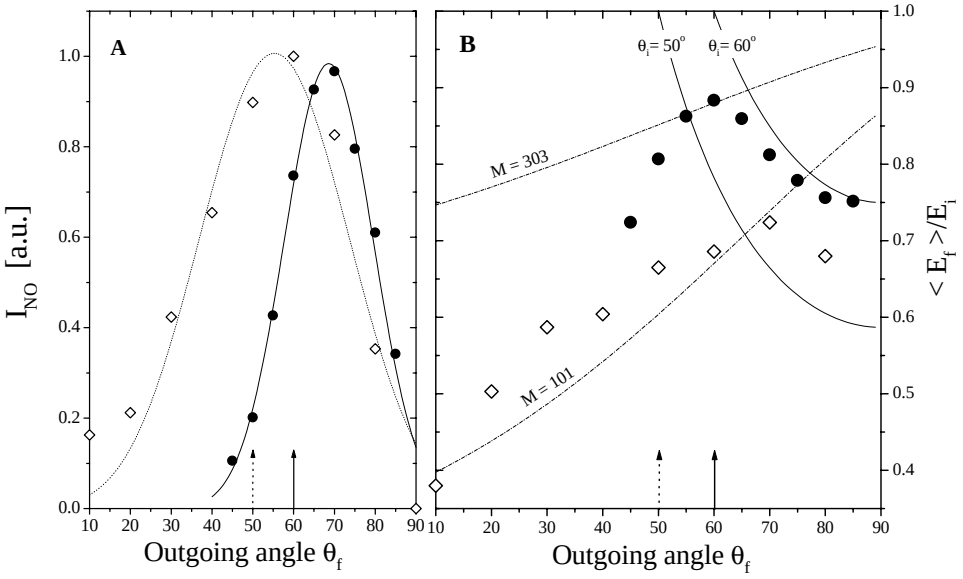

Figure 5.4: *The normalized scattered intensity (panel* **A***) and ratio of final to initial energy* E_f/E_i *(panel* **B***) as a function of the final angle* θ_f*, for NO molecules scattered from:* • *Ru(0001) at* E_i= *0.70 eV,* θ_i= 60^o*,* T_s= *550 K and* ⋄ *Ru(0001)-(2x2)NO at* E_i= *2.06 eV,* θ_i= 50^o*,* T_s= *140 K. The dashed curves hold for the binary collisions of hard spheres with two different mass ratios; one with the NO mass (30 amu) colliding with a single Ru mass (101 amu) and with three times the Ru mass (303 amu). The solid lines hold for the conservation of parallel momentum in the collision for the two angles of incidence. The arrows indicate the outgoing angle in case of specular scattering.*

5.3.3 Angular and energy distributions

Measurements of the angular distribution and normalized energy of the NO scattering from the clean Ru(0001) surface are depicted in Fig. 5.4. This figure is also showing data of the O-saturated surface as comparison. The difficulty of experiments on the clean surface lies in the rapid build up of NO due to the high sticking probability. As a check, the signal after a beam dosage of four times the measurement time was recorded to be less than 10%. Although conditions are different (θ_i= 60^o, E_i= 0.70 eV for the clean, and θ_i= 50^o, E_i= 2.06 eV for the O-saturated surface), it is clear from the angular distribution that the surface appears much less corrugated for the bare surface (FWHM = 27^o vs. 43^o). This width can also be expressed by fitting simple cos^n-functions through the data of Fig. 5.4.A resulting in n= 28 and n= 10 respectively. Note also the width's reported for the inert NO/Ag(111) [38]

and the reactive NO/Pt(111) [89] systems, of 28^o and 36^o respectively. Furthermore, the scattered distribution from the clean surface is peaked relatively super-specular, implying high conservation of parallel momentum. This can directly be observed in the energy distributions shown in Fig. 5.4.B, where the data closely approaches the solid line, drawn for $\theta_i = 60^o$, which holds for the ideal conservation of parallel momentum, consistent with scattering from an uncorrugated surface. The absence of such a convergence for the scattering of the oxygen layer indicates strong mixing of parallel and normal momentum by the corrugation. Molecules scattered sub-specular, undoubtedly experienced surface corrugation in the collision event. The dashed lines represent the final energies of particles scattered in a binary collision of hard spheres; one with the NO mass (30), the other with one or three times the Ru mass of 101. From the angular and energy distributions of the scattered NO molecules it is clear that the Ru(0001)-(2x1)O surface is experienced fairly corrugated, with an effective surface mass closely resembling that of individual ruthenium atoms.

The most surprisingly feature of Fig. 5.4.B however, is the remarkably small average energy loss of only 12% for the specular scattered NO molecules from the clean surface. For comparison, the O-saturated surface results in about 35% energy loss, a amount very common for the NO/Ag(111) and NO/Pt(111) systems [38, 89]. Apparently, the NO molecules scattered from the bare surface experience a relatively *heavy* surface resulting in energy transfers almost as small as those reported for the NO/Ru(0001)-(1×1)H system [10]. In combination with the small corrugation observed, this suggests a Potential Energy Surface (PES), possibly dependent on molecular orientation, with classical trajectory turning points positioned far from the surface, thus interacting with multiple Ru atoms and probing little corrugation.

The small amount of energy lost by the non-sticking molecules is remarkable considering the 100% translational energy loss of the majority of (sticking) molecules. The fact, on the other hand, that about 10% of the NO molecules manage to escape from the surface despite their small incident energies compared to the $E_{ads} = 1.49$ eV chemisorption well [16], is consistent with the inefficient energy transfer observed.

5.4 Summary

In summary, the interaction (adsorption) dynamics of NO and the Ru(0001) surface are studied using molecular beam methods aiming to unravel the different adsorption mechanisms from the presented data. Though the presented data set is not sufficient to provide conclusive evidence on adsorption-dissociation pathways over the entire energy region, some worth while statements and suggestions can be made.

The initial drop in $S_{0,D}$ over the range 0 - 0.25 eV is consistent with a physisorption mediated precursor. For low temperatures ($T_s = 140$ K) the sticking is clearly non-dissociative for beam energies up to at least 0.45 eV. The independence of $S_{0,D}$ in the $0.25 \leq E_i \leq 2.4$ eV region can not easily be accounted for by molecular chemisorption mediated dissociation alone, though the cube model predicts a much more gradual fall

off than the NO/Pt system. The data set presented here does not contain evidence of a direct pathway to dissociation. By invoking such a channel, similar to that theoretically predicted for NO/Pt(111) [8], the absence of the drop in $S_{0,D}$ can be explained. Possibly the non-sticking 10% scatters of the (small) chemisorption barrier; far from the surface, consistent with the elasticity observed in TOF. This barrier might well depend on molecular orientation as reported for the NO/Pt(111) system [37].

Chapter 6

Elastic scattering in a reactive environment: NO on Ru(0001)-(1×1)H

Local variations in the reactivity of NO on the Ru(0001)-(1×1)H surface have been probed with a supersonic molecular beam. The presence of adsorbed hydrogen atoms creates an elastic scattering channel in the specular direction, concomitant with a suppression of the initial sticking probability. Argon is scattered in a qualitatively similar, but instrumentally limited specular peak from the same surface. The well characterized position of the hydrogen atoms allows the scattering to be related to collisions at the three-fold hollow sites within the surface unit cell.

6.1 Introduction

One of the recurrent questions in the field of gas-surface dynamics has been the lateral surface site dependence of the reaction probability. It is generally accepted that the reactivity of semiconductor surfaces is dominated by highly localized, dangling bonds. The saturation of these dangling bonds by hydrogen results in the remarkable inertness of silicon surfaces treated with HF [92, 84]. In contrast, on metal surfaces, the jellium model of a completely delocalized electron bath predicts a laterally uniform potential energy for a molecule above the surface unit cell, although little experimental information exists to indicate how realistic this is. Recent theoretical work by Wilke *et al.* [87] suggests considerable local differences may exist on transition metal surfaces. In order to investigate the importance of these effects in a reactive environment, we have studied the catalytic NO reduction reaction on Ru(0001), where a number of associative and dissociative adsorption states exist.

Measurements of the sticking probability alone are generally unable to provide information on the position of the adsorption sites within the surface unit cell. The most informative probe of the interaction dynamics is provided by the angle and energy resolved measurement of the directly scattered molecules [26]. In this letter we report the remarkably elastic, specular scattering of NO from a Ru(0001) surface in which the adsorption channel has been partially closed by the presence of hydrogen atoms in the FCC three-fold hollow sites.

6.2 Experimental

The experiments were performed in an ultra-high vacuum (UHV) scattering chamber equipped with a three stage supersonic molecular beam source [58]. The sample was aligned and polished to within 0.1^o of the (0001) crystal face and cleaned by repeated flashing to a surface temperature (T_s) of 1500 K in $2{\cdot}10^{-8}$ mbar of O_2(g). A single flash to 1600 K in UHV was found to remove all the remaining oxygen and leave a clean ordered surface, ascertained by a Debye-Waller plot of the thermal helium reflectivity which extrapolated to $I/I_0 = 1.0$ at 0 K, where I_0 is the incident He beam intensity. The Ru(0001)-(1×1)H overlayer was prepared by dosing $5{\cdot}10^{-7}$ mbar of H_2(g) for 300 seconds at $T_s \leq 200$ K. Sticking probability experiments were performed using the reflection detection technique of King and Wells [31]. Angle resolved time-of-flight scattering experiments were performed using a chopped beam and a differentially pumped rotatable mass spectrometer. All the adsorption and scattering results were taken in the zero NO coverage limit.

6.3 Results

The behavior of NO on the Ru(0001) surface is dependent on T_s. Below 200 K a strongly chemisorbed molecular state is formed ($E_{ads} \cong 1.49$ eV), either on top of a

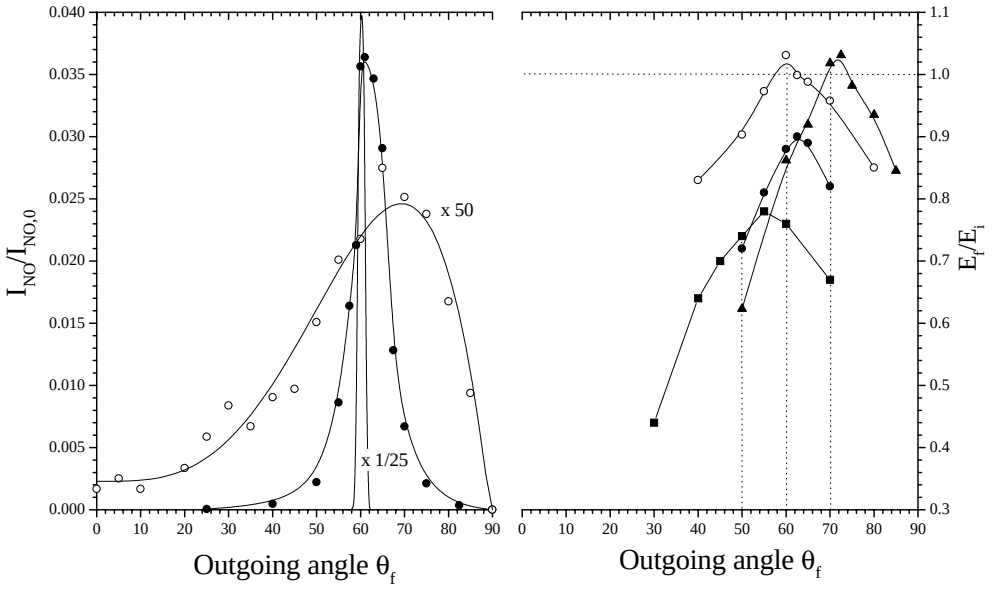

Figure 6.1: *Left panel: Angular distribution of NO molecules scattered from the Ru(0001) (diamonds, E_i= 1.56 eV, T_s= 650 K, θ_i= 60^o along the $< 11\bar{2}0 >$ direction) and Ru(0001)-(1×1)H (circles, E_i= 2.1 eV, T_s= 140 K, θ_i= 60^o along the $< 11\bar{2}0 >$ direction) surfaces, normalized to the direct beam intensity. Direct beam profile is shown for comparison. Right panel: Final energy distributions of NO scattered from Ru(0001)-(1×1)H. E_i= 0.34 eV (open symbols) and 2.1 eV (filled symbols), T_s= 140 K, θ_i= 50^o (squares), 60^o (circles) and 70^o (triangles) along the close packed $< 11\bar{2}0 >$ direction.*

ruthenium atom, in a two-fold bridging or in a three-fold hollow site, depending on the surface coverage [86, 16]. Above 200 K, NO can dissociate into N_{ads} and O_{ads} ad-atoms, given the availability of free sites. Above 450 K, molecular NO_{ads} desorbs from the surface. Finally, N_{ads} and O_{ads} associatively desorb as N_2 and O_2 at ∼500 and ∼1500 K respectively.

The result of scattering NO from the clean Ru(0001) surface is shown in Fig. 6.1. Due to the reactivity of the system very few molecules are directly scattered. Those that are form a broad angular distribution (full width at half maximum FWHM $\cong 37^o$), similar to that observed in the NO-Ag(111) [38] and Pt(111) [89] systems. However, on Ru(0001) it is possible to reduce the surface reactivity by blocking all the FCC three-fold hollow sites with hydrogen atoms [44]. Fig. 6.1 shows the final energy and angular distributions of NO molecules scattered directly from the Ru(0001)-(1×1)H surface. Strikingly, the angular distribution (top panel) now forms a sharp peak in the specular scattering direction (FWHM = 8^o) and can be approximated

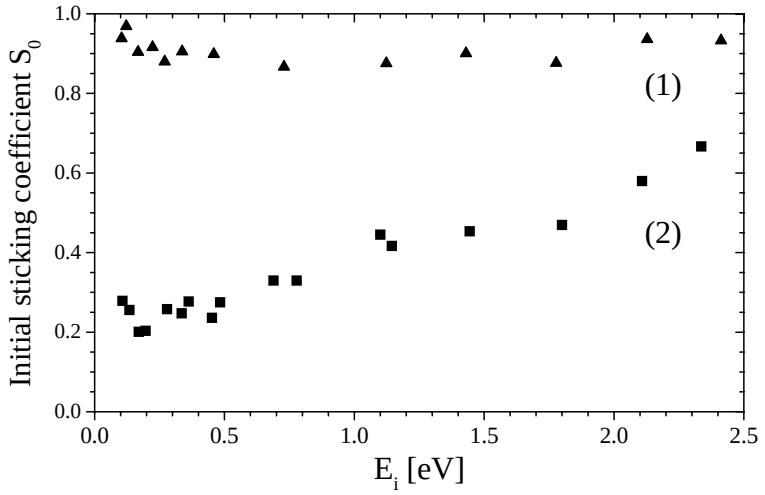

Figure 6.2: *(Same as Fig. 2.3) Initial sticking probability of NO on Ru(0001) (T_s= 650 K, up triangles) and Ru(0001)-(1×1)H (T_s= 140 K, squares) as a function of E_i. θ_i= 0°.*

by a $\cos^n(\theta_f - \theta_{spec})$ function where n = 380 ± 170, far higher than any previously reported value for a heavy, reactive molecule. Comparison with the direct beam profile reveals a slightly asymmetric broadening towards super-specular directions, consistent with some rotational excitation at the expense of normal translational energy ($E_i \cos^2\theta_i$) [33]. The final energy of the scattered molecules (bottom panel) confirms the extremely small energy transfer in the collision. E_f/E_iincreases at more grazing angles of incidence and at lower incidence energies, so that at θ_i= 60°, E_i= 0.34 eV, and θ_i= 70°, E_i= 2.1 eV, molecules scatter along the specular direction in a truly elastic collision (E_f/E_i= 1.0).

In order to measure the effect of H_{ads} on the surface reactivity, the initial sticking probability of NO (S_0) was measured on both the clean and hydrogen covered surfaces (Fig. 6.2). On the clean surface S_0 is high (¿0.7) at all incidence energies. This data was obtained at a surface temperature of 650 K, where the adsorption of NO is dissociative. However, S_0 was found to be independent of the surface temperature and adsorption into the molecular state at 140 K follows the same curve. The effect of H_{ads} on the Ru(0001)-(1×1)H surface is to suppress S_0 but still leaves a significant reaction probability (S_0= 0.17-0.47). Because of the desorption temperature of hydrogen from Ru(0001) (350 K [29]) this data could only be measured at low temperatures, where NO adsorption is entirely molecular. Fig. 6.3 shows the thermally programmed desorption (TPD) spectra for masses 2 (H_2) and 30 (NO) from the Ru(0001)-H+NO overlayer formed by the adsorption of NO on Ru(0001)-(1×1)H. The only other species observed was mass 28 (N_2) formed from the well

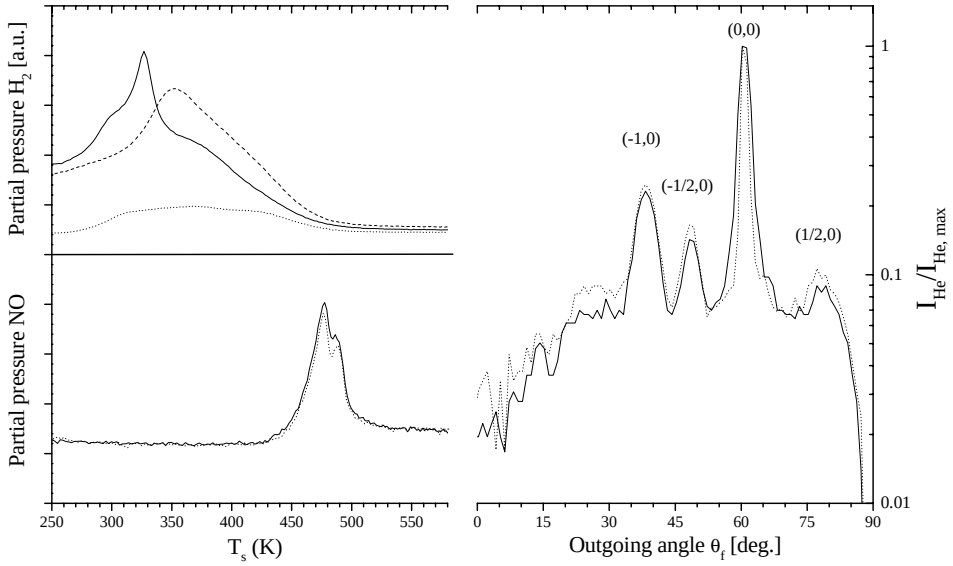

Figure 6.3: *Left panel: TPD spectra of H_2 and NO from Ru(0001)-(1×1)H (dashed lines); Ru(0001)-(2x2)NO (dotted lines) and Ru(0001)-(1×1)H exposed to an NO beam (solid lines). Heating rate 5 Ks^{-1}. Right panel: Normalized scattered helium intensity from Ru(0001)-(2x2)NO and Ru(0001)-(1×1)H + NO, E_i= 65 meV, θ_i= 60° along the close packed $< 11\bar{2}0 >$ direction, T_s= 140 K. Labels show diffraction peak indices.*

known decomposition of NO on Ru(0001) [16]. The associative desorption of H_2 from the Ru(0001)-(1×1)H overlayer and the desorption of NO from the Ru(0001)-(2x2)NO overlayer accurately reproduce previously reported spectra [16, 29]. When NO is adsorbed on the Ru(0001)-(1×1)H surface the H_2 desorption peak narrows and shifts from 350 K to 325 K, with a shoulder at higher temperatures, characteristic of compressed Ru(0001)-nH overlayers observed by Jachimowski [29] (1.0< n <1.4). In contrast, in the presence of H_{ads}, the NO desorption peak remains completely unchanged in both shape and peak position. The area under the desorption peaks remains unchanged for both H_2 and NO, demonstrating that hydrogen is not desorbed during NO adsorption, nor is the number of NO adsorption sites reduced by the presence of hydrogen. These results suggest that where the NO is adsorbed on the Ru(0001)-(1×1)H surface, a Ru(0001)-(2x2)NO region is created, surrounded by a region of compressed hydrogen ad-atoms.

Fig. 6.3 also shows the diffraction of a helium beam by the Ru(0001)-(2x2)NO and Ru(0001)-H+NO surfaces. Both surfaces show almost identical diffraction peaks, indicating that NO adsorbs in the same (2x2) structure on the hydrogen pre-covered

surface as on the clean Ru(0001) surface. This conclusion is supported by the observation of a (2x2) low energy electron diffraction (LEED) pattern on both surfaces. The long range order of the Ru(0001)-(2x2)NO overlayer seen and the high saturation coverage (0.75 monolayers [86, 16]) shows that NO adsorption cannot occur only at surface defects.

Our discussion will concentrate on whether the experimental results are consistent with a local site dependence of the molecule-surface interaction. The suppression of S_0 and the increase of direct scattering show that part of the surface is rendered inert to NO by the presence of H_{ads}. If H_{ads} were to passivate the entire unit cell, then ~30% of the sites in the Ru(0001)-(1×1)H surface would need to be vacant to account for the remaining sticking probability. This is extremely unlikely on such a well defined surface and we can conclude that both scattering and adsorption sites must exist within the same surface unit cell. By occupying the Ru bonding orbitals in the FCC three-fold hollow sites H_{ads} reduces the binding energy for NO significantly. The narrow specular reflection indicates that for certain impact parameters this results in a locally smooth, flat potential energy surface. However, the reactivity of the surface (S_0= 0.17-0.47) shows that other parts of the unit cell continue to interact strongly with NO.

Recent theoretical studies on the dissociation of H_2 have shown that where strongly attractive geometries lie close to repulsive ones, the local potential gradient will 'steer' the molecule into an adsorption site [21, 30]. The result is a tendency for S_0 to approach unity at low energies where the molecule is traveling slowly, and a chaotic scattering of those molecules not adsorbed. However, the remarkably narrow angular distribution observed here suggests that steering does not have a significant effect on the dynamics at the impact parameters of these particular molecules.

In order to compare the behavior of NO with an inert, physisorbed particle, argon was also scattered from the hydrogen covered ruthenium surface and the angle resolved results are shown in Fig. 6.4 for four different incidence angles. A sharp peak is seen at the specular angle, superimposed on a broad background, similar to observations on the 2H-W(100) surface [71]. The specular peak, which increases in intensity at more grazing angles of incidence, is even sharper than that observed for NO and is essentially limited by the angular profile of the direct beam (FWHM = 2^o). Like NO, this is consistent with two distinct scattering regimes. The specular peak suggests a smooth, flat surface, while the diffuse component has experienced a more corrugated potential and undergone inelastic, possibly multiple collisions in the physisorption well, as seen in calculations of Ar on Ag(111) [41]. It is this component which for NO leads to sticking in the deep chemisorption well which still exists in some parts of the unit cell.

We will now turn our attention to the most remarkable observation, that the collision of NO with the inert part of the unit cell can be elastic. The simplest model is for a collision between two non-interacting particles. In this case E_f/E_i= 0.74 for particles of mass 30 (NO) and 101 (Ru). This rises to 0.86 for a surface mass

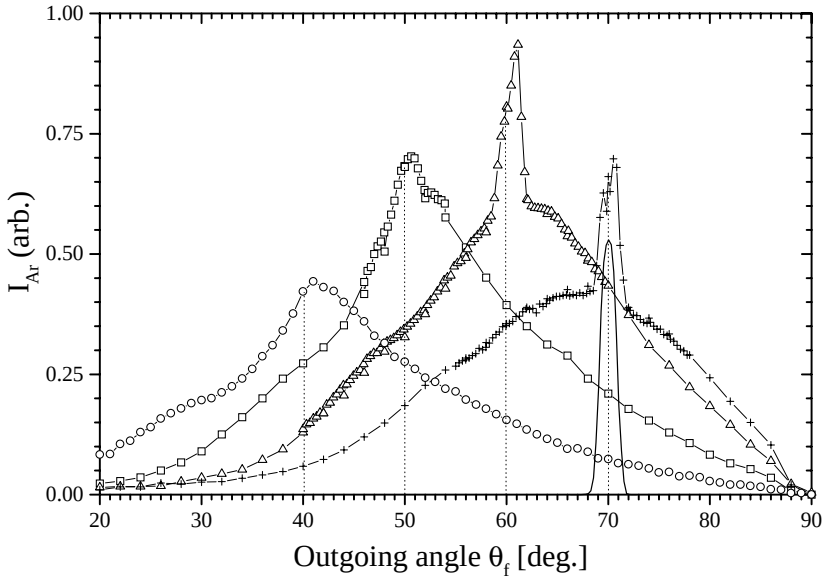

Figure 6.4: *Angular distribution of Ar scattered from the Ru(0001)-(1×1)H surface. E_i=65meV, T_s= 140 K, θ_i= 40^o (circles), 50^o (squares), 60^o (triangles) and 70^o (crosses) along the close packed $< 11\bar{2}0 >$ direction. Angular profile of the direct beam (70^o) is shown for comparison.*

of M = 202, 0.90 for M = 303 and 0.94 for M = 505 amu. Including an attractive molecule-surface interaction in the model would only increase the energy transfer in the collision. Hence E_f/E_ican only approach unity when the interaction energy approaches zero and the mass of the surface scatterer becomes extremely large. This model neglects the quantized nature of the surface phonons. However, the phonon energies extend from 0 meV upwards and have been measured on the Ru(0001)-(1×1)H surface at only 21 meV [76], easily accessible at the incidence energies used here.

A more likely explanation is related to the stiff binding and high coordination of the hydrogen in the three-fold hollow site with which an NO molecule collides. The high vibrational frequency of H_{ads} perpendicular to the Ru(0001) surface ($\nu\perp$= $3.4{\cdot}10^{13}$ Hz [76]) corresponds to a period of 29 fs. In this time the motion of an NO molecule along the surface normal (E_i= 0.34 eV, θ_i= 60^o) will be only 0.22 Å. Hence the H-Ru_3 vibration will adjust adiabatically to the perturbation caused by the NO, leading to the elastic scattering seen in the experiments. The precise dependence of the interaction dynamics on impact parameter will of course be a complicated func-

tion over the whole of phase space. However, the very sharp scattering distributions suggest a rather discontinuous change in behavior, with a local scattering extremum at the three-fold hollow sites. A weaker dependence on impact parameter would lead to the typical broad angular and energy distributions observed on silver and platinum.

6.4 Conclusions

In conclusion, we are able to distinguish two distinct and contrasting interactions of NO within the Ru(0001)-(1×1)H unit cell. Directly above H_{ads}, the NO experiences a weak physisorption well, similar to that of argon. Such an interaction will be smooth and flat leading to the specular, elastic scattering of NO from the hydrogen filled three-fold hollow site. Collisions at other impact parameters within the unit cell will be inelastic and occur on a more corrugated potential energy surface. This leads to efficient sticking (in the case of NO, where a deep chemisorption well exists) and diffuse scattering (in the case of argon). The adsorption of NO results in a migration of H_{ads}, forming compressed overlayers of hydrogen ad-atoms.

Chapter 7

Rotational Excitation of NO on Ru(0001)-(1×1)H

The rotational state distributions of NO molecules scattered of the (1×1)H-covered Ru(0001) surface have been investigated by resonance enhanced multi photon ionisation (REMPI). Angular and energy distributions reported earlier for this scattering channel, show an angular spread of only $\simeq 8^o$ *(*$\theta_i = 60^o$*,* $E_i = 2.1$ *eV), combined with minimal translational energy loss in the collision (*$E_f/E_i = 0.91$*) [10] (Chapter 6). These observations suggest scattering with minimal experienced corrugation and a high probability to yield* cold *rotational distributions. Analysis of the REMPI-spectra, however, reveals substantial rotational excitation, accompanied by rotational rainbows for higher quantum numbers (*$J > 20$*). The rotational temperatures increase from* $< T_{rot} > = 450$ *K at an incidence energy* $E_i = 0.32$ *eV, to* $< T_{rot} > = 950$ *K at* $E_i = 1.50$ *eV. Comparing the standard linear fit* $< E_{rot} > = \alpha \cdot (E_i + \epsilon)$ *to other systems shows* α*, the kinetic to rotational energy transfer efficacy, to be slightly higher than NO scattering of the fairly* inert *Ag(111) surface. This system though has much wider angular spread and larger energy losses. The contribution of the rotational excitation to the NO/Ru angular broadening is studied assuming parallel momentum conservation. For an incoming angle of* $\theta_i = 15^o$*, this contribution seems minor.*

7.1 Introduction

Scattering atoms and molecules from surfaces using molecular beams has been applied very successfully to the study the fundamentals of gas-surface interactions. NO-molecules as projectiles have been widely studied in scattering from various surfaces. The lone pair electron on NO makes this molecule exceptionally accessible for (laser) spectroscopy, and it's $^2\Pi$ ground state allows orientation upon focusing through a hexapole state selector. These experimental advantages are very fortunate since analysis of angular and time of flight (TOF) energy distributions alone usually yield limited information. The angular spread is often due to several totally different mechanisms [88]. Contributions such as surface corrugation, surface temperature, rotational and vibrational excitation typically result in angular distributions with FWHM's in the order of 27^o (for NO/Ag(111) [38]) to 34^o (for NO/Pt(111) [89]). The application of Resonance Enhanced Multi Photon Ionisation (REMPI) allows the discrimination between the contributions of surface corrugation and the molecular anisotropy to the broadening of the angular distribution.

For NO molecules scattered off hydrogen covered Ru(0001) we previously reported very narrow angular distributions of FWHM $\cong 8^o$, with close to elastic scattering (E_f/E_i= 0.91 for $\theta_i = \theta_f = 60^o$) [10]. Comparison to similar scattering measurements on silver (FWHM $\cong 27^o$, E_f/E_i= 0.60 for θ_{spec}) and platinum (FWHM $\cong 34^o$, E_f/E_i= 0.66 for θ_{spec}) show how unconventional the H-covered Ru(0001) surface behaves. A satisfactory explanation for these combined features has not yet been given, but when relating to the hard cube model, the energy distributions point to an effective surface mass as high as three times the Ru atom weight of 101 amu. We previously suggested this to be accomplished by a *stiffening* of the surface lattice layer by the adsorbed hydrogen atoms [10]. Recent time of flight experiments on the clean Ru(0001) surface [4](Chapter 5) however reveal similar small energy losses (E_f/E_i= 0.90 for specular scattering), while the scattered flux is diffusely spread over a 27^o wide angular distribution, as to be expected for reactive scattering from the 1.5 eV deep chemisorption well. Apparently the turning point of the scattering trajectories lies relatively far from the surface. Knowing that the elasticity has to be a feature of the Ru substrate, the strong reduction of corrugation has to be attributed to the *smoothing* of the potential energy surface by the hydrogen atoms. This is confirmed by similar experiments using other gases, like N_2 [53], CH_4 and CO [68, 67] on this H-covered Ru(0001) surface, showing a remarkable correspondence in the scattering channel. The CO/Ru-H angular distribution for example, is indistinguishable from that of NO.

While the hydrogen overlayer has a drastic influence on the angular spread, the high initial sticking coefficient ($S_0 > 0.90$) is less dramatically affected, remaining between 0.20 at thermal energies to 0.60 (E_i= 2.1 eV) for NO/Ru-H [10]. When considering the rotational excitation, the question arises if the (1×1)H-overlayer switches off the rotational anisotropy in the gas surface interaction potential. The combined *inert* scattering and *reactive* sticking of this system gives us essentially three possi-

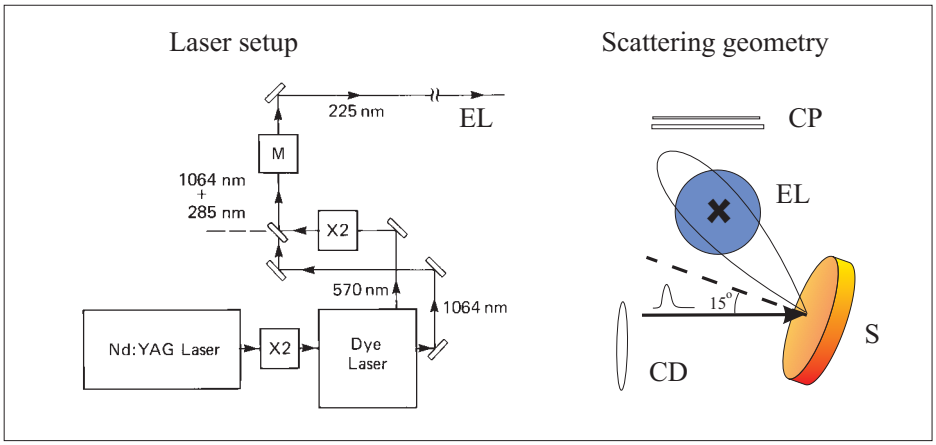

Figure 7.1: *Schematic representation of the laser setup and scattering geometry used to perform (1+1) resonance enhanced multi photon ionisation (REMPI) on a chopped (CD) molecular NO beam scattered from the hydrogen covered Ru(0001) surface (S). As shown in the left panel, the excitation laser (EL) emerges from a Nd:Yag pumped dye laser (Quanta-Ray, DCR2/PDL1) which is frequency doubled (×2) and mixed (M) with residual 1064 nm light to provide 1-2.3 mJ, ∼8 ns pulses of tunable radiation with a bandwidth of ∼0.5 cm^{-1} at a repetition rate of 10 Hz [65]. Ions are detected by multi channel plates (CP).*

ble scenarios: **1**) No surface corrugation nor rotational anisotropy. The gas-surface interaction is purely repulsive. Molecules that make it over the (activated) chemisorption barrier stick. The rotational excitation will be extremely small. **2**) No surface corrugation but substantial rotational anisotropy. The interaction still is repulsive. The ellipsoid or *egg*-shaped molecule bounce of a flat surface resulting in pronounced rotational rainbows [34]. **3**) The chemisorption well is partially probed. The interaction is not just repulsive, resulting in strong rotational excitation and *scrambling* by the attractive potential, leading to Bolztmann distributions with high rotational temperatures.

In this paper the rotational excitation of NO molecules and its influence on the angular spread is discussed. We report substantial rotational excitations very comparable to the *inert* NO/Ag(111) system [35, 65].

7.2 Experimental

The experimental facilities for this study were provided by IBM Almaden Reasearch centre. The apparatus has been described previously [65]. In short the system consists of a 4-stage molecular beam source connected to a 320 l scattering chamber (see

also Fig. 5.1), combined with a UV laser. Time of flight (TOF) experiments were performed using a rotatable doubly differentially pumped QMS (Nuclear Instruments Extrel). For the resonance enhanced multi phonon ionisation (REMPI) study, the incoming angle $\theta_i = 15^o$ was obtained by tilting the sample backwards causing the scattering plane to be vertical.

The excitation laser and scattering geometry are schematically shown in Fig. 7.1. The (REMPI) detection scheme is based on the one-photon resonance to the NO $A^2\Sigma^+$ state using laser light of ~225 nm, followed by ionisation through absorption of a second photon. Collection of the ions done by multi channel plates. The laser spot has a diameter of about 8 mm and is positioned at ~15 mm from the surface. Due to the small width of the angular distribution this provides an angle integrated measurement. No attempts have been made to collect time of flight information.

The Ru(0001) surface was prepared using standard polishing techniques and further cleaned by argon sputtering. The miss cut of the ruthenium crystal was checked using von Laue diffraction and was determined to be $<0.5^o$. Contamination was monitored with Auger Electron Spectroscopy. Sputtering 20 minutes at 2 μA was sufficient to obtain almost oxygen free spectra with excellent agreement to the reference data. Standard flashing of the sample in an oxygen background ($5{\cdot}10^{-8}$ mbar) was performed to remove possible carbon atoms not visible by AES because of overlapping peaks [10]. The H-overlayer on the Ru(0001) surface was obtained by dosing >50 ML [29] with a second beam line.

The translational energy of the beam was varied by seeding in H_2 or He combined with resistive heating of the stainless steel nozzle. At ~600 K water was formed in the nozzle from a reaction NO with H_2. Because of the non zero sticking coefficient for NO, care was taken to ensure nearly zero NO coverage limit. A one-slit chopper and a fast beam flag were used to minimize the NO dose per laser shot. Typically the intensity of the rotational lines did not vary more than 10% after 30 minutes of measuring. The spectra were obtained in several fractions. In order to correct for fluctuations in laser output, dependence of the intensity on laser power was determined for several transition to be $I_{corr} \simeq I_{raw} \cdot P^{1.15}$.

Assigning these corrected spectra was done by comparing peak position with simulated spectra. Subsequently the intensities were determined by manually measuring the peak heights and estimating the base line and error bars. This allowed reasonable analysis of the lower J-states of which the lines are mostly not totally resolved. The R_{11}+Q_{21} and the Q_{11}+P_{21} transitions seem hardly saturated; the rotational distributions show approximately the same maximum intensity. We corrected the relatively lower ion yield $I(J)$ for the R_{21} branch by invoking a Höhn-London dependence in the saturation. This gives a correction $I_{HL}(J) = I(J)/(1 - e^{-C \cdot HL_{R_{21},J}})$ in which C stands for the saturation parameter. A value of approximately 8 was chosen as to obtain the same maximum intensity in the fitted Boltzmann distributions for all three analyzed braches (Section 7.3).

Incidence energy	R_{21}	$R_{11} + Q_{21}$	$Q_{11} + P_{21}$
$E_i = 1.5$ eV	850 K	850 K	900 K
$E_i = 0.70$ eV	500 K	470 K	480 K
$E_i = 0.32$ eV	400 K	400 K	430 K

Table 7.1: *Rotational temperatures ($< T_{rot} >$) derived from the three REMPI spectra by fitting Boltzmann curves through the first 20 J-numbers (Fig. 7.2).*

7.3 Results and Discussion

Three rotational (REMPI) spectra of NO molecules scattered from the Ru(0001)-(1×1)H surface for the initial energies of 0.32, 0.70 and 1.50 eV (θ_i= 15^o) are depicted in Fig. 7.2. In contrast to expectations based on the elastic scattering already reported for higher incoming angles (Chapter 6 of this thesis), the currently reported rotational distributions show considerable population of relatively high rotational states. Boltzmann curves are fitted through the first 20 J-numbers yielding rotational temperatures ($< T_{rot} >$) of 400 K, 500 K and 850 K for the R_{21}-branch. At higher J-numbers considerable deviations from these Boltzmann curves are observed which are attributed to the presence of rotational rainbows [34, 33, 46]. Keeping in mind that such rainbows are generally observed for specific, super-specular outgoing angles, the clear presence in our angle integrated measurements are indicative of very pronounced rainbow scattering.

The dependence of the rotational temperature of the scattered molecules on initial energy (E_i) is summarized in Table 7.1 and graphically represented in Fig. 7.3. A linear fit of the form $< E_{rot} > = \alpha \cdot (E_i + \epsilon)$ makes comparison to other systems possible. The inclination α denotes the efficiency of conversion of translational to rotational energy. In an earlier paper, Kleyn *et al.* interpreted ϵ as the effectively experienced well depth. Later theoretical work however showed this to lead to overestimated depths. The results of similar fits for the NO/Ag(111) and NO/Pt(111) systems are shown in Table 7.3. There is a very close similarity between our NO/Ru(111)-H and the *inert* NO/Ag(111) system, with α even slightly higher for Ru-H. Both have a much smaller efficiency for kinetic to rotational energy transfer than observed for the *reactive* NO/Pt(111) system. The (general) mechanism behind the narrowing of the angular distribution by the H-overlayer clearly does not annul the rotational excitation. While the lateral corrugation of the PES is strongly reduced, the molecular anisotropy remains substantial. Still, the rotational energy is only a small fraction of the amount of translational energy lost. The 9% energy loss quoted (θ_i= 60^o, E_i= 2.1 eV) accounts for the specular direction only, while integration over the entire angular distribution adds up to an average of about 18%. Smaller incoming angles lead to lower values of E_f/E_i and even more energy transfer to other degrees of freedom. Though 82% energy conservation still is amazingly high, the majority of the

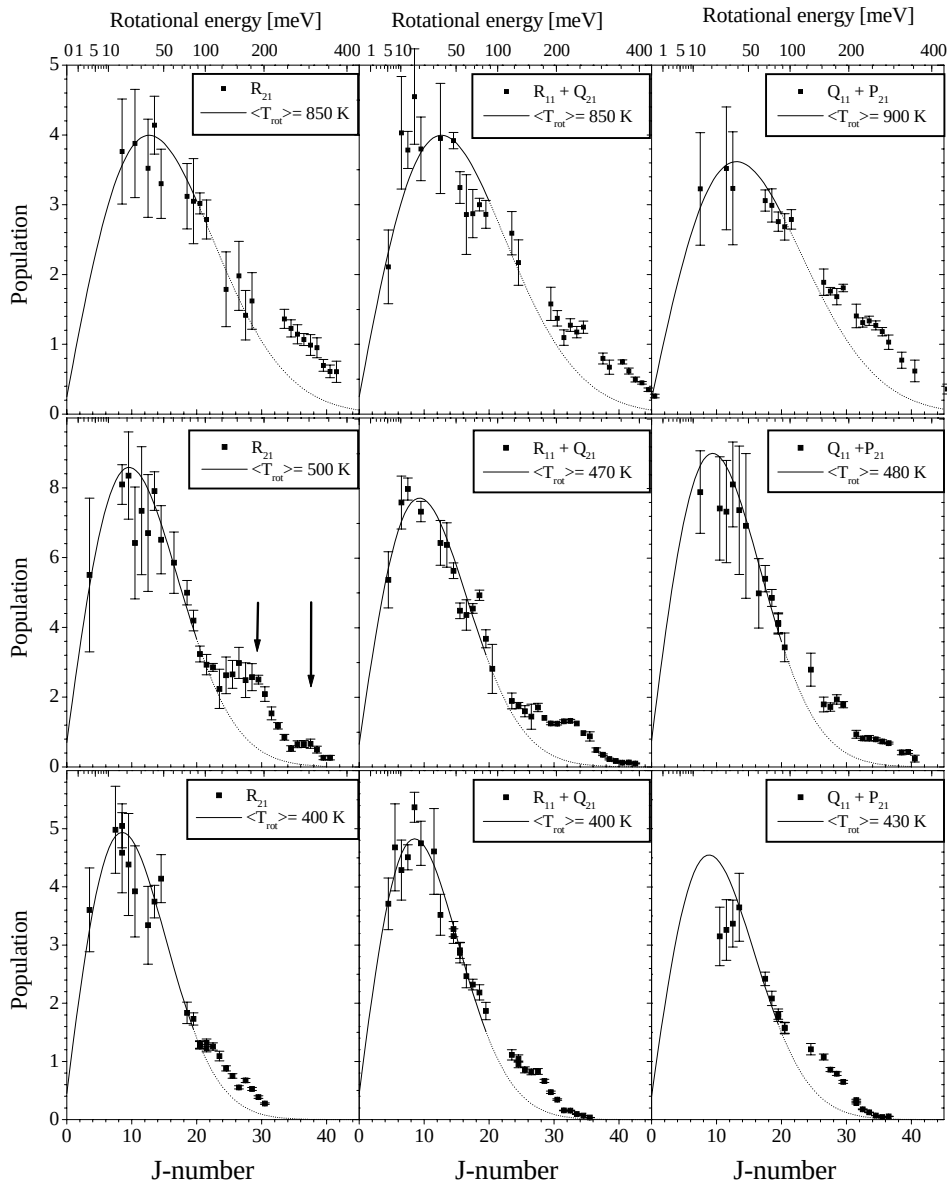

Figure 7.2: *Angle integrated rotational distributions of NO molecules scattered from the Ru(0001)-(1×1)H surface for three different beam energies: 1.5 eV (top row), 0.7 (middle) and 0.3 eV (bottom) at T_s= 85 K and θ_i= 15°. Boltzmann curves are fitted through the first 20 J-numbers to obtain average rotational temperatures (< T_{rot} >). The deviations at higher J-numbers are assigned to rainbow scattering.*

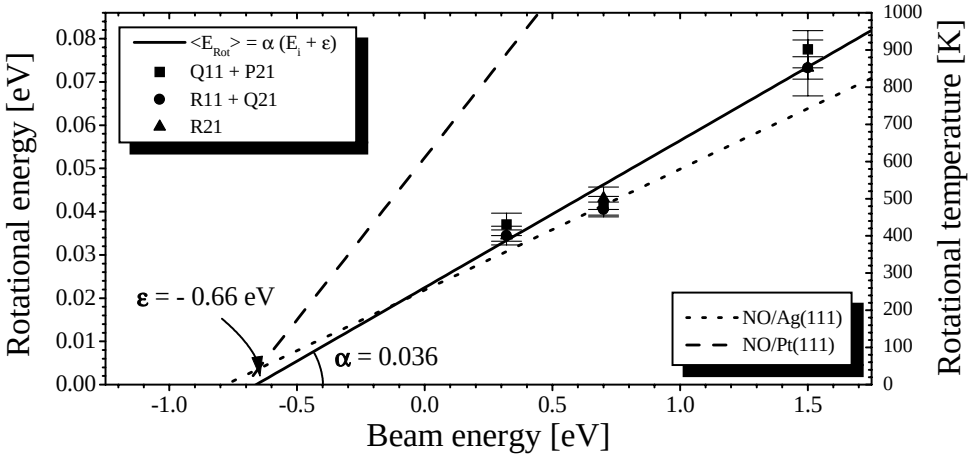

Figure 7.3: *Average rotational temperature* $< T_{rot} >$ *vs. beam energy for three different branches* (Q_{11}, R_{11} *and* R_{21}). *A linear dependence is suggested by fitting with* $< E_{rot} >= \alpha \cdot (E_i + \epsilon)$. *While the interpretation of* ϵ *is not clear, parameter* α *gives the efficiency for conversion of translational to rotational energy. Also shown are the result of similar fits for the Ag(111) (dotted)[35] and Pt(111) systems (dashed)[90].*

$(0.18 \cdot 2.1$ eV $\simeq)$ 0.4 eV energy is transferred to the crystal lattice, clearly consistent with the observed rotational temperatures of ∼1000 K ($< E_{rot} > \cong$ 86 meV). For the NO/Ag(111) system this transfer is much larger (typically about 40% at $\theta_i = 60^o$), even though the molecular chemisorption well is believed to be shallow. This provides additional evidence to support the conjecture of the extreme separation between scattering, dominated by the repulsive potential, and sticking in the deep chemisorption well. These two channels are most likely impact site dependent (see Chapter 8).

As mentioned in section 7.2, the incoming angle for this REMPI study was limited to $\theta_i = 15^o$. The previously reported angular and energy distributions however were taken at $40^o \leq \theta_f \leq 70^o$ with $\theta_i + \theta_f \geq 60^o$ [10]. It was shown that the angular distribution broadens upon a decrease in the incoming angle, combined with an increase

System	Authors	Ref.	α	ϵ [eV]
NO/Ag(111)	Kleyn *et al.*	[35]	0.028 ±.002	-0.78 ±.08
NO/Ru(0001)-(1×1)H	This paper	[-]	0.034 ±.003	-0.66 ±.15
NO/Pt(111)	Wiskerke *et al.*	[90]	0.075	-0.70

Table 7.2: *The linear dependence of rotational energy on initial energy,* $< E_{rot} >= \alpha \cdot (E_i + \epsilon)$, *compared to other systems.*

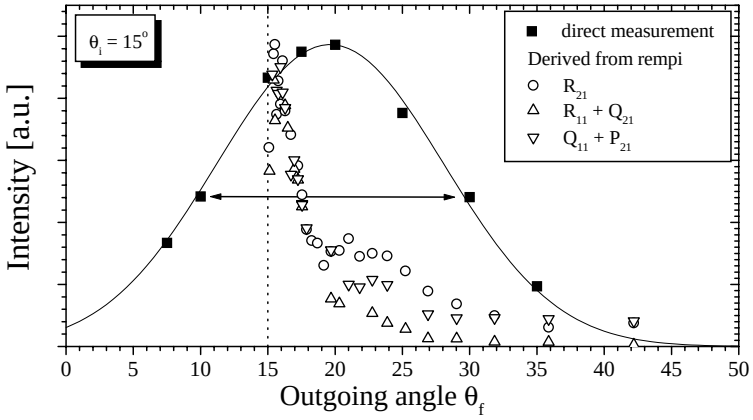

Figure 7.4: *The directly determined angular distribution ($\theta_i = 15^o$, $E_i = 0.25$ eV), compared to those derived from the REMPI-data. Parallel momentum conservation is assumed. The solid line is drawn to guide the eye only. The vertical dashed line indicates the specular scattering direction ($\theta_f = \theta_i = 15^o$).*

in the energy transfer to other degrees of freedom, like rotational energy [10]. This wider angular spread has also been observed for NO/Ag(111) by Rettner *et al.* [65]. Measurements for 0.98 eV NO (J=$\frac{1}{2}$) show an increase in the FWHM from $\sim 26^o$ to $\sim 46^o$ upon changing the incoming angle from 45^o to 30^o. Using the second (hexapole) beam source on the FOM beam machine, mounted 45^o with respect to the conventional beam source [7](Chapter 8). This molecular beam produces rather low energy molecules and does not provide TOF-resolution,. The FWHM of the angular distribution for $\theta_i = 15^o$ and $E_i = 0.25$ eV is determined at $\simeq 20^o$ (Fig. 7.4). Substantially wider than the before mentioned 8^o, this is consistent with the observed trend and still remarkably narrow. Fig. 7.4 also shows the super-specular broadening of the angular distribution assuming the collisions to obey parallel momentum conservation, and the rotational excitation to be solely at the expense of the normal momentum. Clearly the rotational excitation play only a minor role in the angular broadening. Since the low surface temperature excludes large thermal roughening, surface corrugation has to account for most of the angular spread.

Returning to the three different scenarios suggested for the PES (Introduction), we can exclude alternative **1**; the effective smoothing of the surface corrugation by the hydrogen overlayer is not accompanied by cancellation of the molecular anisotropy. Rotational excitations, solely according to alternative **3**, i.e. excitation through the molecular chemisorption well, would most probably result in higher rotational temperatures and scrambling of the pronounced rotational rainbows. Scattering from the edges of the chemisorption well is very realistic though, be it that the low rotational temperatures primarily suggest scattering from a rather flat repulsive potential (**2**).

This conclusion is very similar to observations of Tenner *et al.* [82] on the NO/Ag(111) interaction potential.

7.3.1 Possible double rainbow

Much to our surprise, the R_{21}-branch of Fig. 7.2 shows a double peak structure at $J = 29\frac{1}{2}$ and $37\frac{1}{2}$. This theoretically predicted effect has not been experimentally observed before despite attempts from Rettner *et al.* for NO/Ag(111) [65]. Quantum calculations by Lemoine show that *inclusion of the corrugation strongly attenuates the interference structures due to the rotational rainbows* [12]. This suggest the now possibly observed double rainbow from the Ru(0001)-(1×1)H to be related to the much smaller surface corrugation than that of Ag(111). This is nicely consistent with the narrow angular distributions observed for this NO/Ru-H system (FWHM of about 8^o) (Chapter 6). Disturbing is the absence of a double feature in the well accessible R_{11}-branch while the information in each branch is usually expected to be similar. Earlier calculations by Lemoine *et al.* [43] however show considerable differences per branch.

Though it's tempting to claim the first observation of quantum interferences for the scattering of a 'heavy' molecule in surface scattering, more data is needed to do so.

7.4 Conclusions

The rotational distributions observed for the NO scattering of the Ru(0001)-(1×1)H surface are clearly not unprecedentedly cold, despite the earlier reported unusually narrow angular distributions. While the strong reduction of the Ru(0001) surface corrugation by the (1×1)H-overlayer seems apparent for a range of gases, the considerable rotational temperatures indicates the persistence of the molecular anisotropy. The rotational excitation efficiency is very much comparable to the NO/Ag(111) system which indicates the excitation to occur on a similar hard potential. Since the NO/Ag angular and energy distributions differ substantially, these measurements demonstrate molecular anisotropy and surface corrugation to be largely decoupled.

Chapter 8

Steric asymmetry of NO scattering on Ru(0001)-(1×1)H

Molecular orientation dependence in the scattering of NO from (1×1)H covered ruthenium (0001) surface has been observed. The scattering of this system has previously been shown to result in extremely narrow angular distributions. With a hexapole beam source we discriminate contributions of the two molecular orientations. The O-end down molecules yield a relatively narrow angular distribution. The N-end down molecules scatter broader and are only slightly super specularly shifted with respect to the O-end collisions. While the centre of the angular distribution is dominated by the inert O-end collisions, this situation is reversed in the wings, resulting in changes of the sign of the steric asymmetry, $R = 2 \cdot [I^- - I^+]/[I^- + I^+]$*, which are very symmetric around the specular direction. The magnitude of* R *is found to increase with incoming angle, ranging from 0.05 to 0.15 for* $20^o \leq \theta_i \leq 60^o$*, while the width of the angular distributions decreases. This points to a minor contribution of the molecular anisotropy to the angular spread. Using a double-cosine fit, two scattering channels are separated; one preferentially specularly scattered, emerging from relatively* flat *parts of the unit cell and a broader and super specular shifted scattering channel of an intermediate* corrugated *region.*

8.1 Introduction

Over the past decades, the fundamentals of surface chemistry have been studied for systems widely varying in reactivity. The scattering of particles from a potential energy surface with or without a chemisorption well gives much insight in the behavior of reactive vs. inert systems. In order to discriminate different interaction mechanisms, scattering experiments have been designed to control an increasing amount of collision parameters. The use of nitric oxide (NO) has always been widespread for its outstanding properties in laser spectroscopy; this molecule allows (relatively) easy determination of it rotational distribution. Additionally the $^2\Pi_{1/2}$ state can be oriented by the combination of a hexapole state selective electrostatic lens and an orientation field. State to state scattering of NO on Ag(111) has first been performed by Tenner and Geuzebroek [81, 19]. These steric measurements allow very direct comparison of the interaction of two end of the molecule with the surface. The steric asymmetry in the scattered intensity is defined as $R = 2 \cdot [I^- - I^+]/[I^- + I^+]$, with I^- and I^+ the scattered intensities with negative or positive orientation field, respectively (see experimental section 8.2). There are several situations that lead to $R \neq 0$. Shifts in the angular distribution due to e.g. different rotational excitations for the two sides of the molecule. These shifts will lead to $\int_{-\frac{\pi}{2}}^{\frac{\pi}{2}} R(\theta_f) \cdot I(\theta_f) d\theta_f = 0$, with $I(\theta_f) = I^-(\theta_f) + I^+(\theta_f)$. In case of selective removal, as is the case for NO/Pt(111), this integral will be unequal to zero [18].

We have previously shown the NO/Ru(0001)-(1×1)H system to contain a peculiar combination of an extremely inert scattering channel as well as a ∼50% sticking channel [10]. Especially the very small width of the angular distribution (FWHM of only 8^o at $\theta_i = 60^o$ and $E_i = 2.1$ eV) indicates effective smoothing of the interaction potential by the hydrogen overlayer as associated with inert scattering of a flat and hard surface. Surprisingly, the scattered molecules hardly appear to be affected by the presence of the chemisorption well. In a later study we characterized the rotational excitation [5] (Chapter 7) to be relatively large, i.e. very similar to the NO/Ag(111) system. This observation reveals the considerable rotational anisotropy of the NO molecule on this almost uncorrugated surface, a combination which makes it interesting to study the contributions of the two ends of the molecule to the broadening of the angular distribution.

In this paper we present a study on the difference in interaction of the two ends of the NO molecule in the scattering from the H-covered Ru(0001) surface. A model will be presented separating the gas-surface interaction in three channels. Besides the sticking, the scattered flux is separated in two contributions; one component scattered from the smoothest part of the unit cell, and the other from a more corrugated region around the edges of the chemisorption well. A model of the surface unit cell can in principle be constructed from a quantitative analysis of the orientation dependence of the relative amplitudes of these channels.

8.2 Experimental

The UHV scattering setup and sample preparation have been described in detail in a number of earlier studies [58] and the previous chapters of this thesis. In short it consists of a main chamber with a base pressure of $1 \cdot 10^{-10}$ mbar, which contains the sample, mounted on a 3-axis goniometer [59] enabling the study of azimuthal dependencies. For this study we used the hexapole beam source which produces state selected ($^2\Pi_{1/2}$) NO-molecules. The second of three differential pumping stages contains six 1 meter long rods, of 4 mm diameter, in a hexapole configuration, separated 2 mm from each other. A pulsed valve (General Valve with a 100 μm orifice at a repetition rate of 40 Hz) is used to produce NO molecules in the J = $\frac{1}{2}$ rotational state with energies up to $\simeq$ 0.25 eV. Orientation of the molecules takes place in the last 10 mm of flight before impact by through the application of an electric field of 12.5 kVcm^{-1}. At this field strength the effective orientation is about 90% [80]. A positive high voltage results in the N-end of the NO molecule being preferentially directed towards the surface. The degree of orientation depends on initial energy according to the following expression: $< \cos\gamma_E > = \frac{M\Omega}{J(J+1)}$ [80]. A quadrupole mass spectrometer QMS (Extranuclear Labs.) is mounted on a doubly differentially pumped rotatable cover in order to provide angular resolution. The scattered intensity for the two orientations of the molecule is measured by switching the high voltage on the orientation pole each 100 pulses. Care was taken to make sure the total NO dose did not yield more than only a couple of percents coverage.

8.3 Results and discussion

Angular distributions obtained for the scattering of preferentially oriented NO molecules of the Ru(0001)-(1×1)H surface are shown in Fig. 8.1. For a 0.15 eV beam, data taken for incoming angles of θ_i= 20^o, 40^o and 60^o. For this last outgoing angle also a higher energy molecules ($E_i \simeq$ 0.25 eV) have been scattered. The angular distributions obtained for the O-end vs. N-end down scattering are shown in the left panel. The differences in the two distributions might seem subtle, but these values are not corrected for the orientation probability distribution $< \cos\gamma_E >$ which especially affects the higher energy data. In an earlier study this was corrected for [19]. We however made no such attempts since the rotational state distribution of the molecular beam is not accurately known.

The scattering of O-end down oriented molecules (I^-) dominates in the specular direction. The broader angular spread of N-end collisions (I^+) leads to a higher yield in the wings. This shift, upon changing orientation, results in a change of sign in the steric asymmetry R ($= 2\cdot[I^- - I^+]/[I^- + I^+]$), as depicted in the right panel of Fig. 8.1. The curve plotted is R generated from the cos^n-fits (using this same relation). The broader N-end distribution is consistent with particles probing the deeper molecular chemisorption well, consistent with the known N-end down molecular chemisorption

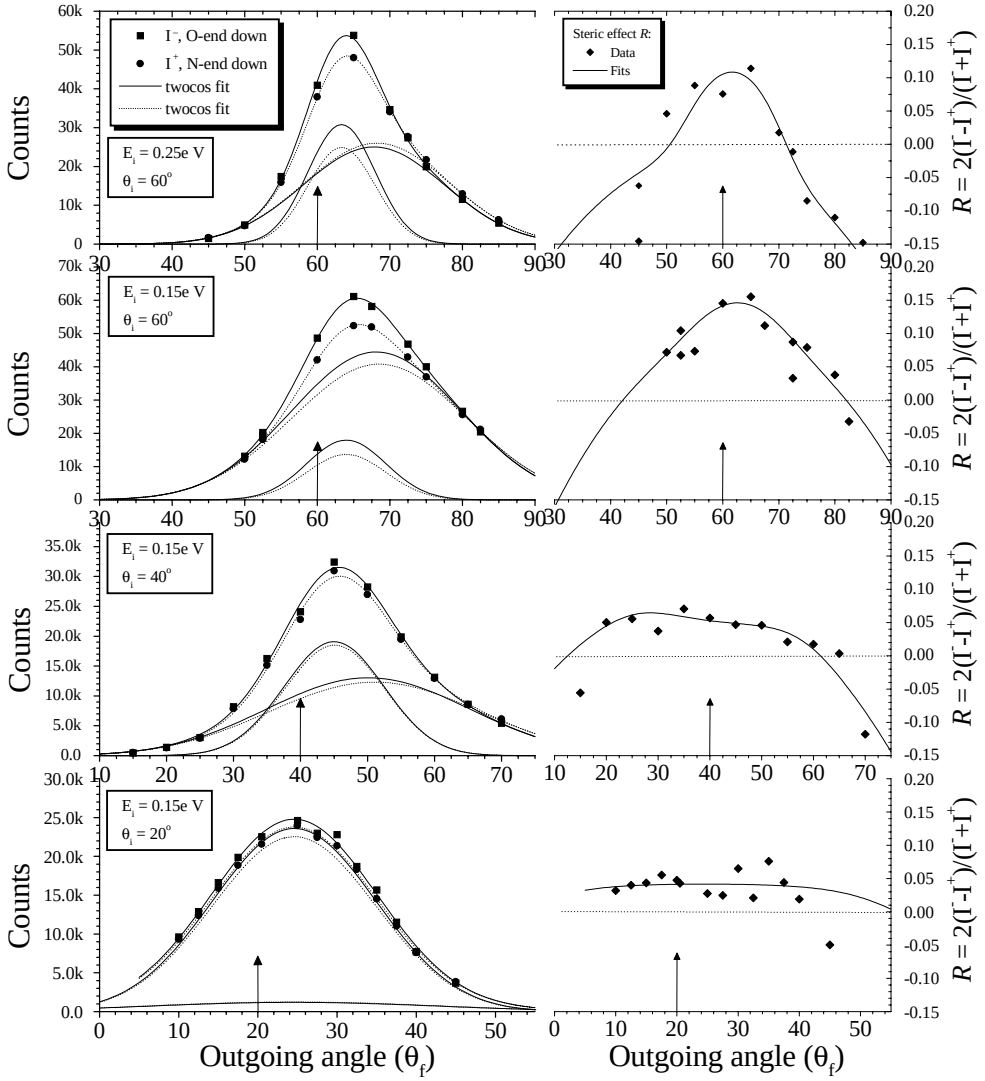

Figure 8.1: *Angular distributions (left column) and steric asymmetry (right column) $R = 2 \cdot (I^- - I^+)/(I^- + I^+)$ for preferentially oriented NO, scattered from Ru(0001)-(1×1)H (θ_i= 20°, 40° and 60° for $E_i \simeq 0.15$ eV and θ_i= 60° for $E_i \simeq 0.25$ eV). Vertical arrows indicate the specular scattering direction ($\theta_i = \theta_f$). No correction has been made for changes in beam intensity or detector settings. The angular distributions are each fitted by a double cosines as defined in Eqns. 8.1 and 8.2 in order to disentangle the contributions from relatively flat or corrugated regions of the unit cell. Table 8.1 contains the results of this procedure. Clearly the O-end down oriented molecules yield a higher intensity in the specular direction (I^-) while the broader N-end scattering dominates the wings of the distribution. This results in the change in the sign of R (right column).*

θ_i	$E_{i\,[\mathrm{eV}]}$	HV	A_F	θ_F	n_F	A_C	θ_C	n_C	$\Phi_{F\,[\%]}$	$\Phi_{C\,[\%]}$	$\Phi_{T\,[\%]}$
60^o	2.1	0	0.028	62.2	377	0.010	62.2	57.9	52.4	47.6	100
60^o	0.25	-	0.573	63.4	153	0.466	67.8	34.1	18.9	32.0	50.9
60^o	0.25	+	0.514	63.4	153	0.536	68.2	32.8	15.3	33.8	49.1
60^o	0.15	-	0.296	64.0	110	0.733	68.1	24.3	8.60	43.7	52.3
60^o	0.15	+	0.259	64.0	110	0.775	68.6	22.7	6.54	41.2	47.7
40^o	0.15	-	0.606	45.1	59.0	0.414	50.1	14.5	22.1	28.7	50.9
40^o	0.15	+	0.616	45.1	59.0	0.410	51.1	13.4	21.4	27.7	49.1
20^o	0.15	-	0.952	24.6	30.9	0.048	24.6	10.0	47.3	3.69	51.0
20^o	0.15	+	0.950	24.6	30.9	0.052	24.6	10.0	45.2	3.83	49.0

Table 8.1: *Results of the two-cosine fits as defined in Eqns. 8.1 and 8.2. The last three columns show the integrated flux expressed in percentages of the total flux, i.e.* $\int_{-\pi/2}^{\pi/2} I^+(\theta_f) + I^-(\theta_f) d\theta_f$.

configuration [22].

We introduce a two-channel scattering mechanism assuming the reflective part of the unit cell to be divided in a two regions: one relatively flat heavy (*inert*) and the other more corrugated with larger normal momentum transfer (*reactive*). We propose these two surface areas, as well as the size of the chemisorption well, to depend on molecular orientation. In order to disentangle the angular distributions for the two preferential orientations (I^- and I^+) we fit the curves with a two-cosine function:

$$I^+(\theta_f) = A_F^+ \cos^{n_F}(\theta_f - \theta_F) + A_C^+ \cos^{n_C}(\theta_f - \theta_C) \tag{8.1}$$

$$I^-(\theta_f) = A_F^- \cos^{n_F}(\theta_f - \theta_F) + A_C^- \cos^{n_C}(\theta_f - \theta_C) \tag{8.2}$$

In fitting the distributions (I^- and I^+), we tied the peak position (θ_F) and width (n_F) of the contribution from the flat (F) area, while width and position of the corrugation related cosine were allowed to variate freely. *Runaways* for the θ_i= 20^o distributions demanded n_C to be set manually. The values resulting from this procedure are given in Table 8.1. Differences in the amplitudes reveal the changes in the effective surface area of the three proposed channels. Especially for the E_i= 0.25 eV data a clear shift in the populations of the scattering can be observed from narrow (A_F^-) to broad (A_C^+), when switching the orientation field from negative to positive HV. Integration of the two cosine functions for a given molecular orientation ($\Phi_F^\pm$, $\Phi_C^\pm$) shows relative contributions to the total in-plane flux ($\Phi_T^\pm$). In order to compare the fluxes from all four channels (double cosine for two orientations) we normalized each cosine to the total in-plane flux, i.e. $\Phi_T^- + \Phi_T^+ = 100\%$ (see Table 8.1). The contributions of the two orientations to the total scattered flux (Φ_T^- and Φ_T^+) are almost equal, excluding a large steric asymmetry in the sticking channel.

The magnitude of the steric asymmetry R increases with larger incoming angle as

shown in Fig. 8.1. The maximum R, positioned at a slightly super specular scattering angle, increases from $R = 0.05$ at $\theta_i = 20^o$ to 0.15 at $\theta_i = 60^o$. Consistent with earlier observed trends [10], we can see the angular distribution narrowing. These two trends appear to be contradicting; on the one hand the narrowing of the angular distribution upon increasing the incoming angle (θ_i) seems to indicate a decrease in the experienced surface corrugation, while on the other hand the steric asymmetry, the effective molecular anisotropy, becomes larger. This increase of experienced molecular anisotropy is expected to broaden the angular distribution, but apparently the balance between the increasing anisotropy and the decrease in the experienced surface corrugation is in favor of the latter.

The symmetry of R around the specular is remarkable, especially when comparing to the steric asymmetry curves as determined for the NO/Ag(111) and the NO/Pt(111) systems. In these cases the asymmetry is caused by the larger rotational excitation of the O-down oriented molecules, resulting in increased super specular shifts. In the Ru-H case, flipping the orientation of NO leads to symmetric changes in the spread of scattered particles. This symmetry of R indicates rotational excitation to be similar for both sides of the molecule. This is surprising, for the generally the NO molecule is found to exhibit more of and *egg* shape than an ellipsoidal (American) *footbal* shape.

The observed molecular anisotropy is consistent with earlier measurements on the final rotational state distribution [5].

8.4 Conclusions

Molecular asymmetry has been observed in the angular distributions of preferentially oriented NO molecules, scattered of the Ru(0001)-(1×1)H surface. The NO molecules are preferentially specularly scattered for the *inert* O-end directed towards the surface vs. the more diffuse spread of the *reactively* scattered N-end down molecules. This confirms a very general conjecture between the *inertness/reactivity* of the interaction and the narrowness/broadness of the angular distribution. The observed symmetric behavior of the steric asymmetry R indicates the rotational excitation to be similar for the two ends of the molecule. Counter intuitively the steric asymmetry increases for larger incident angles while this does not result in broader angular distributions. Apparently the molecular anisotropy forms a minor contribution to the angular broadening when compared to the effect of the reduced effective surface corrugation.

Upon reversing the orientation of the molecules, the separation of the unit cell into two scattering regions shows the flat area to be effectively larger for N-end down molecules, while the more corrugated area dominates for the O-end particles. Integration of the in-plane flux changes suggest a minimal dependence of the sticking probability on molecular orientation.

Chapter 9

Orientation dependent sticking of NO on Al(111)

Preliminary results of a collaborating study on the initial sticking probability of oriented NO molecules on Al(111) are presented. The initial sticking coefficients for the O-end vs. N-end down, S_0^O and S_0^N respectively are shown to increase with incidence energy, as well as the relative difference $R = 2 \cdot [S_0^O - S_0^N]/[S_0^O + S_0^N]$.

Previous scanning tunneling microscopy (STM) and Auger electron spectroscopy (AES) studies indicate the dissociative sticking to result in excess oxygen on the surface. Abstraction of N-atoms has been posted as a likely process. In order to be consistent with the currently reported higher trapping probabilities for preferentially N-end down oriented molecules one has to picture the molecule flipping around after being captured in the molecular precursor state. The excess energy subsequently allows the ejection of the N-atom into the vacuum.

9.1 Introduction

The sticking of NO on Al(111) has recently received special attention. Partly this interest comes from its connection with the O_2/Al(111) discussion initiated by Brune *et al.* who claimed the observation of highly mobile *hot* oxygen atoms upon dissociation of thermal O_2 [9]. With scanning tunneling microscopy (STM), only randomly distributed O-atoms were observed, on average separated 80 Å from each other. From the absence of pairs of ad-atoms it was concluded that upon dissociation of an O_2 molecule, the two O-atoms on average move at least these 80 Å before their translational energy parallel to the surface is dissipated into the solid. This explanation has encountered some criticism and alternative explanations are investigated. Especially the possible ejection or abstraction of an O-atom into the vacuum, using the excess adsorption energy, is studied. The experimental data necessary to refute the original hypothesis seems conclusive. Preliminary results by Hasselbrink (Essen) *et al.* indicate successful REMPI detection of ejected O atoms from O_2 adsorption, despite spectroscopic difficulties, the low sticking coefficient of O_2 on Al(111) and the high background of O_2 gas. Accurate values of the initial (dissociative) sticking probability of O_2/Al(111) were determined by Österlund *et al.* [51]. They showed both translational and vibrational energy to enhance the sticking probability from $S_0 \simeq 10^{-2}$ at $\approx$ 30 meV till near unity for $E_i \simeq 0.6$ - 2.0 eV. The $\approx$1% sticking probability at thermal energies supports the idea of this sticking to be an exceptional event with limited phase space, with the molecular orientation possibly being an important parameter.

The recent interest in NO/Al(111) comes from the close analogy with the O_2 system, explaining why several groups are currently investigating the details of NO dissociation on Al(111). Using molecular beams to vary the incidence energy E_i of the NO molecules, Igor Zoric (Chalmers University of Technology, Göteborg), studied the dissociation process with the adsorption-reflection technique of King & Wells and Auger electron spectroscopy (AES). Quantitative analysis of the Auger spectra turns out to be difficult for this system because of the interference between Al_2O_3 and Al peaks. Despite these problems attempts are currently being made by Komrowski and Kummel (UCSD) and Igor Zoric to analyze spectra in order to produce plots of the ratio of nitrogen and oxygen ad-atoms vs. coverage. Attempts by Komrowski and Kummel (UCSD) to detect ejected N-atoms with a standard QMS system failed up till now due to experimental problems. Hasselbrink is working on N-atom detection using the above mentioned REMPI technique. Both Komrowski-Kummel [36] and Zoric-Kasemo [94] have observed that NO/Al(111) chemisorption results in a non-stoichiometric surface coverage; rich in O-atoms compared to N-atoms. Using Auger electron spectroscopy, Komrowski-Kummel determined this ratio to be $\Theta_N/\Theta_O \simeq 0.3$ - 0.5). However, this selectivity decreases rapidly with coverage and may be greatly affected by the surface roughness. Even without the full characterization of these details it is to be expected that if NO/Al(111) abstracts, then O_2/Al(111) probably does too, thereby directly explaining the randomly distributed O-atoms observed by Brune *et al.* [9].

The excess oxygen in the ad-layer could could, besides to abstraction of N-atoms, also be due to N_2O_g formation. This reaction $2NO_{ads} \rightarrow N_2O_g + O_{ads}$ is known to occur at higher coverages and temperatures on Al. Pashutski *et al.* [54] showed the formation of N_2O on an Aluminum surface. At high exposures of thermal NO the catalytic activity of the 80 K Al(100) surface enabled the following reaction: $NO_{ads} + N_{ads} \rightarrow N_2O_{ads}$. However, Komrowski *et al.* observe chemical selectivity at 300 K, with a maximum selectivity at minimum coverage. Since $2NO_{ads} \rightarrow N_2O_g + O_{ads}$ should be second order in NO coverage, it is expected to provide an ignorable contribution at the lowest coverage.

Prior to the collision an *harpooning* electron can transfer charge from the surface to the NO molecule. Both this transfer and the subsequent chemisorption will probably depend on molecular orientation since the lowest unoccupied molecular orbital (LUMO) on NO and NO^- lack inversion symmetry. It is likely that the sticking probability for NO/Al(111) favors a N-end first geometry since the N-end contains most of the LUMO. However, dissociation-abstraction probably does not occur until a second electron is transferred. Therefore the sticking probability will possibly have a different orientation dependence than the chemical selectivity.

In this chapter we present the results of a collaborative study with the group of prof. A.C. Kummel (UCSD) aiming to elucidate the effect of the (preferential) molecular orientation on the initial sticking probability of NO molecules impinging on Al(111). We have observed the N-end down orientation to be yield the higher sticking coefficient.

9.2 Experimental

The experiment has been described in detail in previous chapters (8), but recent modification enabled orientation dependent sticking probability measurements with very high sensitivity. Especially the purchase an new quadrupole mass spectrometer from ABB-Extrel (type MEXM060 2.9C3/4P8: $\frac{3}{4}$ inch rods, 2.9 MHz 300 W Q-head, off-axial cross beam ionizer in pulse counting mode) resulted in a large improvement in signal to noise. Differential pumping of this probe is possible by installation of the pump housing shown in Fig. 9.1 combined with a 260 ls^{-1} turbo molecular pump.

In short the hexapole beam source consists of a three pumping stages. In the source chamber, NO gas pulses are produced by expansion of mixtures of NO in He, Ne or Kr from a pulsed valve (General valve, 2 mm orifice). After a flight path of 200 mm, the second stage is entered through a 5 mm aperture. In this stage the electrostatic hexapole lens is entered, composed of six 1 m long rods of 4 mm diameter, mounted 2 mm from each other to yield in inner circle of 8 mm. Another 200 mm flight and a 6 mm diaphragm leads to the third 350 mm long chamber. The main chamber is then entered through a 100 mm long tube of 5 mm diameter entrance positioned at 470 mm from the sample. The hexapole lens only affects NO molecules in the ($J = \frac{1}{2}$) rotational ground state. Focusing or defocusing occurs, for the upper and lower

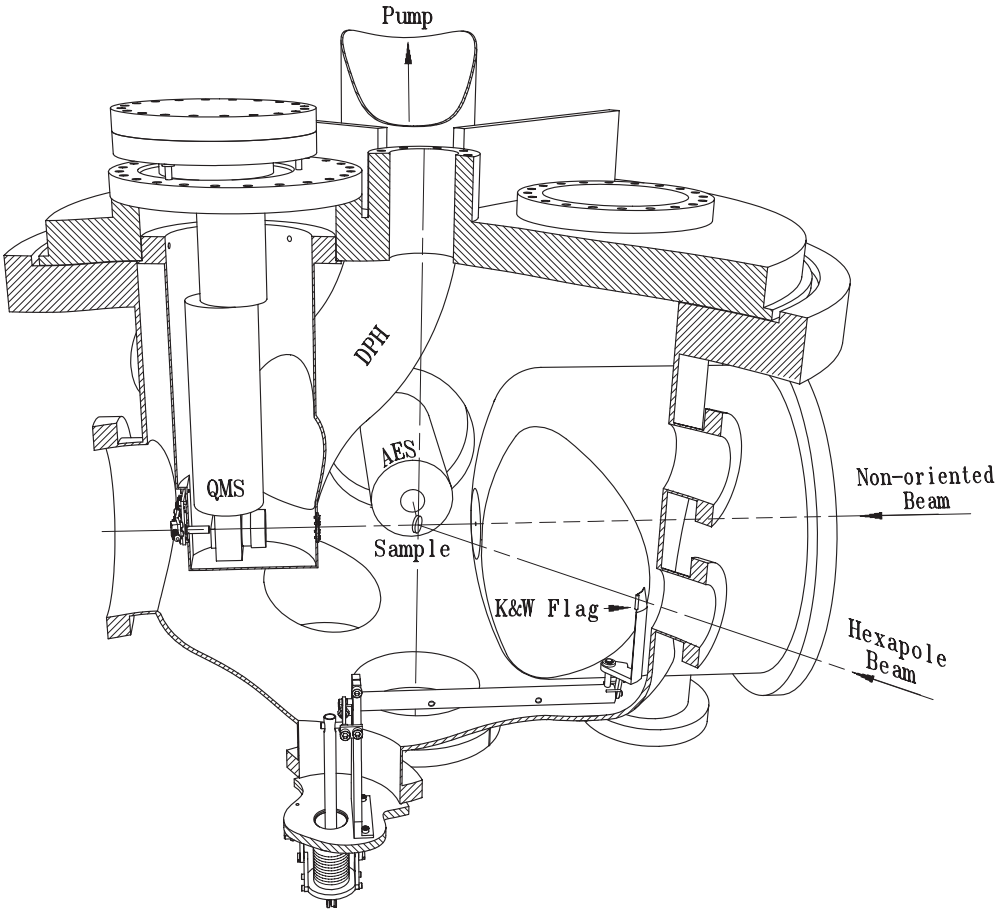

Figure 9.1: *Design for the mounting of the newly purchased QMS (ABB-Extrel). This probe is mounted on the main chamber through an adaptor flange which is height and tilt adjustable. Optimum differential pumping of the ionizer, essential for future scattering experiments, can be obtained when installing the differential pumping house (DPH). The large diameter tubing, aimed directly at the ionizer region, ensures maximum effective pumping speed. In order to enable sensitive angularly resolved desorption studies, the exit of this pump house can be closed by a shutter. The currently described sticking measurements demanded precise determination of the (changes in) NO partial pressure in the main chamber. We therefore discarded the differential pumping of the QMS. The pneumatic controlled K&W flag allows the state selected (hexapole) beam to be blocked. Sample cleanliness and ad-layer composition are checked with AES.*

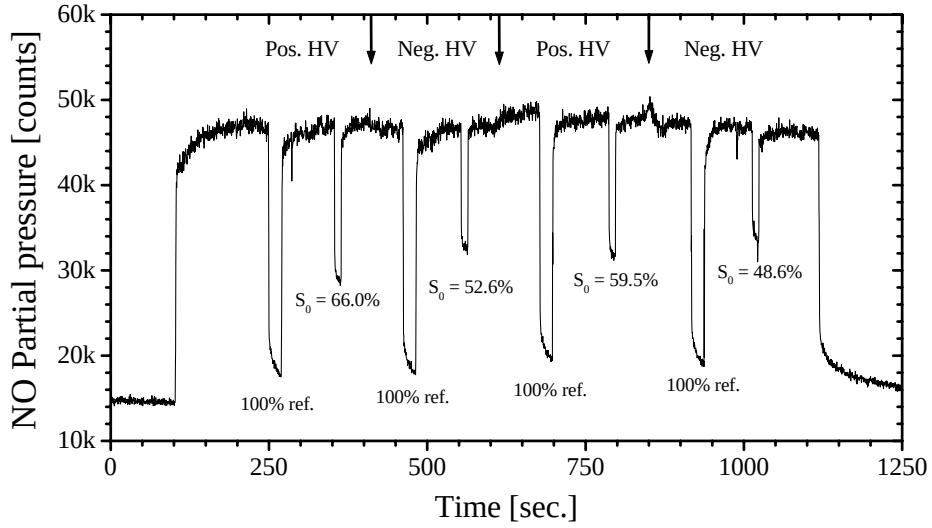

Figure 9.2: *Typical data of a King&wells sticking measurement for oriented molecules. Vertical arrows indicate the switching of the orientation voltage. Clearly the slow response of the vacuum chamber upon changes in the gas load can be observed. These deviations from the ideal K&W data are tackled using the analysis procedure described in Chapter 2.*

component of the Λ-doublet, respectively. Within the geometry described here, the maximum translational energy for which complete focusing can be achieved (0.3 eV) is limited by the breakdown voltage of the hexapole lens, approximately 30 kV. Applying a high voltage ($\simeq$15 kV/cm) to a vertical rod positioned approximately 10 mm from the surface, produces an electric field with respect to the sample (ground) plane which approximately 95% effective orients the NO molecules. This orientation of the NO molecules is not the ideal probability distribution, but one of preferentially oriented molecules $< cos(\gamma) >_E \simeq 0.95$, with γ being 0 and 1 for O-end vs. N-end down molecules, respectively [81]. Furthermore the hexapole electrostatic lens produces a distribution of J-states and Λ-doublets, resulting in a non-ideal orientation distribution. Especially considering the preliminary character of this thesis we permit ourselves to roughly estimate the beam 90% pure, resulting in $< cos(\gamma) > \approx 0.30$ ($\frac{1}{3}$ ideally). Together with the non-infinite orientation field this results in a correction according $R = C_{orr} \cdot R_{raw}$, with $C_{orr} = \cdot \frac{0.3333}{0.30 \cdot 0.95}$.

The ≈10 mm diameter Al crystal (Monocyrstals Company) is 99.999% pure and polished within 1^o of the (111) face. Pre-cleaning by 1.5 days of Ar^+ sputtering (3 kV at room temperature), was done at UCSD before shipping the sample to the FOM-Amolf. Further cleaning was done by sputtering with 1 keV Kr^+ ions ($\simeq$ 0.6 μA). Before annealing the crystal to 800 K, surface cleanliness was carefully checked with

Auger electron spectroscopy to ensure all oxygen was removed. Between measurements about 4 hours of sputtering was needed to obtain an atomically clean surface.

The orientation dependent initial sticking coefficients are determined with the *adsorption-reflection* technique of King and Wells [31, 32]. Since the combination of this technique with the hexapole beam source is new to us this required the construction of a K&W flag which can block the beam inside the main chamber (see bottom of Fig. 9.1). A typical measurement of the orientation dependent initial sticking probability is shown in Fig. 9.2. At $t = 100$ s the gate valve between source chamber and second stage of the beam line is opened to allow the beam to hit the K&W flag. The subsequent slow exponential partial pressure rise, due to trapping-desorption of NO molecules on the stainless steel chamber walls [3], is expected to equilibrate in $\sim$150 s. In order to mimic the situation for 100% sticking, the gate valve between source chamber and second stage of the beam line is closed. This provides an accurate reference since the effusive component of the beam was determined to be $\leq$0.1%. The sticking probabilities are obtained through a sequence of closing-opening the gate valve (20 s), retracting K&W flag allowing the beam to hit the surface (10 s) and switching the polarity of the orientation (high) voltage. In order to accurately measure the partial pressures of the main chamber we chose to exploit the much higher sensitivity of the Extrel-QMS by leaving out the differential pumping arrangement shown in Fig. 9.1. Without the shielding properties of this pump house however, the sensitivity of the QMS is influenced by the changes in high voltage orientation field; especially for the weaker NO/Kr beam this effect is $\simeq$20%. Therefore we measure the 100% sticking reference each time after switching the orientation field. In Fig. 9.2 this switching of the HV on the orientation pole is indicated by vertical arrows. In this configuration, the TMP on the top flange and the main TMP act together yielding a total effective pumping speed of about 600 ls^{-1}. No attempt has been made to detect the possible N_2O formation. For all sticking measurements the incoming angle θ_i has been kept constant at approximately 15^o. For closer to normal incidence angles the beam would be blocked by the orientation pole. Though these measurements are lengthy, contamination of the sample by the partial NO pressure rise in the chamber was minimal, as checked by AES. When the sticking coefficients within one measurement decrease because of built up coverage, these values are extrapolated to yield the initial sticking probabilities.

9.3 Results and discussion

The initial sticking coefficients for preferentially oriented NO molecules on the Al(111) surface, S_0^N and S_0^O, have been determined for three incidence energies (all at $\theta_i \simeq 15^o$). Results are summarized in Table 9.1 and shown in the top panel of Fig. 9.3. The preferred sticking geometry is N-end down, consistent with the suggestion made in the introduction of the LUMO being on the N-side of the molecule. This process however does not seem to critically dependent on orientation while even for preferen-

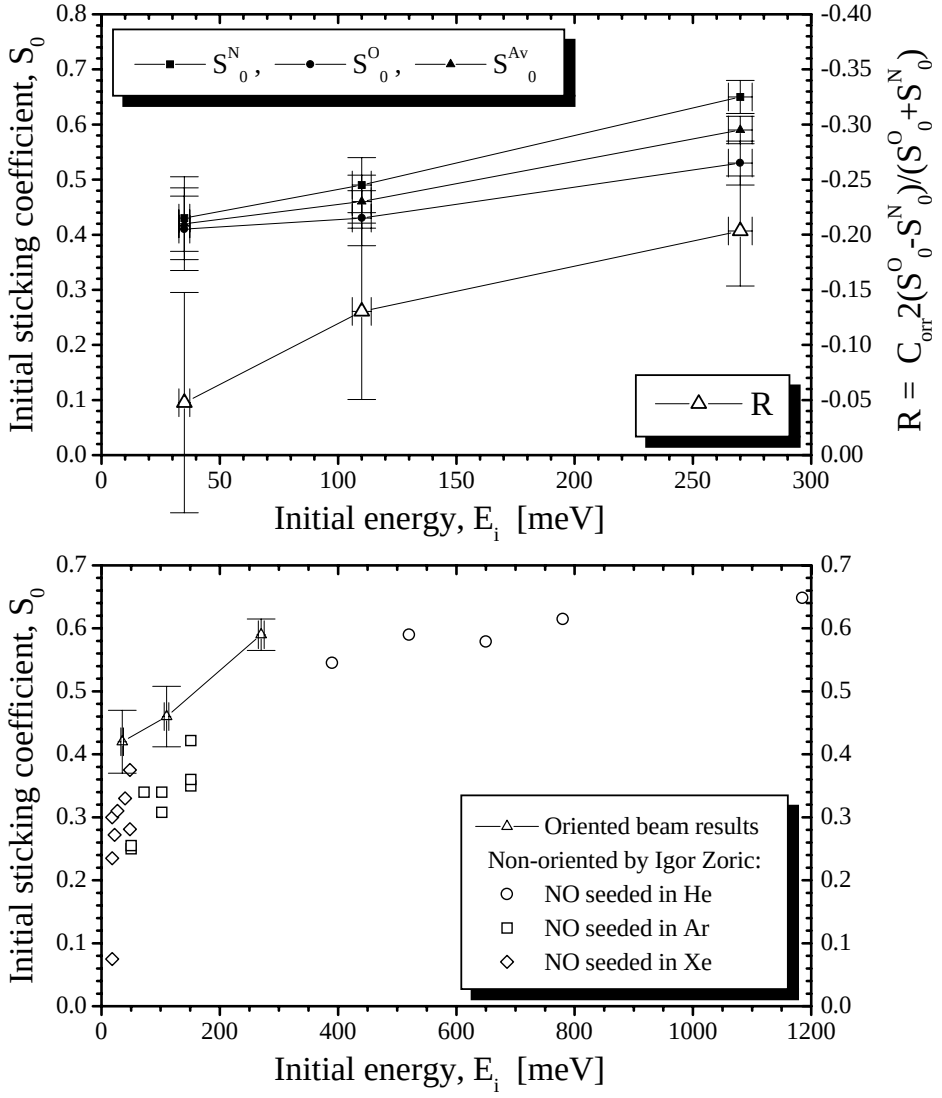

Figure 9.3: *Top panel: Initial sticking coefficient (S_0) for preferentially oriented NO molecules on Al(111) (see Table 9.1). The chemical selectivity can be derived from the N-end down (S_0^N) and O-end down (S_0^O) sticking probabilities according to $R = C_{orr} \cdot 2 \cdot [S_0^O - S_0^N]/[S_0^O + S_0^N]$, with C_{orr} a factor correction for experimental imperfections. Bottom panel: Preliminary results by Igor Zoric* et al., *of the initial dissociative sticking coefficient S_0 of NO on Al(111). These sticking coefficients are derived from AES spectra. Analysis of these spectra is complicated due to overlap of the peaks (Section 9.2).*

E_i[meV]	35	150	300
S_0^N	0.43	0.49	0.65
S_0^O	0.41	0.43	0.53
S_0^{Av}	0.42	0.46	0.59
R_{corr}	-0.056	-0.153	-0.238

Table 9.1: *Initial sticking coefficients for the two preferential orientations of NO molecules (S_0^N and S_0^O) on an Al(111) surface, determined for three beam energies (E_i). From these values the average sticking S_0^{Av} and the (corrected) chemical selectivity $R = C_{orr} \cdot 2 \cdot [S_0^O - S_0^N]/[S_0^O + S_0^N]$ are derived (see section 9.2).*

tial orientation most molecules are aligned parallel with the surface. These relatively high sticking coefficient clearly require a large phase space. It is well possible that only a small fraction of (close to) perpendicular aligned molecules is responsible for the observed chemical selectivity.

The average of the sticking probabilities determined seems consistent with the initial dissociative sticking coefficients determined by Zoric *et al.* for non-oriented molecules as depicted in the bottom panel of Fig. 9.3 [94]. This sticking probability curve lies slightly below our values and shows an increase with beam energy from S_0= 0.24 at 20 meV to S_0= 0.65 at 1175 meV, characteristic of an activated channel. Considering the complicated analysis and preliminary nature of the Auger data, the correspondence with our values appears satisfactory.

In view of the excess oxygen atoms observed on the surface upon NO exposure the preferred N-end down sticking geometry seem contradicting. It suggests the molecules to flip orientation after being trapped, followed by ejection of the N-atoms. The dissociative chemisorption-abstraction of NO on Al(111) is likely to be non-adiabatic; a sudden transfer of the molecule from NO to NO^- to NO^{2-} followed by dissociation. Possibly the first step consists of an electron harpooning to the N-end of the molecule, explaining the higher sticking probability for preferentially N-end down oriented molecules. When transferring a second electron, the intramolecular bond breaks. While the more electro negative O-atoms bind to the surface, the excess binding energy is partly dissipated to translational energy of the N-atom which now can escape into the vacuum.

9.4 Preliminary conclusions

The preferred orientation for sticking of NO molecules on the 300 K Al(111) surface is N-end down; consistent with arguments based on the position of the LUMO on the N-side of the molecule. The chemical selectivity (R) increases with beam energy. Averaging the sticking coefficients for the two molecular orientations shows very satisfactory agreement with the sticking probabilities determined by Zoric *et al.*, es-

pecially when considering the preliminary nature of both these data sets. We picture the abstraction of N-atoms to proceed through the flipping of preferentially N-end down oriented molecules. Ejection of the N-atoms from the surface can occur when transferring excess binding energy into translational energy.

Chapter 10

Summary

In chapters 2-9 of this thesis, eight studies on the interactions between various combinations of gases and surfaces are presented. The common aspect in these studies is the mono-energetic beam of gas particles colliding with a crystalline metallic surface. In these experiments, we can determine the fraction of particles that sticks to the surface. We can subsequently determine the velocity and direction of the scattered part. From these scattering angles and energy losses we can deduce information on the forces between gas particle and surface during the collision. These insights in the *dynamics* of the interaction form the main difference with microscopic and spectroscopic techniques, exposing *static* processes at surfaces.

Fundamental surface science is usually conducted under ultra high vacuum conditions (UHV) because a perfectly clean sample is essential. At a pressure of $1{\cdot}10^{-10}$ mbar ($\simeq$ 0.000 000 000 0001 atmosphere) the surface stays clean for some minutes, up to one hour. Well defined experiments can only be conducted under these ideal conditions. Except for the aluminum crystal used in chapter 9, we used the hexagonal close packed surface of a ruthenium crystal. Our attention was especially caught by the drastic modifications to the scattering properties upon adsorbing a monolayer of hydrogen atoms which makes this Ru(0001)-(1×1)H surface behave as a 'molecular mirror' (Fig. 11.1).

Different gases have been scattered: argon (Ar), nitrogen (N_2), hydrogen (H_2), helium (He) but mostly nitric oxide (NO). Experimental techniques like Temperature Programmed Desorption (TPD), adsorption-reflection sticking probability measurements (technique of King & Wells), Time Of Flight (TOF) scattering measurements, Rotationally Enhanced Multi Photon Ionisation (REMPI) and steric asymmetry measurements have been applied in order to elucidate different features. Especially Chapters 5, 6, 7 and 8 are very closely linked through the different insights they contain on the surprising influence of a hydrogen ad-layer on the Ru(0001) surface. In this summary I will devote most attention to our beloved NO/Ru(0001)-(1×1)H system in order to construct a consistent view on the most likely (emperic) Potential Energy

Surface (PES).

The sticking probability measurements using the standard *adsorption-reflection* technique of King & Wells [31, 32] are in practice often complicated by NO molecules interacting with the stainless steel chamber walls. This disturbing behavior is characterized by the development of mathematical model which allowed an elegant solution to be formulated. After correction for this systematic error, the initial sticking probability of NO on the clean Ru surface turned out to be very high, between 90 and 100%. Adsorbing a (1×1) hydrogen layer, reduces the sticking probability to 20-60% (depending on particle energy); still substantial.

The scattering of argon atoms from the clean ruthenium surface turned out surprisingly complicated. While the interaction between a noble gas and the highly symmetric single crystalline surface appears to be relatively simple, the balance between the energy exchange mechanisms turns out subtle. Classical trajectory calculations using the simulation code TACO (by Rob Lahaye) did not result in satisfactory correspondence to the experimental data. The analytical *washboard model* on the other hand, does yield surprising agreement which are, in view of the simplified interactions (Fig. 3.1) hardly quantitatively reliable. This model does however lead to easy insight in the energy transfer between gas particle and surface.

Calculations on the N_2/Ru(0001) interaction potential by the group of Jens Nørskov reveal a possible meta-stable molecular state on the Ru surface. Flat lying and somewhat stretched nitrogen molecules could spend up to milliseconds in this state. The measurements presented in chapter 4 are consistent with this suggestion.

The interaction of NO with clean ruthenium is mapped in chapter 5. The high sticking probability (chapter 2) prove to be the combined result of several mechanisms acting in conjunction. The analysis of the energies of the ≃10% scattered particles reveal remarkably small energy losses; a feature already known for the hydrogen covered surface (chapter 6).

The incredibly narrow angular distributions of scattered particles presented in Chapter 6 started what appeared to be the mystery around the (1×1)H overlayer. An angular spread of only 8^o FWHM is simply unprecedented. Together with the before mentioned elasticity of the collisions this indicates a relatively flat and heavy surface. The scattered molecules, hardly seem to be affected by the sticking channel, suggesting two extremes: Either the impinging particles stick to the surface by transferring 100% of their initial translational energy, or they scatter in the specular direction (incoming angle = outgoing angle) as if the surface was a *molecular mirror*. A cartoon of this situation is depicted in Fig. 10.1.

Counterintuitively the angular distribution narrows upon increasing the beam energy (Chapter 6). Generally more initial energy puts the turning point of the trajectory closer to the surface causing the particle to experience more corrugation. This argumentation does explain the broadening of the angular distributions for less grazing incoming angles. The larger deflection angles are caused by harder collisions

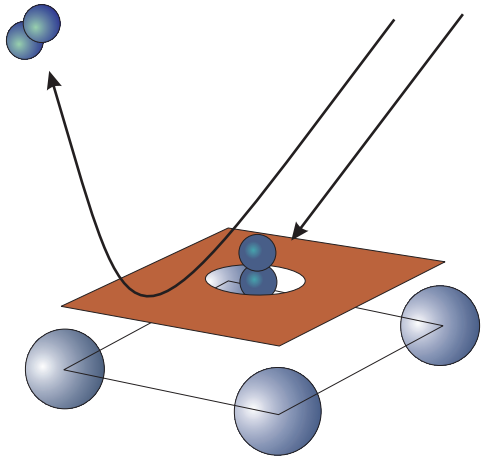

Figure 10.1: *The extreme differences between the adsorption and scattering channels are chematically depicted by this so-called* hole model *by Steve Holloway: either the molecules stick and transfer 100% of their initial energy to the surface, or the scatter almost elastically, narrowly spread around the specular direction ($\theta_f = \theta_i$), as if the surface was a* molecular mirror.

probing more corrugation.

The 'molecular mirror' like scattering made us wonder whether the molecules are rotationally excited in the collision with the Ru(0001)-(1×1) surface. The REMPI study reported in Chapter 7 shows the rotational excitation of scattered NO molecules to be far from extremely small. While the angular distributions indicate minimal surface corrugation, the molecular anisotropy is substantial. Apparently surface corrugation and molecular asymmetry are largely decoupled in the interaction potential.

The steric effect measurements reveal the reactive features in the scattered distribution, by separating the contributions of the differently oriented molecules (Chapter 8). The molecular chemisorption geometry is known to occur N-end down. The molecules impinging in this orientation are scattered over a broader spatial distribution as a result of the stronger interaction with the surface. The magnitude of this steric asymmetry goes up for larger incoming angles (Chapter 8). Again not an expected trend since this anisotropy is expected to broaden the angular distributions, contrary to the observed narrowing. Apparently the decrease in effective surface corrugation dominates over the molecular anisotropy.

In order to develop a consistent view on the interaction potential of the NO/Ru(0001)-(1x1)H system these different observations have to be combined like pieces of a jigsaw puzzle. Especially the experiments with oriented molecules suggest the lattice unit cell to be composed of three different regions:**1)** a flat section of which the molecules are predominantly specularly scattered, **2)** *reactive* scattering of a second more

corrugated area, **3)** the chemisorption well responsible of the sticking of molecules to the surface. In this picture, translational energy, incoming angle and molecular orientation determine the relative size of these three regions. The increase in sticking probability on the H-covered surface for increasing particle energy for instance, can be viewed upon as a widening of the chemisorption well. Tough many questions about this fascinating system remain unanswered sufficient experimental data is obtained to justify a detailed theoretical study. A comparison of (DFT) calculations and (semi) classical trajectory simulation to the data presented in this thesis will probably allow the construction of a reliable interaction potential.

The orientation dependent sticking probability measurements for NO on Al(111) presented in Chapter 9 are the result of a collaboration with Andrew Komrowski and Andrew Kummel (UCSD, USA). The interest in this system originates from the observed non-stochiometric composition of the surface after NO dissociation. Preliminary result of other groups suggest this oxygen rich surface to be the result of N-atoms being ejected from the surface (abstraction) by *consuming* the released excess binding energy. Our experimental capabilities to orient molecules prior to the impact allowed us to determine the preferred sticking geometry to be N-end down. For the abstraction mechanism this means that the molecule has to rotate before the dissociation.

Chapter 11

Samenvatting

In de hoofdstukken 2-9 van dit proefschrif, vertaald getiteld 'Adsorbaat Geinduceerde Gedeeltelijke Passivering van Gas-Oppervlakte Interacties', worden acht onderzoeken gepresenteerd op het gebied van interacties tussen gassen en oppervlakken. Het gemeenschappelijke aspect in deze studies is het gebruik van de bundel mono energetische gasdeeltjes die we op een kristrallijn metaal oppervlak laten botsen. De mogelijkheid om de snelheid van de inkomende deeltjes te varieren maakt het mogelijk processen aan oppervlakken te testen op hun energieafhankelijkheid. We kunnen bijvoorbeeld bepalen welke fractie van de deeltjes blijft plakken. Van de verstrooide deeltjes kunnen we de snelheid en richting bepalen. Uit deze strooihoek en energieverliezen kunnen we informatie herleiden over het krachtenspel *tijdens* de botsing. Deze inzichten in de dynamica van de interactie vormen het grote verschil met microscopische en/of spectroscopische technieken, gericht op de statische evenwichtssituatie van deeltjes *na* de botsing met het oppervlak.

Fundamenteel oppervlakte onderzoek vind bijna altijd plaats onder ultra hoog vacuum (UHV) omdat een perfect schoon sample vereist is. Bij een druk van $1{\cdot}10^{-10}$ mbar ($\simeq$ 0.000 000 000 0001 atmosfeer) blijft het oppervlak enkele minuten tot ongeveer een uur lang schoon. Alleen onder deze ideale condities kunnen goed gedefinieerde experimenten gedaan worden. Behalve het aluminium sample, gebruikt voor hoofdstuk 9, hebben we alle experimenten gedaan met het hexagonale dichtbepakte oppervlak van een rutheen kristal. Onze aandacht werd al snel gegrepen door de drastische invloed van een monolaag waterstof atomen op de verstrooiende eigenschappen van dit Ru(0001) oppervlak. In tegenstelling tot Fig. 11.1 waar dit oppervlak is weergegeven als een verzameling bolletjes blijkt dit met waterstof bedekte Ru(0001)-(1×1)H oppervlak zich te gedragen als een 'moleculaire spiegel'.

Verschillende gassen zijn verstrooid: argon (Ar), stikstof (N_2), waterstof (H_2), helium (He) maar hoofdzakelijk stikstofoxide (NO). Experimentele technieken als temperatuur geprogrammeerde desorptie (TPD), adsorptie-reflectie plakkans metingen (techniek van King & Wells), vluchttijd verstrooiings metingen (TOF), rotationeel

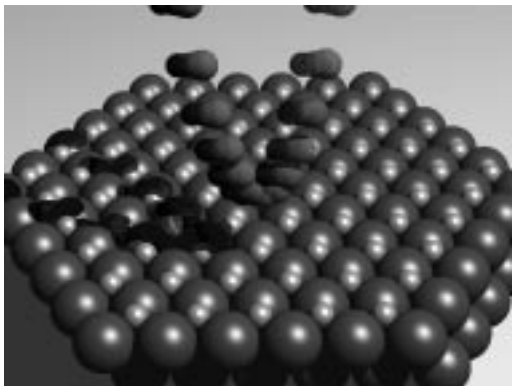

Figure 11.1: *Schematische voorstelling van een verstrooiend NO molecuul aan het met een monolaag waterstof bedekte Ru(0001) oppervlak.*

vermeerderde multipele fotonen ionisatie (REMPI) en sterische asymmetrie metingen zijn ingezet om verschillende aspecten te onderzoeken. Vooral de hoofdstukken 5, 6, 7 en 8 zijn onderling nauw verbonden door de verschillende inzichten die verkregen worden op de verrassende invloed van de waterstof overlaag op het Ru(0001) oppervlak.

In dit hoofdstuk zal ik proberen de weldadige hoeveelheid aan resultaten samen te vatten. De meeste aandacht zal hierbij uitgaan naar ons geliefde Ru(0001)-(1×1)H systeem om zodoende een consistent beeld te vormen van het meest waarschijnlijke (emperische) potentiële energie oppervlak (PES).

De plakkans metingen met de standaard *adsorptie-reflectie* techniek, begin jaren '70 ontwikkeld door de heren King en Wells [31, 32], worden in de praktijk vaak bemoeilijkt doordat NO moleculen niet alleen op het sample plakken, maar ook een sterke wisselwerking met de wanden van de UHV-kamer hebben. Dit storende gedrag is in hoofdstuk 2 door middel van een wiskundig model in kaart gebracht waarna een elegante oplossing geformuleerd kon worden. Na correctie voor deze systematische fout blijkt de plakkans van NO moleculen op het schone rutheen oppervlak zeer hoog, tussen de 90 en 100%. Het aanbrengen van een waterstof laag op het oppervlak heeft slechts een gedeeltelijk passiverende werking. De plakkans verminderd tot 20-60% (afhankelijk van de deeltjesenergie); nog steeds aanzienlijk.

De verstrooiing van argon atomen van het schone rutheen oppervlak is verrassend gecompliceerd gebleken. Hoewel de wisselwerking tussen een edelgas deeltje en het hoog symmetrische oppervlak van het rutheen één-kristal relatief eenvoudig lijkt is het samenspel van verschillende energie uitwisselinde mechanismen toch der-

mate subtiel dat het door ons gebruikte geavanceerde simulatieprogramma (TACO van Rob Lahaye, draaiend op de SP2 supercomputer van rekencentrum SARA) niet in staat is de experimenten quantitatief te reproduceren. Het analytische *washboard model* levert resultaten die een opvallende gelijkenis vertonen met de experimentele data, maar behandelt de verstrooiing dermate simplistisch dat aan deze quantitatieve overeenkomsten niet veel waarde gehecht kan worden. Zo wordt het oppervlak bijvoorbeeld voorgesteld door een één-dimensionele rimpel, analoog met een ouderwets wasboord (zie Fig. 3.1), in plaats van de realistische twee-dimensionele hexagonale structuur van Fig. 11.1. Dit model bewijst zich echter wel heel geschikt voor het verkrijgen van inzichten in de relevante processen achter de energieoverdracht tussen gasdeeltje en kristal rooster.

Berekeningen aan de N_2/Ru(0001) interactiepotentiaal door de groep van Jens Nørskov laten een mogelijke metastabiele moleculaire toestand zien; een toestand waarbij de stikstof moleculen plat en enigszins uitgerekt een korte tijd (tot enkele milliseconden) aan het oppervlak kunnen verblijven. De metingen die in hoofdstuk 4 gepresenteerd worden zijn consistent met deze voorspelling.

De interactie van NO met schoon rutheen is in kaart gebracht in hoofdstuk 5. De hoge plakkans van NO moleculen op het oppervlak (zie hoofdstuk 2) blijkt het gevolg van een combinatie van verschillende mechanismen. Dat NO moleculen bij de verstrooiing van het waterstofbedekte oppervlak bijna geen energie verliezen was al bekend (hoofdstuk 6). Tot onze grote verrassing blijkt dit ook te gelden voor de weinige ($\sim$10%) deeltjes die op het uiterst reactive schone oppervlak niet plakken.

De spectaculair smalle hoekverdeling van verstrooide NO-moleculen gepresenteerd in hoofdstuk 6 vormde het beginpunt van het mysterie rond de (1×1)H overlaag. Een hoekverbreding van slechts $\sim 8^o$ (FWHM) is simpelweg nooit eerder vertoond. Samen met de eerder genoemde bijna elastische verstrooiing suggereert dit een relatief ongecorrugeerd en zwaar oppervlak. Dit gegeven lijkt echter lastig te rijmen met de aanzienlijke plakkans (S_0) van NO moleculen op dit met waterstof bedekte oppervlak. Deze ogenschijnlijke tegenstelling is in Fig. 10.1 geillustreerd door middel van het zogenaamde 'hole model' van Steven Holloway. De moleculen kunnen of plakken, door 100% van de initiële energy over te dragen naar het oppervlak, of bijna elastisch verstrooien in een nauwe verdeling rond de speculaire richting (hoek van inval = hoek van uitval: $\theta_f = \theta_i$), alsof het oppervlak een *moleculaire spiegel* is.

Tegen de intuitie in blijken de hoekverdelingen smaller te worden bij toenemende bundelenergie. In het algemeen betekent meer initiële energy dat het omkeerpunt van de verstrooiingsbaan dichter bij het oppervlak ligt waardoor het deeltje meer oppervlaktecorrugatie ervaart. Dit argument verklaart namelijk wel waarom de hoekverdeling verbreedt bij minder scherende inkomende hoeken. De grotere afbuighoeken moeten het resultaat zijn van hardere botsingen (meer kracht betekent een dichtere nadering van het oppervlak) waardoor dus meer corrugatie ervaren wordt. In de oorspronkelijke publicatie van dit werk [10] hebben we gesuggeerd dat de bijna elastische verstrooiing het gevolg zou zijn van een *verstijvende* werking van de waterstof laag

op het kristalrooster. De latere bij (IBM-research) bepaalde energieverdelingen van het schone kristal (hoofdstuk 5) tonen echter aan dat deze elasticiteit een eigenschap is van het rutheen substraat.

Doordat de 'moleculaire spiegel' karakteristiek van de verstrooiing vroegen wij ons af of er in de botsing enige **rotatie-excitatie** optreedt (in de botsing kan torsie op het molecuul ervoor zorgen dat deze het oppervlak tollend verlaat). Deze excitatie is echter niet extreem klein (hoofdstuk 7) en vertoont opvallende gelijkenis met de NO verstrooiing van het zilver (111) oppervlak. Hoewel de hoekverdelingen wijzen op minimale oppervlakte corrugatie (hoofdstuk 6) blijkt de moleculaire anisotropie aanzienlijk. Kennelijk zijn deze anisotropie en oppervlakte corrugatie grotendeels ontkoppeld in de interactiepotentiaal.

De sterisch effect metingen leggen reactieve eigenschappen bloot in de ruimtelijke verdeling door deze te ontbinden in bijdragen van de twee moleculaire oriëntaties (hoofdstuk 8). De stand van het molecuul vóór de botsing is een zeer elementaire botsingsparameter die we door gebruik van een electrostatische (hexapool-) lens en een hoogspanningsveld kunnen manipuleren. Uit de literatuur is bekend dat het molecuul met de N-kant naar het oppervlak bindt. Consistent met deze wetenschap worden de in deze voorkeursoriëntatie verstrooide moleculen door de sterkere interactie met het oppervlak over een grotere ruimtehoek verspreidt.

Een consistent beeld van de interactiepotentiaal van het NO/Ru(0001)-(1x1)H systeem kan verkregen worden door de verschillende bevindingen in elkaar te passen. De experimenten met georiënteerde moleculen wijzen er op dat een eenheidscel waarschijnlijk in drie gebieden onderverdeeld kan worden: **1)** een vlak gedeelte waarvan de moleculen voornamelijk speculair verstrooien, **2)** *reactieve* verstrooiing van een tweede gebied met meer oppervlakte rimpel, **3)** de chemisorptie put waar de deeltjes aan het oppervlak gebonden worden. De afmetingen van deze gebieden zijn in dit beeld afhankelijk van de oriëntatie van het molecuul en de energie van de inkomen NO moleculen. Zo valt het feit dat de plakkans toeneemt voor snellere NO-moleculen te verklaren door het groter worden van de chemisorptieput.

Het mag duidelijk zijn dat veel vragen over dit merkwaardige systeem voorlopig open blijven staan. Hoewel dit systeem door additioneel experimenteel werk veel uitgebreider gekarakteriseerd kan worden is nu genoeg materiaal geleverd voor een gedetailleerde theoretische aanpak. Door (DFT-)berekeningen en (semi-)klassieke baanberekening te toetsen aan de in dit proefschrift gepresenteerde data kan waarschijnlijk een betrouwbare quantitatieve interactie potentiaal bepaald worden.

De oriëntatie afhankelijke plakkans van NO op Al(111), beschreven in het laatste hoofdstuk 9, is het gevolg van een recente samenwerking met Andrew Komrowski en Andrew Kummel (University of California, San Diego, USA). De interesse in dit systeem volgt op de bevinding dat na dissociatie (het opbreken) van het NO molecuul minder stikstof dan zuurstof atomen op het aluminium oppervlak aanwezig zijn. Voorlopige resultaten van andere groepen suggereren dat de bij de dissociatie vrijkomende bindingsenergie gebruikt wordt om het N-atom van het opper-

vlak te schieten (abstractie). Door onze experimentele middelen om de moleculen te oriënteren voor de botsing, hebben we kunnen vaststellen dat de plakkans het grootst is voor deeltje met de N-kant richting het oppervlak. Voor het abstractiemechanisme betekent dit dat het molecuul aan het oppervlak moet roteren voor het dissocieert.

Nawoord

Modern experimenteel wetenschappelijk onderzoek is niet mogelijk zonder een gezond teamverband. Afgezien van de intense samenwerking met groepsleden, ondersteunende diensten en vele (internationale) contancten is het in dit proefschrift gepresenteerde werk in allereerste instantie mogelijk gemaakt door mijn beide promotoren Aart Kleyn en Steven Stolte. Hun vertrouwen in mij, opgebouwd tijdens mijn langdurige stage periode bij het Amolf, maakte het mogelijk aan dit project beginnen. Door het aanstekelijke enthousiasme van deze twee complementaire karakters kon ik deze klus afmaken.

In dienst van de scheikunde faculteit van de VU maar gedetacheerd bij het Amolf was ik in alle benodigde randvoorwaarden voorzien: de gecombineerde wetenschappelijk kennis en ervaring van twee groepen, de uitgebreide technische ondersteuning van groepstechnici, constructie buro, electronische en mechanische werkplaatsen van het Amolf. Ook voor de aankoop van apparatuur en conferentie bezoek bleek altijd voldoende budget beschikbaar. Zo konden Bernd en ik, voorafgaand aan de Gordon Research Conference (Endover '99), bij de firma ABB-Extrel (Pittsburg, USA) onderhandelen over de State-of-the-Art quadrupool detector waar uiteindelijk de data voor hoofdstuk 8 mee is gemeten. Naast de bovengenoemde randvoorwaarden heeft een gezond mengsel van botte pech en veel geluk tot verrassende inwikkelingen van dit project geleid. De bedekking van het rutheen oppervlak met een laagje waterstof, dat zoveel verrassende resultaten heeft opgeleverd, was bijvoorbeeld niet gepland.

Het binnenhalen van het *dr. van Dierendonck Stipendium* leverde extra finaciele steun boven het ruime reisbudget van het Amolf, waardoor een intense tien-weekse samenwerking met Charlie Rettner en Dan Auerbach (IBM-research San Jose, USA) mogelijk werd. Dit bezoek, aan de wetenschappelijke broedkamer van enkele toonaangevende vakgenoten (waaronder Aart zelf), bood een indrukwekkende en inspirerende blik achter de schermen van veel baanbrekend oppervlaktefysica onderzoek.

Nu dit proefschrift (bijna) af is wil ik graag een aantal mensen bedanken. Allereerst mijn directe groepsgenoten François, Bernd, David, Dimitrios, Richard, Mike, Laurent, Silvie vooral ook mijn productieve studenten Martijn en Sander. Ook dank ik de 'nazorg' van illustere voorgangers als Age, Arjan, Rob en ook nog heel even de pret van Frans Vitalis. Dank natuurlijk ook voor de technische ondersteuning van het

Amolf met een bijzondere vermelding voor Idsart, Jan, Henk (N), Menno en Wim (B) omdat zij, naast hun inzet voor de vacuum apparatuur, makkelijk enthousiast krijgen waren voor een motor-beun op Amolf niveau.

Buiten de werksfeer heb ik natuurlijk veel te danken aan de warme steun, inspiratie en gezelligheid van familie, vrienden en vriendinnen, muziekmakers, vage bekenden en andere 'meelevers': Eveline, Margot, Alex, (opa) Cees, Bep, Jacques, Ellen, Arnoud, Marco, Maritsa, Hans, Yvonne, Marije, Mascha, Kirsten, Wim, Steven (dV), Illya, Gerard, Henk (S), Doede, Hermien (en het overige personeel van café 'East of Eden'), Anton, Audrey, Katelijne, Amanda, Sandra, Mar, Ilse, Karin, Gea, Teske, Bas (vD), Jannekke, Mirna, Laurent, Rob (O), Jimmy, Daniël, Rob vD. en Michiel.

Hoewel het afzweren van het wedstrijdroeien een voorwaarde voor mijn aanstelling was, heb ik ook tijdens mijn promotie veel moois uit deze prachtige sport gehaald. Bij mijn eigen rustige roeivereniging RIC vooral met roeimakker Bart (vdH) en daarnaast ook met dr. Jeroen en roeigoden Franco en Marc. De laatste tijd beleef ik de roeisport minder lichamelijk actief, maar zeker zo betrokken en ontspannend, door het coachen van de 1^e-jaars zware heren 8+ bij mijn vroegere studenten roeivereniging Skøll. Dank aan 'Fast Forward': David, Robin, Pieter, Viljo, Jaap, Alexander, Peter, Marijn, Olivier, Victor, Ester, Eva maar vooral medecoaches Joyce en Nienke die mijn coachtaken zonder problemen overnamen in mijn periodes van proefschrift deadline stress.

Amsterdam, 15 mei 2000

Bibliography

[1] A.B. Anton, N.R. Avery, B.H. Toby, and W.H. Weinberg. Electron energy loss spectroscopy of the decomposition of formic acid on Ru(001). *J. Electron. Stectr. Relat. Phenom.*, 29:181, 1983.

[2] J.L. Beeby. The scattering of helium atoms from surfaces. *J. Phys. C. (Solid State Physics)*, 4(18):L359, 1971.

[3] B. Berenbak, D.A. Butler, B. Riedmüller, D.C. Papageorgopoulos, S. Stolte, and A.W. Kleyn. Sticking probability measurements in a reactive system. *Surf. Sci.*, 414(1):271–278, 1998. This thesis Chapter 2.

[4] B. Berenbak, B. Riedmüller, D.A. Butler, C.T. Rettner, D.J. Auerbach, S. Stolte, and A.W. Kleyn. Molecular beam study on interaction dynamics in a reactive system: NO on bare Ru(0001). *Phys. Chem. Chem. Phys.*, 2:919, 2000. This thesis Chapter 5.

[5] B. Berenbak, B. Riedmüller, C.T. Rettner, D.J. Auerbach, S. Stolte, and A.W. Kleyn. Decoupling of rotational excitation and parallel momentum transfer: NO scattered from Ru(0001)-(1×1)H. *In preparation*, 2000. This thesis Chapter 7.

[6] B. Berenbak, S. Zboray, B. Riedmüller, D.C. Papageorgopoulos, S. Stolte, and A.W. Kleyn. Ar/Ru(0001) experiments compared to washboard model and trajectory simulations. *In preparation*, 2000. This thesis Chapter 3.

[7] B. Berenbak, S. Zboray, B. Riedmüller, S. Stolte, and A.W. Kleyn. Reactive vs. inert surface scattering: Steric effect of NO from Ru(0001)-(1×1)H. *In preparation*, 2000. This thesis Chapter 8.

[8] J.K. Brown and A.C. Luntz. NO sticking on a Pt(111) surface. *Chem. Phys. Lett.*, 204(5,6):451–454, 1993.

[9] H. Brune, R.J. Behm, and G. Ertl. Surface migration of 'hot' adatoms in the couse of dissociative chemisorption of oxygen on Al(111). *Phys. Rev. Lett.*, 68(5):624, 1992.

[10] D.A. Butler, B. Berenbak, S. Stolte, and A.W. Kleyn. Elastic scattering in a reactive environment: NO on Ru(0001)-(1×1)H. *Phys. Rev. Lett.*, 78:4653–4556, 1997. This thesis Chapter 6.

[11] H. Dietrich, P. Geng, K. Jakobi, and G. Ertl. Sticking coefficient for dissociative adsorption of N_2 on Ru single-crystal surfaces. *J. Chem. Phys.*, 104(1):375, 1996.

[12] T. Duhoo and D. Lemoine. The role of surface corrugation in the rotational rainbow scattering of NO from Ag(111). *J. Chem. Phys.*, 109(7):2851–2855, 1998.

[13] R.C. Egeberg, J.H. Larsen, and I. Chorkendorff. private communication.

[14] T. Engel. A molecular beam investigation of the catalytic oxidation of CO on Pd(111). *J. Chem. Phys.*, 69(3):373, 1978.

[15] G. Ertl. *Catalytic Ammonia Synthesis, eds. J.R. Jennings (Plenum, New York)*, page 109, 1991.

[16] P. Feulner, S. Kulkarni, E. Umbach, and D. Menzel. A multimethod investigation of the adsorption of NO on Ru(001). ii. delta phi, thermal desorption and LEED results. *Surf. Sci.*, 99:489, 1980.

[17] P. Feulner and D. Menzel. Unusual coverage dependence of a sticking coefficient: N_2 Ru(001). *Phys. Rev. B*, 25:4295, 1982.

[18] F. Geuzebroek. *State to State Molecule-Surface Scattering.* PhD thesis, Universiteit van Amsterdam, (1991).

[19] F.H. Geuzebroek, A.E. Wiskerke, M.G. Tenner, A.W. Kleyn, S. Stolte, and A. Namiki. Rotational excitation of oriented molecules as a probe of molecule-surface interaction. *J. Phys. Chem.*, 95(21):8409, 1991.

[20] J.T. Grant and T.W. Haas. *Surf. Sci.*, 21(76), 1970.

[21] A. Gross, S. Wilke, and M. Scheffler. Six-dimensional quantum dynamics of adsorption and desorption of H_2 at Pd(100): Steering and steric effects. *Phys. Rev. Lett.*, 75(14):2718, 1995.

[22] B. Hammer. Bond activation at monatomic steps: NO dissociation at corrugated Ru(0001). *Phys. Rev. Lett.*, 83(18):3681, 1999.

[23] T.F. Hanisco and A.C. Kummel. The effect of surface passivation on rotationally inelastic scattering: N_2 scattered from W(110), W(110)-(2x2)N, W(110)-(1×1)H, and Pt(111). *J. Chem. Phys.*, 99(9):7076, 1993.

[24] Martin Head-Gordon, C.T. Rettner, B.C. Mullins, D.J. Auerbach, and John C. Tully. On the nature of trapping and desorption at high surface temperatures. theory and experiments for the Ar-Pt(001) system. *J. Chem. Phys.*, 94(12):1516, 1991.

[25] Martin Head-Gordon, H. Schlichtling, D. Menzel, and John C. Tully. The coverage dependence of the sticking probability of Ar on Ru(001). *J. Chem. Phys.*, 95(12):9266, 1991.

[26] S. Holloway, M. Karikorpi, and J.W. Gadzuk. Dynamics of molecular collisions with surfaces: excitation, dissociation and diffraction. *Nucl. Instr. Meth. B*, B27(1):37, 1987.

[27] A. Hopkinson. PhD thesis, University of Cambridge, 1993.

[28] A. Hopkinson, X-C Guo, J.M. Bradley, and D.A. King. A molecular beam study of the co-induced surface phase transition on Pt(100). *J. Chem. Phys.*, 99(10):8262, 1993.

[29] T.A. Jachimowski, B. Meng, D.F. Johnson, and W.H. Weinberg. Thermal desorption studies of high-coverage hydrogen overlayers on Ru(001) created with gas-phase atomic hydrogen. *J. Vac. Sci. Technol. A*, 13(3):1564, 1995.

[30] M. Kay, G.R. Darling, S. Holloway, J.A. White, and D.M. Bird. Steering effects in non-activated adsorption. *Chem. Phys. Lett.*, 245(2/3):311, 1995.

[31] D.A. King and M.G. Wells. Molecular beam investigation of adsorption kinetics on bulk metal targets: nitrogen on tungsten. *Surf. Sci.*, 29(2):454, 1972.

[32] D.A. King and M.G. Wells. Reaction mechanism in chemisorption kinetics: nitrogen on the (100) plane of tungsten. *Proc. Roy. Soc.*, 339(1617):245, 1974.

[33] A.W. Kleyn. Rotational rainbow scattering of oriented molecules. *Surf. Rev. Lett.*, 1(1):157, 1994.

[34] A.W. Kleyn and T.C.M. Horn. Rainbow scattering from solid surfaces. *Phys. Rep.*, 199(4):192, 1991.

[35] A.W. Kleyn, A.C. Luntz, and D.J. Auerbach. Rotational energy transfer in direct inelastic surface scattering: NO on Ag(111). *Phys. Rev. Lett.*, 47(16):1169, 1981.

[36] A. Komrowski and A.C. Kummel. private communication.

[37] E.W. Kuipers, M.G. Tenner, A.W. Kleyn, and S. Stolte. Steric effects for NO/Pt(111) adsorption and scattering. *Phys. Rev. Lett.*, 62(18):2152, 1989.

[38] E.W. Kuipers, M.G. Tenner, M.E.M. Spruit, and A.W. Kleyn. Angular and energy distributions of NO scattered from a Ag(111)-surface. *Surf. Sci.*, 189/190:669, 1987.

[39] E.W. Kuipers, M.G. Tenner, M.E.M. Spruit, and A.W. Kleyn. Differential trapping probabilities and desorption of physisorbed molecules: application to NO/Ag(111). *Surf. Sci.*, 205(1-2):241, 1988.

[40] R.J.W.E. Lahaye. *simulation of Surface Scattering.* PhD thesis, Vrije University te Amsterdam, 1995.

[41] R.J.W.E. Lahaye, S. Stolte, and A.W. Kleyn. Site dependent energy loss in Ar scattering from Pt(111). *Surf. Sci.*, 307:187, 1994.

[42] R.J.W.E. Lahaye, S. Stolte, and A.W. Kleyn. Orientation and energy dependence of NO scattering from Pt(111). *J. Chem. Phys.*, 104(21):8301, 1996.

[43] D. Lemoine and D.C. Corey. Close-coupled wave-packet calculations of the direct inelastic scattering of NO($X^2\Pi$) from Ag(111). *J. Chem. Phys.*, 92(10):6175–6189, 1990.

[44] M. Lindroos, H. Pfnür, P. Feulner, and D. Menzel. A study of the adsorption sites of hydrogen on Ru(001) at saturation coverage by electron reflection. *Surf. Sci.*, 180(1):237, 1987.

[45] A.C. Luntz, M.D. Williams, and D.S. Bethune. The sticking of O_2 on a Pt(111) surface. *J. Chem. Phys.*, 89(7):4381, 1988.

[46] K.R. Lykke and B.D. Kay. Rotationally inelastic gas-surface scattering: HCl from Au(111). *J. Chem. Phys.*, 92(4):2614–2623, 1990.

[47] T. Matsushima. Angular distribution of the combinative desorption of nitrogen atoms on Ru(001) surfaces. *Surf. Sci.*, 197:l287, 1988.

[48] J.J. Mortensen, B. Hammer, and J.K. Nørskov. Alkali promotion of N_2 dissociation over Ru(0001). *Phys. Rev. Lett.*, 80(19):4333, 1998.

[49] J.J. Mortensen, Y. Morikawa, B. Hammer, and J.K. Nørskov. Density functional calculations of N_2 adsorption and dissociation on a Ru(001) surface. *J. Cat.*, 169(1):85, 1997.

[50] M.J. Murphy, J.F. Skelly, A. Hodgson, and B. Hammer. Nitrogen recombination dynamics at Cu(111): Rotational energy release and product angular distributions. *J. Chem. Phys.*, 109(9):3619, 1998.

[51] L. Österlund, I. Zoric, and B. Kasemo. Dissociative sticking of O_2 on Al(111). *Phys. Rev. B*, 55(23):15452, 1997.

[52] A. Ozaki and K. Alika. *Catalysis-Science and Technology, eds. J.R. Anderson and M. Boudart (Springer, Berlin)*, 1, 1981.

[53] D.C. Papageorgopoulos, B. Berenbak, M. Verwoest, B. Riedmüller, S. Stolte, and A.W. Kleyn. A molecular beam study of the scattering and chemisorption dynamics of N_2 on Ru(0001). *Chem. Phys. Lett.*, 305:401, 1999.

[54] A. Pashutski and M. Folman. Low temperature XPS studies of NO and N_2O adsorption on Al(100). *Surf. Sci.*, 216:395, 1989.

[55] A. Raukema. *Dynamics of Chemisorption*. PhD thesis, University of Amsterdam, 1995.

[56] A. Raukema, D.A. Butler, and A.W. Kleyn. The interaction of oxygen with the Ag(100) surface. *J. Phys.: Condens. Matter*, 8(14):2247, 1996.

[57] A. Raukema, D.A. Butler, and A.W. Kleyn. O_2 transient trapping-desorption at the Ag(111) surface. *J. Chem. Phys.*, 106(6):2477, 1996.

[58] A. Raukema, R.J. Dirksen, and A.W. Kleyn. Probing the (dual) repulsive wall in the interaction of O_2, N_2, and Ar with the Ag(111) surface. *J. Chem. Phys.*, 103(14):6217, 1995.

[59] A. Raukema, A.P. de Jongh, H.P. Alberda, R. Boddenberg, E. de Haas, A.W. Kleyn, H. Neerings, R. Schaafsma, and H. Veerman. A three-axis goniometer in an uhv molecular beam experiment. *Meas. Sci. Technol.*, 8:253, 1997.

[60] A. Raukema and A.W. Kleyn. Transient trapping desorption of molecules at surfaces. *Phys. Rev. Lett.*, 74(21):4333, 1995.

[61] P.D. Reed, C.M. Comrie, and R.M. Lambert. Chemisorption, surface structural chemistry and electron impact properties of carbon monoxide on Ru(101). *Surf. Sci.*, 59(1):33, 1976.

[62] C.T. Rettner, D.J. Auerbach, J.C. Tully, and A.W. Kleyn. Chemical dynamics at the gas-surface interface. *J. Phys. Chem.*, 100:12021–13033, 1996.

[63] C.T. Rettner, J.A. Barker, and D.S. Bethune. Angular and velocity distributions characteristic of the transition between the thermal and structural regimes of gas-surface scattering. *Phys. Rev. Lett.*, 67(16):2183, 1991.

[64] C.T. Rettner, L.A. DeLouise, and D.J. Auerbach. Effect of incidence kinetic energy and surface coverage on the dissociative chemisorption of oxygen on W(110). *J. Chem. Phys.*, 85(2):1131, 1986.

[65] C.T. Rettner, J. Kimman, and D.J. Auerbach. Inelastic scattering of NO from Ag(111): Internal state, angle, and velocity resolved measurements. *J. Chem. Phys.*, 94(1):734–750, 1991.

[66] C.T. Rettner and H. Stein. Effect of translational energy on the chemisorption of N_2 on Fe(111): activated dissociation via a precursor state. *Phys. Rev. Lett.*, 59(24):2768, 1987.

[67] B. Riedmüller, I.M. Ciobica, D.C. Papageorgopoulos, B. Berenbak, R. van Santen, and Kleyn A.W. CO adsorption on hydrogen saturated Ru(0001). *Submitted to J. Phys. Chem.*, 2000.

[68] B. Riedmüller, D.C. Papageorgopoulos, F. Frechard, B. Berenbak, Kleyn A.W., and R. van Santen. The dynamic interaction of CO with Ru(0001) in the presence of adsorbed CO and hydrogen. *Submitted to Surf. Sci.*, 2000.

[69] L. Romm, G. Katz, R. Kosloff, and M. Assher. Dissociative chemisorption of N_2 on Ru(001) enhanced by vibrational and kinetic energy: Molecular beam experiments and quantum mechanical calculations. *J. Phys. Chem. B.*, 101(12):2213, 1997.

[70] R.A. van Santen, P.W.N.M. Leeuwen, J.A. Moulijn, and B.A. Averill. *Catalysis, An Integrated Approach, Second, Revised and Enlarged Edition.* Elsevier, Amsterdam, 1999.

[71] E.K. Schweizer and C.T. Rettner. Quantum effects in the scattering of argon from 2H-W(100). *Phys. Rev. Lett.*, 62(26):3085, 1989.

[72] E.K. Schweizer, C.T. Rettner, and S. Holloway. Diffraction and rainbows in the scattering of argon from 2H-W(100). *Surf. Sci.*, 249(1/3):335, 1991.

[73] D.C. Seets, M.C. Wheeler, and C.B. Mullins. Dynamics of molecular chemisorption of N_2 on the Ru(001) surface. *J. Vac. Sci. Technol. A*, 14(3):1566, 1996.

[74] D.C. Seets, M.C. Wheeler, and C.B. Mullins. Kinetics and dynamics of nitrogen adsorption on Ru(001): evidence for direct molecular chemisorption. *Chem. Phys. Lett.*, 257(3/4):280, 1996.

[75] H. Shi and K. Jacobi. Evidence for physisorbed N_2 in the monolayer on Ru(001) at 40 K. *Surf. Sci.*, 278(3):281, 1992.

[76] H. Shi and K. Jacobi. Hydrogen vibrations on the Ru(001) surface revisited. *Surf. Sci.*, 313:289, 1994.

[77] H. Shi, K. Jacobi, and G. Ertl. Dissociative chemisorption of nitrogen on Ru(0001). *J. Chem. Phys.*, 99(11):9248, 1993.

[78] M.E.M. Spruit and A.W. Kleyn. Dissociative adsorption of O_2 on Ag(111). *Chem. Phys. Lett.*, 159:342–348, 1989.

[79] M.E.M. Spruit, E.W. Kuipers, M.G. Tenner, J. Kimman, and A.W. Kleyn. Molecular-beam scattering of O_2 and Ar from Ag(111). *J. Vac. Sci. Technol. A*, 5(4):496, 1987.

[80] M.G. Tenner. *Steric Effects in Molecule-Surface Scattering.* PhD thesis, University of Amsterdam, 1990.

[81] M.G. Tenner, F.H. Geuzebroek, E.W. Kuipers, A.E. Wiskerke, A.W. Kleyn, S. Stolte, and A. Namiki. Orientation dependence of rotational excitation in NO scattering from Ag(111). *Chem. Phys. Lett.*, 168(1):45, 1990.

[82] M.G. Tenner, E.W. Kuipers, A.W. Kleyn, and S. Stolte. Classical trajectory study of the interaction of oriented NO and Ag(111). *Surf. Sci.*, 242(1/3):376, 1991.

[83] S.R. Tennison. *Catalytic Ammonia Synthesis, eds. J.R. Jennings (Plenum, New York)*, page 303, 1991.

[84] G.W. Trucks, K. Raghavachari, G.S. Higashi, and Y.J. Chabal. Mechanism of HF etching of silicon surfaces: A theoretical understanding of hydrogen passivation. *Phys. Rev. Lett.*, 65:504, 1990.

[85] J.C. Tully. Washboard model of gas-surface scattering. *J. Chem. Phys.*, 92(1):680, 1990.

[86] E. Umbach, S. Kulkarni, P. Feulner, and D. Menzel. A multimethod study of the adsorption of NO on Ru(001). I. XPS, UPS and XAES measurements. *Surf. Sci.*, 88(1):65, 1979.

[87] S. Wilke, M.H. Cohen, and M. Scheffler. Local isoelectronic reactivity of solid surfaces. *Phys. Rev. Lett.*, 77:1560, 1996.

[88] A.E. Wiskerke. *Direct scattering and chemisorption.* PhD thesis, Unerversity of Amsterdam, 1994.

[89] A.E. Wiskerke and A.W. Kleyn. Angular and translational energy distributions of NO scattered from Pt(111). *J. Phys.: Condens. Matter*, 7(27):5195, 1995.

[90] A.E. Wiskerke, C.A. Taatjes, and A.W. Kleyn. Survival mechanism for rotational rainbows in highly attractive molecule-surface systems: NO scattering from Pt(111). *Chem. Phys. Lett.*, 216:93, 1993.

[91] G.-Q. Xu, S.L. Bernased, and J.C. Tully. Stochastic trajectory studies of small argon cluster scattering from Pt(111). *J. Chem. Phys.*, 88(5):3376, 1988.

[92] E. Yablonovitch, D.L. Allare, C.C. Chang, T. Gmitter, and T.B. Bright. Unusually low surface-recombination velocity on silicon and germanium surfaces. *Phys. Rev. Lett.*, 57:249, 1986.

[93] T. Zambelli, J. Trost, J. Wintterlin, and G. Ertl. Diffusion and atomic hopping of N atoms on Ru(0001) studied by scanning tunneling microscopy. *Phys. Rev. Lett.*, 76:795–798, 1996.

[94] I. Zoric and B. Kasemo. private communication.